

**“High Frequency Electromagnetic  
Propagation/Scattering Codes”**

**Final Technical Report**  
September 1, 2000

Small Business Technology Transfer (STTR) Program (DOD)  
DCMC Hartford

Topic No: AF97T001  
Phase II

Issued by USAF, AFMC  
Air Force Office of Scientific Research under

**Contract No: F49620-97-C-0051**

F.M.A.& H. Corporation  
1020 Sherman Avenue  
Hamden, CT 06514  
Eff. Date of Contract: 8/1/98

P.I.: Frank Geshwind, Ph.D.  
(203)248-8212  
This report covers period:  
8/1/98 – 7/31/00

“The views and conclusions contained in this document are those of the authors and should not be interpreted as representing the official policies, either expressed or implied, of the Small Business Technology Transfer (STTR) Program or the U.S. Government.”

“Distribution is unlimited; approved for public release.”

DNIC QUALITY INSPECTED 4

20000914 064

**REPORT DOCUMENTATION PAGE**

Form Approved  
GSA No. 0704-0188

Public Reporting Burden for this collection of information is estimated to average 1 hour per response, including the time for reviewing instructions, searching existing data sources, gathering and maintaining the data needed, and reviewing the collection of information. Send comments regarding this burden estimate or any other aspect of this collection of information, including suggestions for reducing the burden, to Washington Headquarters Service, Directorate for Information Operations and Reports, 1215 Jefferson Davis Highway, Suite 1204, Arlington, VA 22202-4302, and to the Office of Management and Budget, Paperwork Reduction Project (0704-0188), Washington, DC 20503.

1. AGENCY USE ONLY (Leave blank)		2. REPORT DATE 9/1/00	3. REPORT TYPE AND DATES COVERED Final Technical 8/1/98-7/31/00	
4. TITLE AND SUBTITLE "High Frequency Electromagnetic Propagation/ Scattering Codes"			5. FUNDING NUMBERS F49620-98-C-0051	
6. AUTHOR(S) Dr. Vladimir Rokhlin				
7. PERFORMING ORGANIZATION NAME(S) AND ADDRESS(ES) Fast Mathematical Algorithms & Hardware Corporation 1020 Sherman Avenue Hamden, CT 06514			8. PERFORMING ORGANIZATION REPORT NUMBER 2	
9. SPONSORING/MONITORING AGENCY NAME(S) AND ADDRESS(ES) USAF, AFMC Air Force Office of Scientific Research 801 N. Randolph Street, Room 732 Arlington, VA 22203-1977			10. SPONSORING/MONITORING AGENCY REPORT NUMBER	
11. SUPPLEMENTARY NOTES				
12a. DISTRIBUTION/AVAILABILITY STATEMENT "Distribution is unlimited, approved for public release"			12b. DISTRIBUTION CODE	
13. ABSTRACT (Maximum 200 words)  Whenever band-limited signals are measured or generated, different distributions of a fixed number of receivers and transducers lead to very different resolutions. A Closely related set of issues is encountered in the numerical solution of scattering problems: given a scatterer, one would like to find nodes on its surface leading to most efficient discretizations. In this project, we have constructed numerical algorithms for the determination of such discretizations in one, two, and three dimensions, and used the obtained results for the design of optimal phased antenna arrays. The work will be reported in four papers; copies of two of these papers are attached, and two are in preparation. Also, a preliminary patent application has been submitted.				
14. SUBJECT TERMS			15. NUMBER OF PAGES 27	
			16. PRICE CODE	
17. SECURITY CLASSIFICATION OF REPORT N/A	18. SECURITY CLASSIFICATION OF THIS PAGE N/A	19. SECURITY CLASSIFICATION OF ABSTRACT N/A	20. LIMITATION OF ABSTRACT N/A	

DTIC QUALITY INSPECTED 4

# 1 Report

Whenever band-limited signals are measured or generated, the locations of receivers or transducers have to be selected; it is well-known that different distributions lead to very different resolutions given a fixed number of receivers or transducers. A closely related set of issues is encountered in the numerical solution of scattering problems: given a scatterer, one would like to find nodes on its surface leading to most efficient discretizations.

During Phase I of the STTR project F49620-97-C-0052, we discovered (somewhat serendipitously) that whenever band-limited signals are to be discretized, measured, or generated, the construction of optimal (in a very strong sense) configurations of nodes is a tractable problem. When the nodes are to be located on a line or on a disk in  $\mathbb{R}^2$ , the solution is a fairly straightforward consequence of classical results obtained by Slepian and his collaborators more than 30 years ago. We have constructed the necessary numerical tools, which are quite efficient; the resulting discretizations are a dramatic improvement over the ones currently employed.

The basic analytical apparatus for dealing with band-limited functions are the classical Prolate Spheroidal Wave Functions (PSWFs) and their generalizations. We were surprised to discover that the existing numerical tools for the evaluation of PSWFs leave much to be desired, being based on the so-called Bouwkamp algorithm, constructed in 1941 (see [1]). Indeed, a fairly straightforward analysis shows that the Bouwkamp scheme is numerically unstable, except for small-scale problems; as a result, there appears to exist a belief (see, for example, [18]) that the numerical evaluation of PSWFs presents severe numerical difficulties. When we examined the Bouwkamp algorithm, we discovered that a very simple alteration eliminates the instability completely. In fact, the required change is no more than the use of standard modern numerical techniques for the solution of a fairly simple Sturm-Liouville problem. Needless to say, such techniques did not exist in 1941, when C. J. Bouwkamp developed his scheme. In the process of designing the requisite numerical tools, we discovered that the PSWFs possess an extremely

rich collection of analytical properties; we list some of these properties in [20], where we also describe interpolation and quadrature techniques for band-limited functions.

Next, we applied the constructed apparatus to the design of configurations of transducers for linear phased antenna arrays, and to antenna arrays on disks in the plane. This work is reported in [19] (attached). Construction of optimal configurations of nodes on more complicated regions requires additional mathematical apparatus; such apparatus has been largely designed, and largely implemented numerically. The paper describing it is in preparation. We are also investigating applications of the constructed numerical techniques in the design of receiver configurations in seismic data collection (as encountered in oil exploration and related areas), electronic beam steering, and several other environments. A preliminary patent application has been filed by the Office of Cooperative Research at Yale University.

## 2 Appendix: Antenna Patterns and Corresponding Optimal Element Distributions

### 2.1 Characteristics of an antenna pattern

Depending on the situation, the design of an antenna array attempts to optimize certain characteristics of the resulting far-field pattern, subject to certain constraints on the number, power, etc. of the elements. Since the principal purpose of this work is to develop a technique for the selection of the *locations* of the elements that approximate a user-specified pattern, we could use any reasonable far-field pattern to be approximated. In subsection 2.2, 2.3, we construct optimal element distributions for the so-called sector patterns and cosecant pattern, respectively; a detailed discussion of these (and several other) pattern cans be found, for example in [6].

We will say that the antenna pattern has the  $\epsilon$ -bandwidth  $b$  if

$$\int_{b \leq \|x\| \leq 1} |F(x)|^2 dx = \epsilon^2 \cdot \int_{-1}^1 |F(x)|^2 dx \quad (1)$$

in other words, the proportion of the energy radiated outside the  $\epsilon$ -beamwidth from the axis of the beam is equal to  $\epsilon$ . The *supergain* of an antenna is defined (see, for example, [22]), as the ratio

$$\frac{\int_{-\infty}^{+\infty} |F(x)|^2 dx}{\int_{-1}^1 |F(x)|^2 dx}. \quad (2)$$

The supergain (sometimes referred to as superdirectivity) measures the ratio of the energy associated with the total spectrum of the antenna to the energy in its visible spectrum; while detailed discussion of supergain and related issues is outside the scope of this report, we will observe that antenna arrays with large degrees of supergain would violate the uncertainty principle, and thus are physically impossible. Attempts to construct supergain antennae result in rapidly (exponentially) growing Ohmic losses, prohibitive accuracy requirements, extremely low bandwidth, etc. Thus, any potentially useful procedure for the design of antenna arrays has to limit the supergain of the resulting patterns.

## 2.2 Sector patterns

It is often desirable to construct antenna patterns that are as constant as possible within the main beam, and as small as possible outside it; in other words, ideally, the pattern would be defined by the formulae

$$F_b(x) = 1 \text{ for } |x| \leq b, \quad (3)$$

$$F_b(x) = 0 \text{ for } |x| > b, \quad (4)$$

with  $b$  a real number such that  $0 < b \leq k$ . Needless to say, the function  $F_b$  defined by the formulae (3), (4) is not band-limited, and some approximation has to be used. A standard procedure is to truncate the Fourier Transform of  $F_b$ , approximating it by the function  $\tilde{F}_b$  defined by the formula

$$\tilde{F}_b(x) = \int_{-1}^1 \frac{\sin(b \cdot t)}{t} \cdot e^{i \cdot k \cdot x \cdot t} \quad (5)$$

(see, for example, [21]). An important special case occurs when  $b = k$ , with (5) assuming the form

$$\tilde{F}_k(x) = \int_{-1}^1 \frac{\sin(k \cdot t)}{t} \cdot e^{i \cdot k \cdot x \cdot t}, \quad (6)$$

obviously, the latter expression is a band-limited approximation of the  $\delta$ -function. Another frequently encountered situation is that of  $b = k/2$ , so that (5) assumes the form

$$\tilde{F}_k(x) = \int_{-1}^1 \frac{\sin(\frac{k}{2} \cdot t)}{t} \cdot e^{i \cdot k \cdot x \cdot t}, \quad (7)$$

which is a band-limited approximation to the beam that is equal to 1 for  $-1/2 < x < 1/2$  and to zero elsewhere.

In Section 2.4 below, we demonstrate optimal element configurations that produce approximations to the patterns (6), (7) with  $k = 20\pi, 10\pi, 32.4676\pi$ .

**Remark 2.1** While (5) is by no means the only possible band-limited approximations to  $F_b$ , it is quite satisfactory in most cases, in addition to being simple. Furthermore, the principal purpose of this report is to describe a technique for the selection of *locations* of the nodes, given a pattern to be approximated. Thus, we ignore the issue of the optimal choice of  $F_b$ .

### 2.3 Cosecant patterns

Another standard far-field radiation pattern is the so-called cosecant pattern (see, for example, [8]). Given two real numbers  $0 < a < b < 1$ , the cosecant pattern  $F_{a,b}$  is defined by the formula

$$F_{a,b}(x) = \frac{1}{x} \quad (8)$$

for all  $x \in [a, b]$ , and

$$F_{a,b}(x) = 0 \quad (9)$$

for all  $x \in ([-1, 1] \setminus [a, b])$ . Again, the function  $F_{a,b}$  defined by the formulae (8), (9) is not band-limited. Before our scheme can be applied to  $F_{a,b}$ , the latter has to be approximated with a band-limited function; as discussed in Section 2.1 above, if such an approximation is to be useful as an antenna pattern, its supergain factor has to be controlled. Fortunately, a procedure for such an approximation has been in existence for more than 35 years (see, [7]); the algorithm of [7] is a modification of the least-squares approach *permitting the user to limit the supergain factor of the obtained pattern explicitly*. At the time, the utility of the scheme of [7] was limited by the (perceived) difficulty in the numerical evaluation of Prolate Spheroidal Wave functions; given the present state of numerical analysis, this difficulty is non-existent, and it is this author's impression that the insights of [7], [8] deserve more attention than they have been receiving.

## 2.4 Optimal distributions of elements

In this subsection, we briefly describe an algorithm for the construction of optimal (in the sense defined below) element configurations for the generation of antenna patterns, of which the patterns (4)-(6) are special cases. As will be seen, the procedure is in fact applicable to the design of element configurations for very general far-field patterns.

We start with observing that the far-field pattern  $F$  is an integral over the interval  $[-1, 1]$  of functions of the form

$$\sigma(u) \cdot e^{i \cdot k \cdot x \cdot u}, \quad (10)$$

with  $x = \cos(\theta)$  determined by the direction  $\theta$  in which the far-field is being evaluated. In other words, the problem of finding efficient antenna element distributions is equivalent to that of constructing quadrature formulae for functions of the form (10). In our numerical experiments, the techniques of [2]) (after some tuning) have always been successful in finding the Gaussian quadratures for integrals of the form (3); some of our results are presented in Section 3 below.

## 3 Numerical Examples

In this section, we present examples of optimal element distributions generating the patterns of the preceding Section; all of the results presented here have been obtained numerically. Antenna patterns we present are compared to the antenna patterns given by uniform source distributions; configurations of elements approximating these antenna patterns are compared to equispaced distributions of elements generating the same antenna patterns.

### 3.1 Optimal distributions of elements

In this section, we demonstrate the results of the application of the techniques of Section 2.4 of this report to the types of antenna patterns described in the Sections 2.2, 2.3.

In all cases, we choose the size of an antenna array and a pattern to be reproduced, and use the scheme outlined in Section 2.4 to design a distribution of antenna elements (both the locations and the intensities) located within the chosen array that reproduces the required pattern. For comparison, we also generate optimal (in the least squares sense) approximations to the desired pattern generated by equispaced elements located within the same array. Since the number of equispaced nodes required to obtain a reasonable approximation to the desired pattern is (in many cases) much greater than the number of optimally chosen nodes, for each example we demonstrate patterns generated by several such configurations. In this manner, the numbers of optimally chosen nodes necessary to obtain reasonable approximations to the desired patterns can be compared to the numbers of equispaced nodes required to obtain similar results.

#### 3.1.1 Sector patterns

**Example 3.1** *The first example we consider is of the pattern defined by the formula (7), with  $k = 62.8312$ , so that the size of the array is 20 wavelengths.*

*In Figure 5, we display an approximation to the pattern obtained with 19 elements, overlaid with the exact pattern; the locations of the elements are displayed in Figure 5a; the relative error of the obtained approximation is 5.01%.*

Similarly, in Figure 5g, we display the approximation to the pattern obtained with 21 elements, overlaid with the exact pattern; the relative error of the obtained approximation is 0.443%; in Figure 5h, we display the the approximation obtained with 17 elements. In the latter case, the relative error of the obtained approximation is 6.43%; Figure 5i depicts the 17-node distribution producing the approximation illustrated in Figure 5h. Finally, Figure 5j contains a graph of the values of the sources located at the 17 nodes depicted in Figure 5i and generating the pattern shown in Figure 5h.

For comparison, the optimal approximation obtained with 19, 24, 29, 31, and 34 equispaced elements are displayed in Figures 5b, 5c, 5d, 5e, 5f, respectively; these are also overlaid with the exact pattern.

**Example 3.2** Our second example is identical to the first one, with the exception that  $k = 31.416$ , so that the size of the array is 10 wavelengths.

In Figure 6, we display an approximation to the pattern obtained with 9 elements, overlaid with the exact pattern; the locations of the elements are displayed in Figure 6a; the relative error of the obtained approximation is 11.2%.

Similarly, in Figure 6f, we display the approximation to the pattern obtained with 11 elements, overlaid with the exact pattern; the relative error of the obtained approximation is 0.600%.

For comparison, the optimal approximation obtained with 9, 14, 16, and 18 equispaced elements are displayed in Figures 6b, 6c, 6d, 5e, respectively; these are also overlaid with the exact pattern.

**Example 3.3** Our third example is identical to the preceding two, with the exception that  $k = 102$ , so that the size of the array is about 32.45 wavelengths.

In Figure 7a, we display an approximation to the pattern obtained with 23 optimally distributed elements, overlaid with the exact pattern and with the pattern obtained with 23 equispaced elements.

The relative error of the obtained approximation is 5.4%; needless to say, the error of the approximation obtained with the equispaced nodes is more than 70%. As can be seen

from Figure 7c, the actual size of the obtained 23-element array is about 21 wavelengths; in other words, in order to obtain this precision, the array needs to be about 2/3 of the nominal (maximum permitted) length.

In Figure 7b, we display the approximation to the pattern obtained with 42 and 48 elements, overlaid with the exact pattern.

It is worth noting that with 33 optimally distributed elements, the pattern is approximated to the precision 0.12%; we do not display the obtained pattern since it is visually indistinguishable from the pattern being approximated.

**Example 3.4** Our final example is somewhat different from the preceding ones, in that instead of approximating a sector pattern, we approximate a cosecant pattern (see (8), (9) in Subsection 2.3 above).

In this example, we set

$$a = \sin(15^\circ), \tag{11}$$

$$b = \sin(75^\circ), \tag{12}$$

and use the procedure of [7] to approximate  $F_{a,b}$  with a band-limited function. The band-limit has been more or less arbitrarily set to 110, resulting in an antenna array about 35 wavelengths in size, and the supergain factor of the approximation was set to 1.1.

In Figure 8a, we display an approximation to the pattern obtained with 53 optimally distributed elements, overlaid with the exact bandlimited pattern and with the pattern obtained with 53 equispaced elements.

The relative error of the obtained approximation is 1.79%; the error of the approximation obtained with the equispaced nodes is about 42%.

In Figure 8b, we display the approximation to the pattern obtained with 47 optimally distributed elements, overlaid with the exact pattern; the purpose of this final figure is to demonstrate the behavior of the scheme when the number of elements is insufficient (i.e. when the array is underresolved).

It is worth noting that it takes about 70 equispaced nodes to obtain the resolution obtained with 47 optimally chosen ones.

The following observations can be made from Figures 5 - 8b, and from the more detailed numerical experiments performed by the author.

1. In order to obtain reasonable precision, the scheme requires about 1 point per wavelength in the antenna array; this is more or less independent from the structure of the beam *as long as the pattern is symmetric about the point  $x = 0$* . This fact is observed numerically, even for modest numbers of nodes; for large-scale arrays, this statement (interpreted asymptotically) can be proved rigorously. For certain beam structures, the required number of nodes is even less (see Example 3.3). The reasons for these additional savings are subtle, and have to do with the fact that the continuous source distribution generating the pattern is relatively small on a large part of the antenna array; the algorithm of [2] takes advantage of this fact to reduce the number of nodes. When the beam is not symmetric about  $x = 0$ , the number of elements required does depend on the structure of the pattern, and the dependence is fairly complicated. Generally, the improvement for non-symmetric beams is less than that for the symmetric ones.
2. The qualitative behavior of the scheme is similar to that of the Gaussian quadratures in that it displays no convergence at all until a certain minimum number of nodes is achieved; after that, the convergence is very fast. This behavior is not surprising, since the scheme *is* based on a Generalized Gaussian quadrature.
3. For the sector pattern with the sector  $[-1/2, 1/2]$ , the scheme reduces the required number of nodes by a factor of about 1.5 for small-scale problems, and roughly by a factor of 2 for large-scale ones; again, for large-scale problems, an asymptotic version of this statement can be proven rigorously.
4. For the cosecant pattern with the parameters specified by (11), (12), the number of nodes required is reduced by approximately a factor of 1.4. As the sidelobe level is reduced, the improvement obtained by going from the equispaced discretization to the optimal one increases rapidly.
5. An examination of Figures 5a, 6a shows that while the optimal nodes are by no means uniform, they display no clustering behavior.

6. An examination of Figure 5j shows that the intensities of individual elements do not become large; this is confirmed by the more extensive numerical experiments performed by the author.

7. The combination of the preceding two paragraphs (combined with additional numerical experiments and analysis) provide evidence that configurations of this type should pose no supergain problems.

## 4 Generalizations

The results described above admit radical generalizations in several directions; several such directions are discussed below,

**1. Conformal one-dimensional arrays.** The extension of the techniques of this report to one-dimensional arrays located on curves in  $R^3$  is completely straightforward, involving only a modest increase of the CPU time requirements of the procedure. Improvement in the number of nodes required to produce a prescribed pattern is similar to that in the case of a linear array.

**2. Planar two-dimensional arrays.** A straightforward generalization of the results of Sections 2, 3, is to rectangular planar arrays. Here, a tensor product quadrature can be constructed from the quadratures of Sections 2, 3, possessing all of the desirable properties of the latter. Obviously, the advantage in the number of transducers is squared, so that (for example) replacing 50 nodes in each of the two directions by 23 nodes (see Example 3.3 above) will lead to a factor of  $(50/23)^2 \sim 4.7$  savings in the number of elements.

The theory of Section 2 has been extended for disk-shaped arrays, via (*inter alia*) the techniques developed in [12]. The improvement in the number of nodes is comparable to that obtained in the rectangular geometry, and the CPU time requirements do not differ appreciably from those in the case of linear one-dimensional arrays.

The extension of the theory to more general geometries in the plane is in progress. At the present time, our only numerical experiments have been with arrays on triangles; the results are encouraging, but the CPU time requirements of the algorithms are excessive (we have only been able to design triangular arrays about 6 wavelengths in size). We are now in the process of constructing a more efficient numerical procedure for such computations.

**3. Conformal two-dimensional arrays.** The only environment in which we have a satisfactory theory is when the array is located on a surface of revolution; even in this environment, no experiments have been performed. We have not investigated more general conformal two-dimensional arrays in sufficient detail.

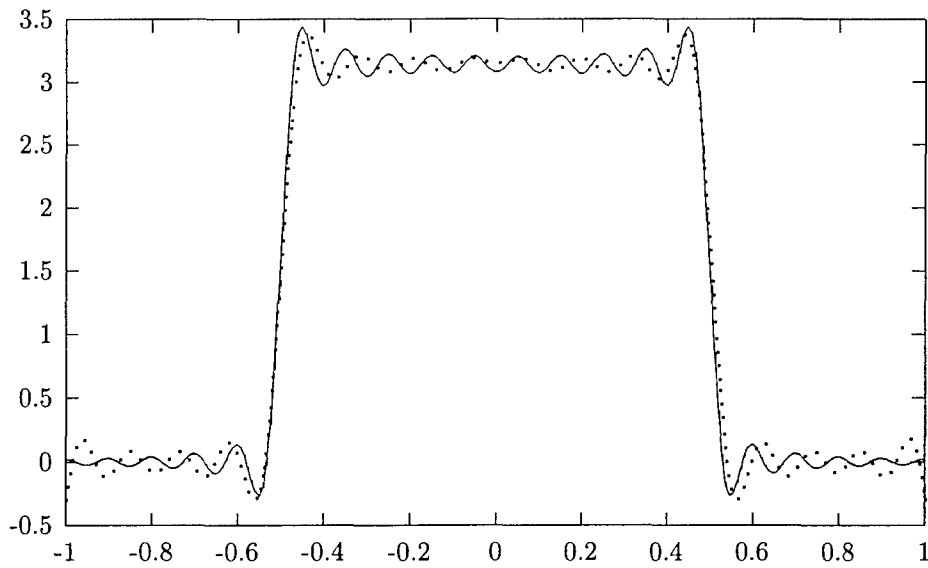


Figure 5: The pattern created by the 19 optimal elements, depicted in Figure 5a as described in Example 3.1

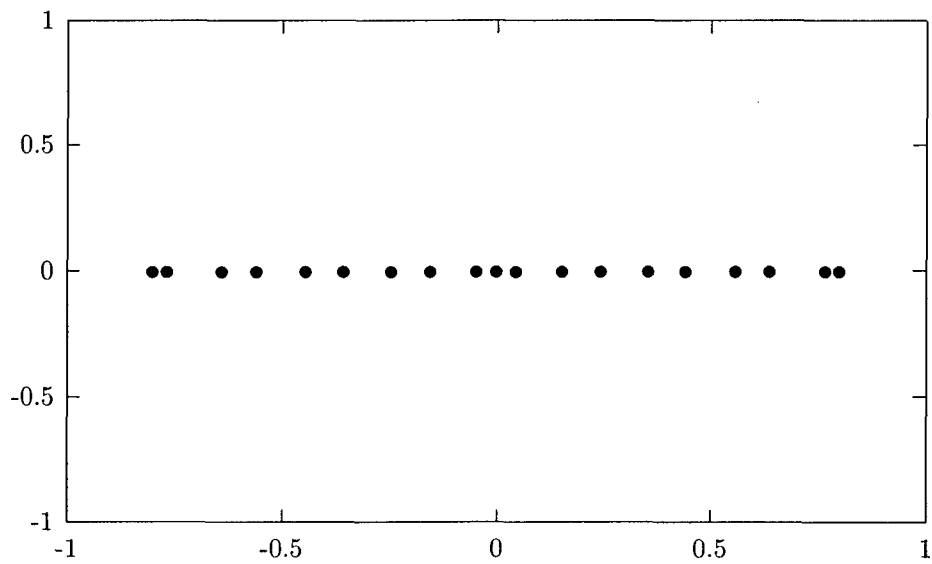


Figure 5a: The distribution of elements creating the pattern depicted in Figure 5, as described in Example 3.1

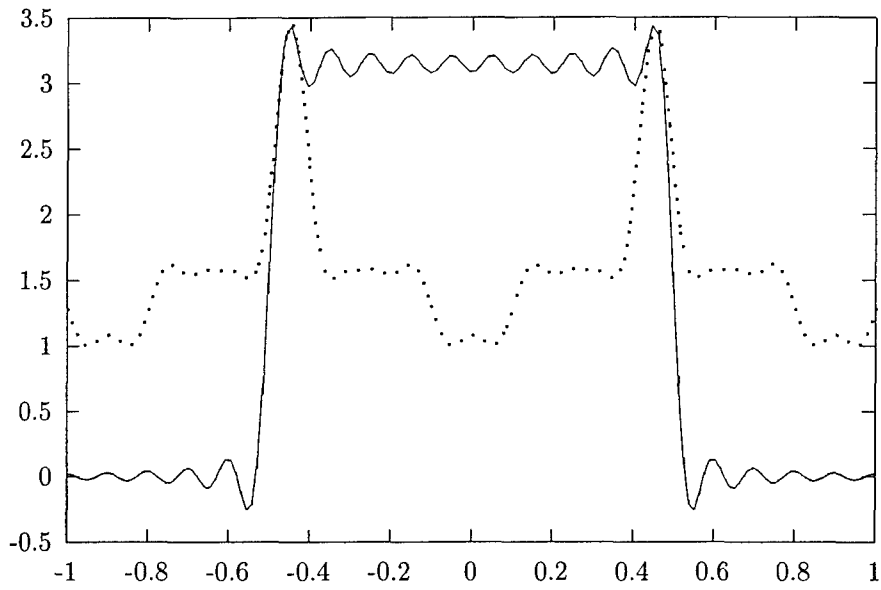


Figure 5b: The optimal approximation to the sector pattern generated by 19 equispaced nodes, as described in Example 3.1

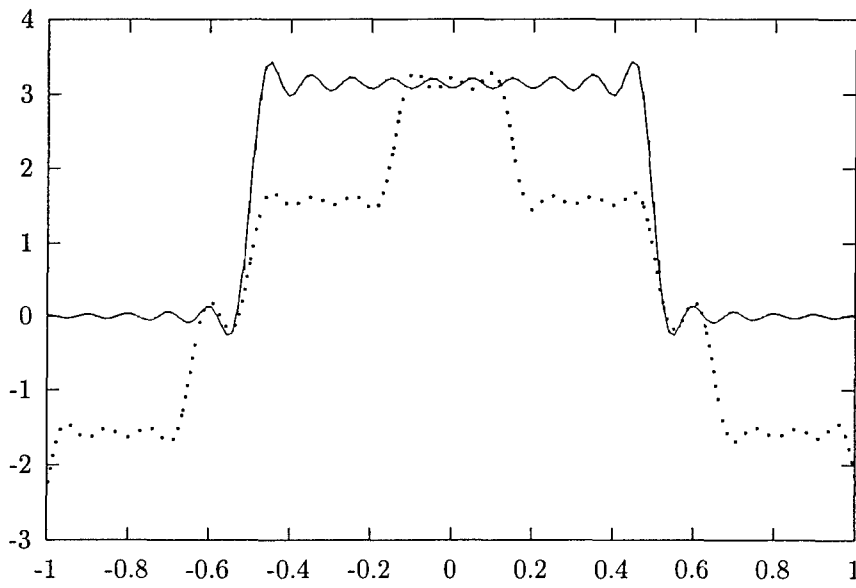


Figure 5c: The optimal approximation to the sector pattern generated by 24 equispaced nodes, as described in Example 3.1

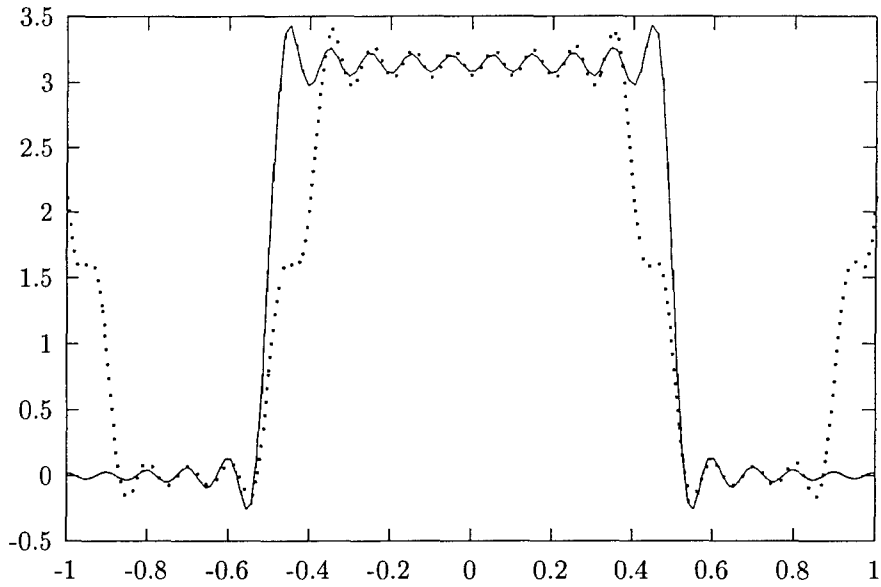


Figure 5d: The optimal approximation to the sector pattern generated by 29 equispaced nodes, as described in Example 3.1

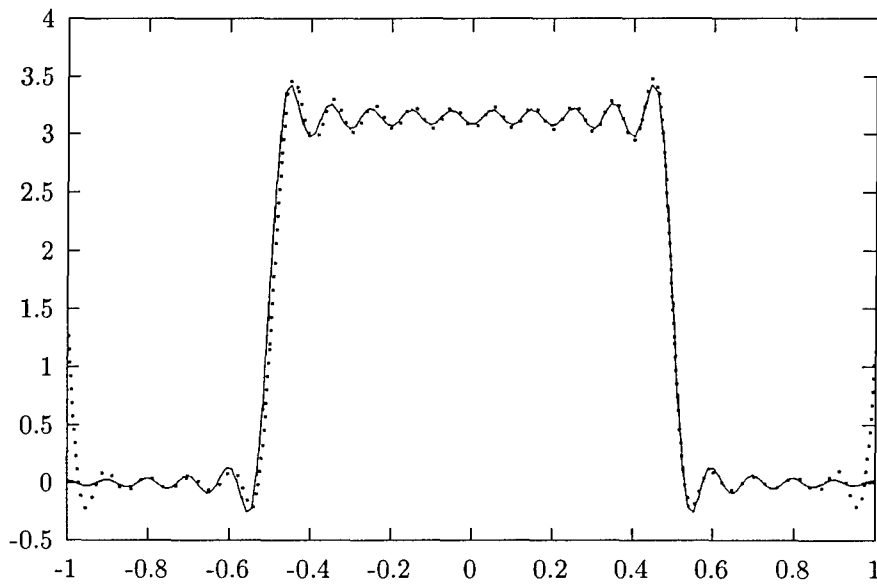


Figure 5e: The optimal approximation to the sector pattern generated by 31 equispaced nodes, as described in Example 3.1

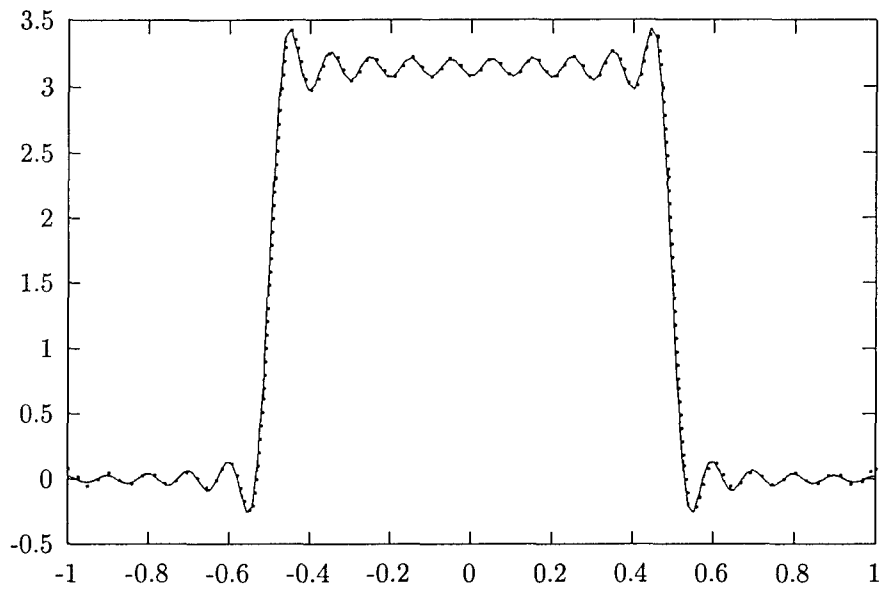


Figure 5f: The optimal approximation to the sector pattern generated by 34 equispaced nodes, as described in Example 3.1

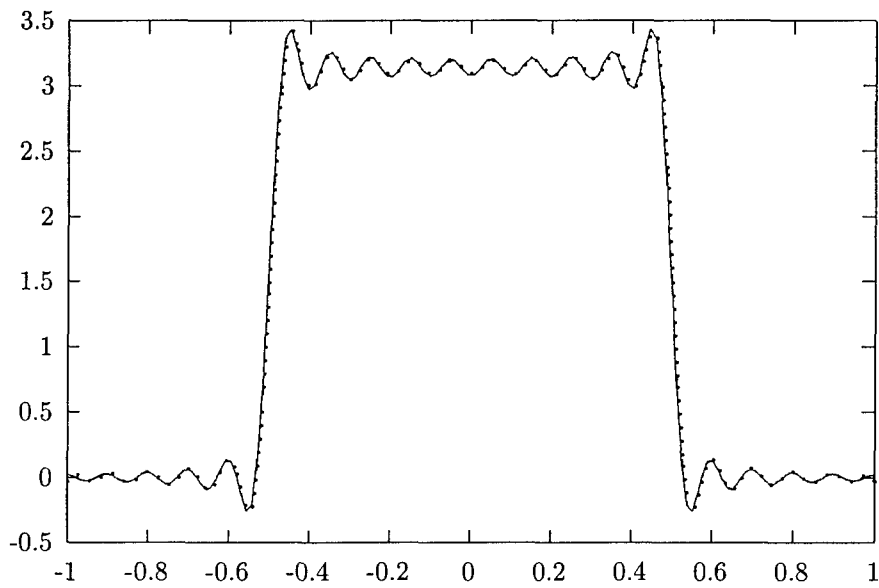


Figure 5g: The optimal approximation to the sector pattern generated by 21 optimal nodes, as described in Example 3.1

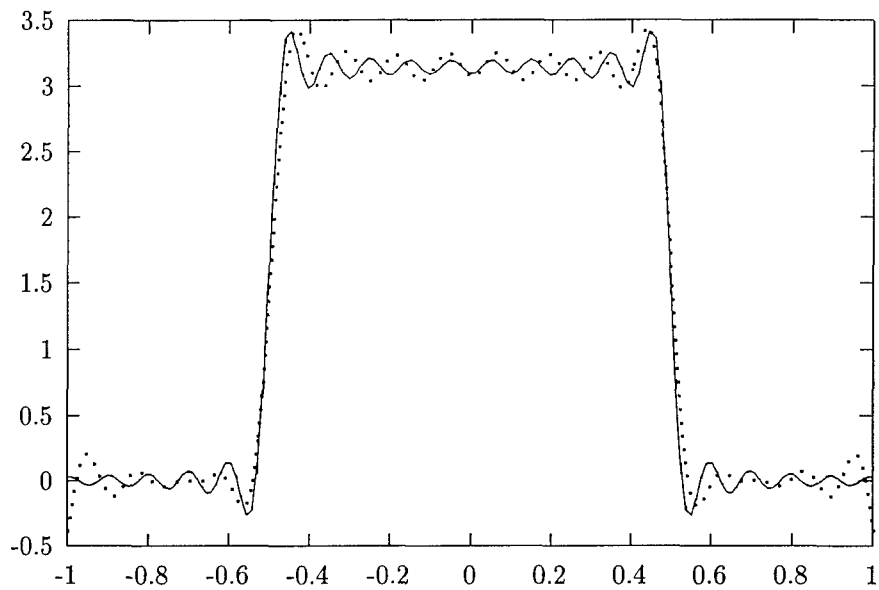


Figure 5h: The optimal approximation to the sector pattern generated by 17 optimal nodes, as described in Example 3.1

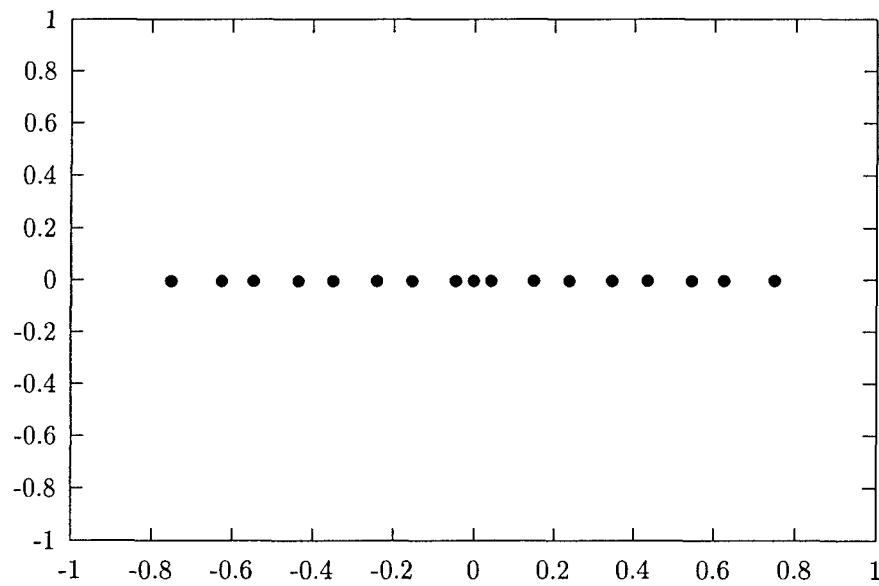


Figure 5i: The distribution of 17 elements creating the pattern depicted in Figure 5h, as described in Example 3.1

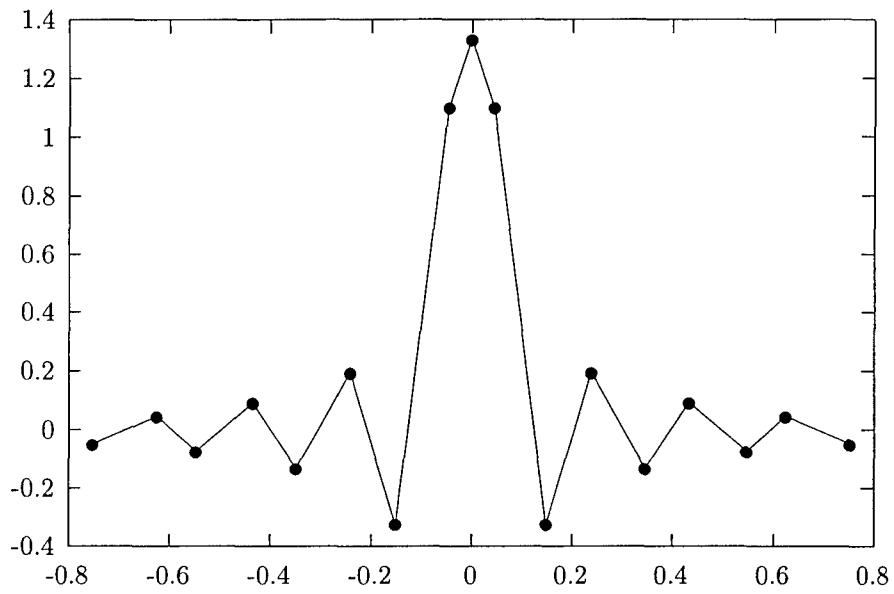


Figure 5j: The values of the sources located at the nodes depicted in Figure 5i and generating the pattern depicted in Figure 5h, as described in Example 3.1

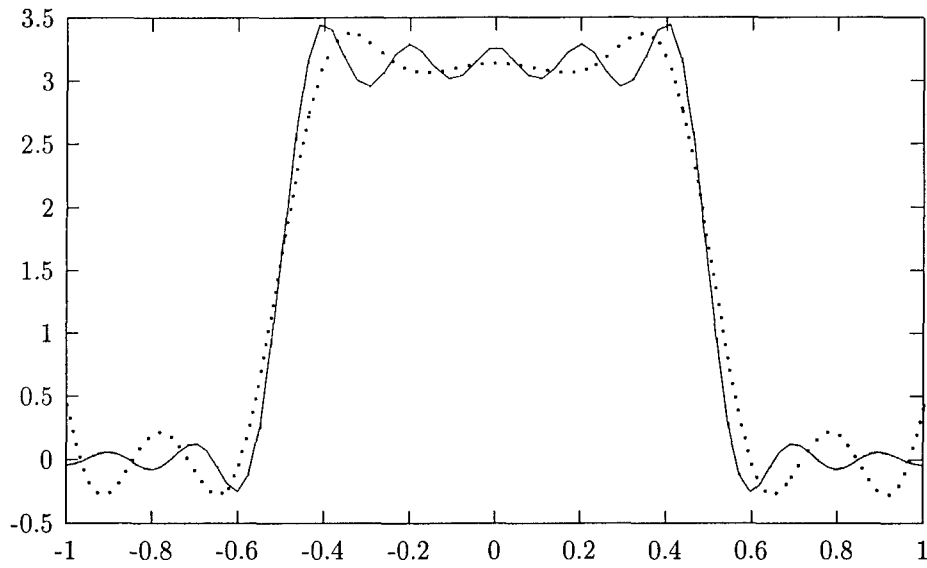


Figure 6: The pattern created by the 9 optimal elements, depicted in Figure 6a as described in Example 3.2

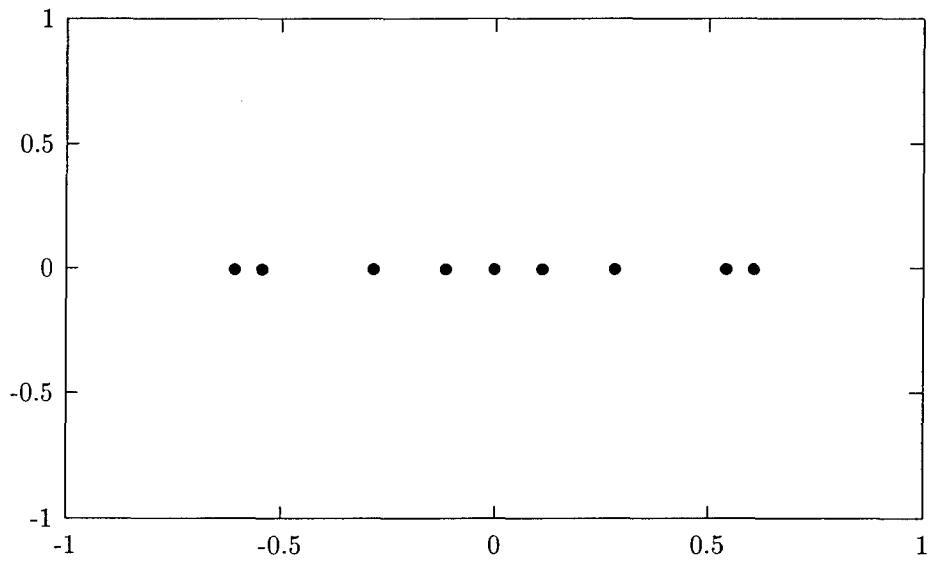


Figure 6a: The distribution of elements creating the pattern depicted in Figure 6, as described in Example 3.2

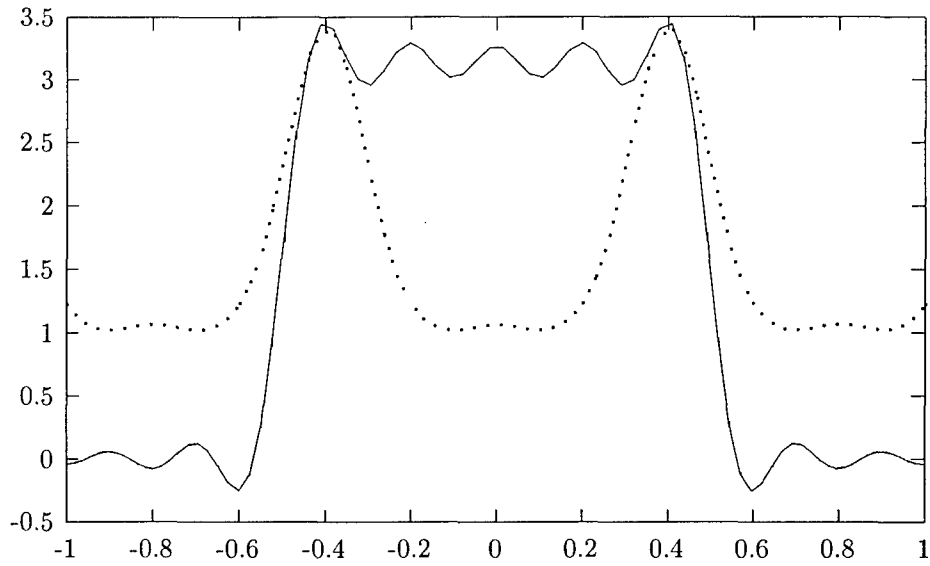


Figure 6b: The optimal approximation to the sector pattern generated by 9 equispaced nodes, as described in Example 3.2

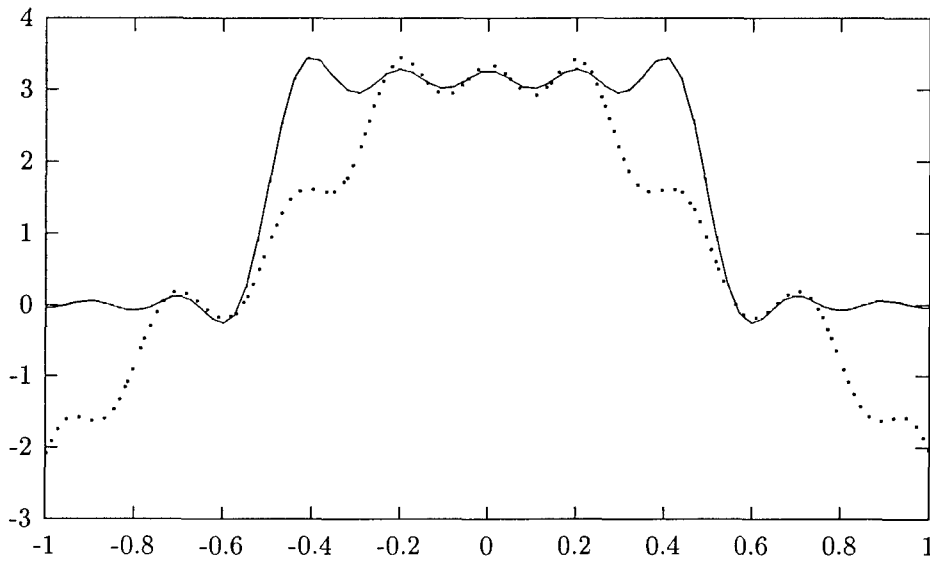


Figure 6c: The optimal approximation to the sector pattern generated by 14 equispaced nodes, as described in Example 3.2

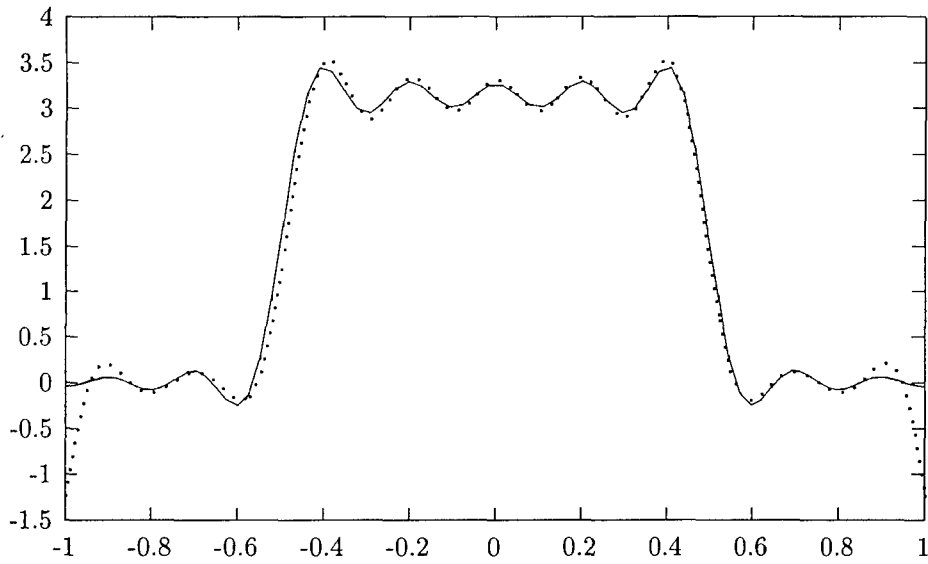


Figure 6d: The optimal approximation to the sector pattern generated by 16 equispaced nodes, as described in Example 3.2

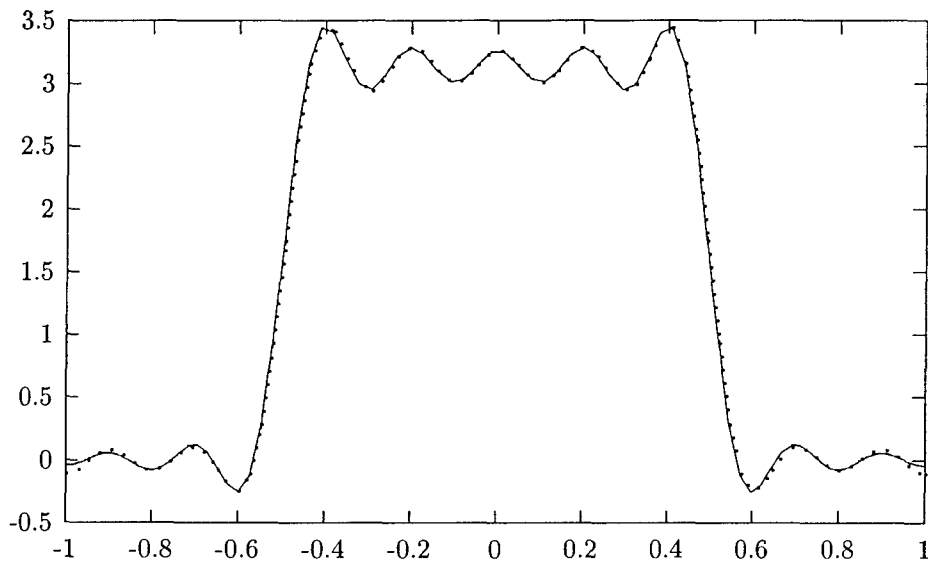


Figure 6e: The optimal approximation to the sector pattern generated by 18 equispaced nodes, as described in Example 3.2

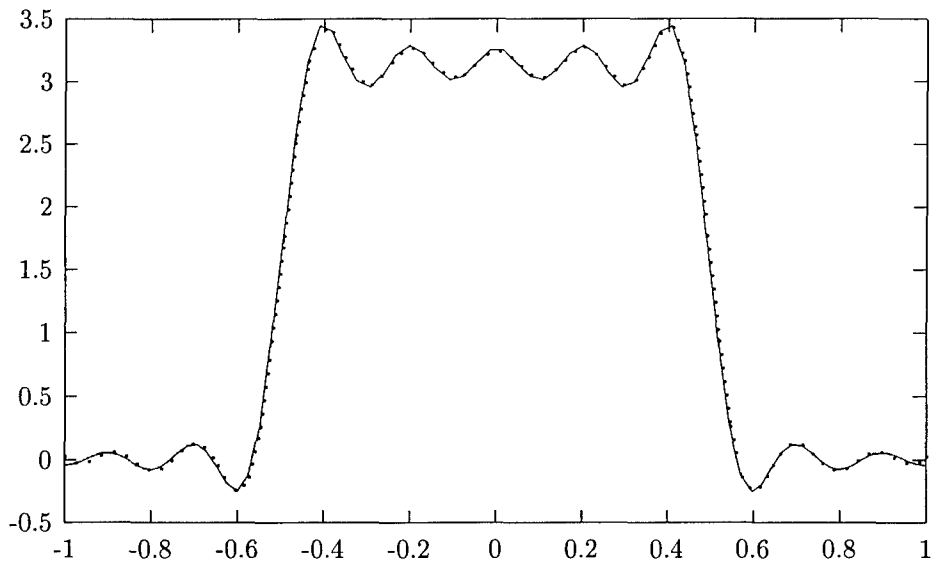


Figure 6f: The pattern created by the 11 optimal elements, in Example 3.2

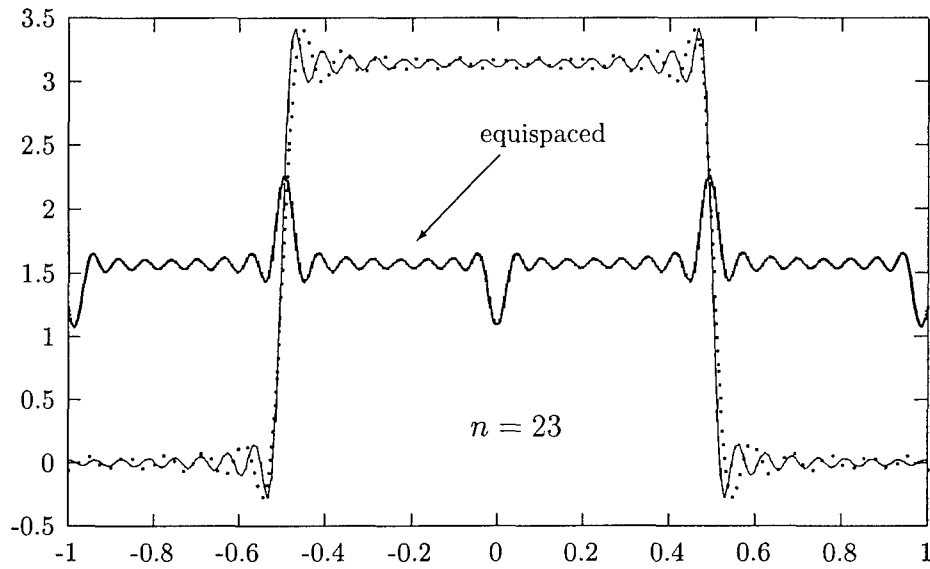


Figure 7a: The approximation to the sector pattern generated by 23 optimal elements, vs. optimal approximation by 23 equispaced nodes, as described in Example 3.3

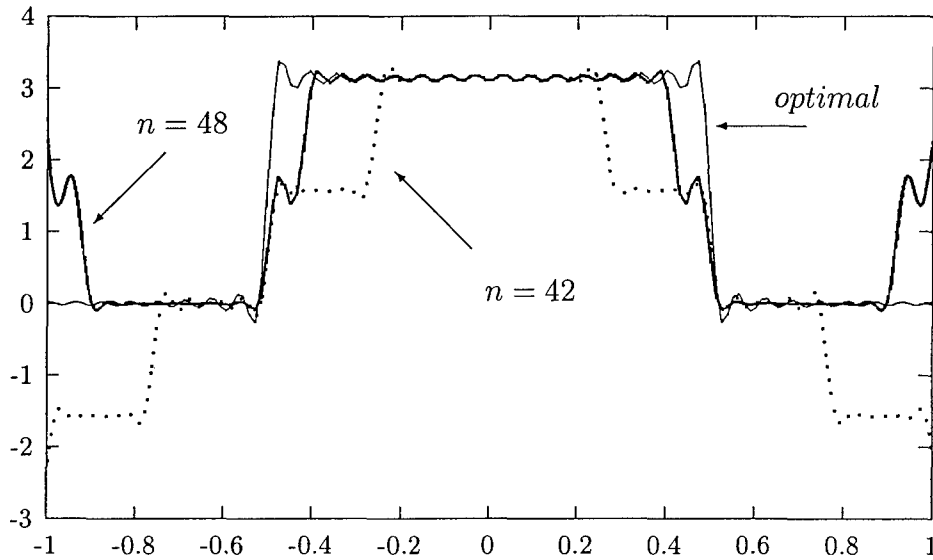


Figure 7b: The optimal approximations to the sector pattern generated by 42 and 48 equispaced nodes, as described in Example 3.3

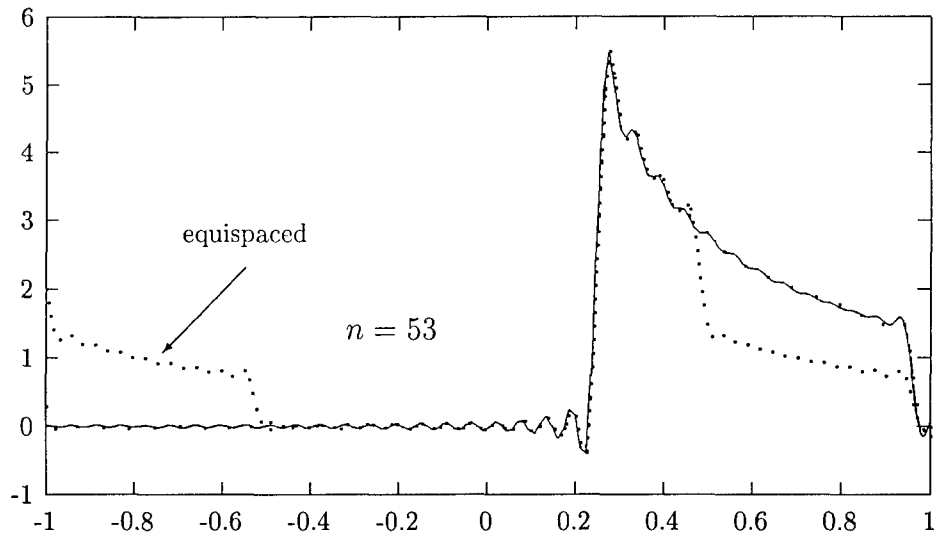


Figure 8a: The approximation to the cosecant pattern generated by 53 optimal elements, vs. optimal approximation by 53 equispaced nodes, as described in Example 3.4

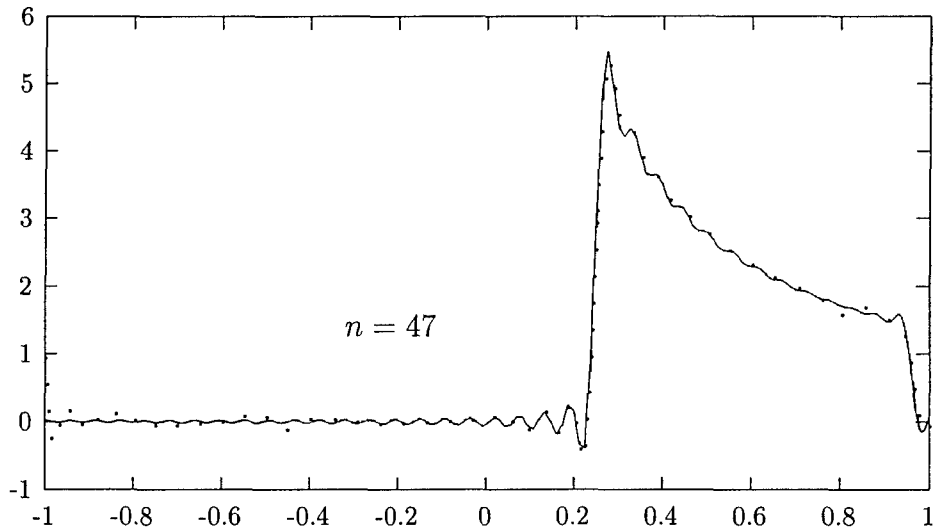


Figure 8a: The approximation to the cosecant pattern generated by 47 optimal elements, as described in Example 3.4

## References

- [1] C.J. Bouwkamp, *Diffraction Through a Circular Aperture; Acoustic Radiation of a Freely Vibrating Circular Plate*, Thesis Groningen 1941.
- [2] H. Cheng, N. Yarvin, V. Rokhlin, *Non-Linear Optimization, Quadrature, and Interpolation*, Yale University Technical Report, YALEU/DCS/RR-1169, 1998, to appear in the SIAM Journal of Non-linear Optimization.
- [3] H.J. Landau, H. Widom, *Eigenvalue Distribution of Time and Frequency Limiting*, Journal of Mathematical Analysis and Applications, 77, 469-481 (1980).
- [4] Y.T. Lo, S.W. Lee, editors, *Antenna Handbook, Theory, Applications, and Design*, Van Nostrand Reinhold Company, 1988.
- [5] J. MA, V. ROKHLIN, AND S. WANDZURA, *Generalized Gaussian Quadratures For Systems of Arbitrary Functions*, SIAM Journal of Numerical Analysis, v. 33, No. 3, pp. 971-996, 1996.
- [6] R.J. Mailloux, *Phased Array Antenna Handbook*, Artech House, 1994.
- [7] D. Rhodes, *The optimum line source for the best mean-square approximation to a given radiation pattern*, IEEE Trans. AP, July 1963.
- [8] D. Rhodes, *Synthesis of planar antenna sources*, Clarendon Press, Oxford, 1974.
- [9] D. Slepian, H.O. Pollak, *Prolate Spheroidal Wave Functions, Fourier Analysis, and Uncertainty - I*, The Bell System Technical Journal, January 1961.
- [10] H.J. Landau, H.O. Pollak, *Prolate Spheroidal Wave Functions, Fourier Analysis, and Uncertainty - II*, The Bell System Technical Journal, January 1961.
- [11] H.J. Landau, H.O. Pollak, *Prolate Spheroidal Wave Functions, Fourier Analysis, and Uncertainty - III: The Dimension of Space of Essentially Time- and Band-Limited Signals*, The Bell System Technical Journal, July 1962.

- [12] D. Slepian, *Prolate Spheroidal Wave Functions, Fourier Analysis, and Uncertainty - IV: Extensions to Many Dimensions, Generalized Prolate Spheroidal Wave Functions*, The Bell System Technical Journal, November 1964.
- [13] D. Slepian, *Prolate Spheroidal Wave Functions, Fourier Analysis, and Uncertainty - V: The Discrete Case*, The Bell System Technical Journal, May-June 1978.
- [14] D. Slepian, *Some Comments on Fourier Analysis, Uncertainty, and Modeling* SIAM Review, V. 25, No. 3, July 1983.
- [15] F. A. Grünbaum, *Toeplitz Matrices Commuting With Tridiagonal Matrices*, J. Linear Alg. and Appl., 40, (1981).
- [16] F. A. Grünbaum, *Eigenvectors of a Toeplitz Matrix: Discrete Version of the Prolate Spheroidal Wave Functions*, SIAM J. Alg. Disc. Meth., 2(1981).
- [17] F. A. Grünbaum, L. Longhi, M. Perlstadt, *Differential Operators Commuting with Finite Convolution Integral Operators: Some Non-Abelian Examples*, SIAM J. Appl. Math. 42(1982).
- [18] D.J. Brown, R.M. Stringfield, *Iterative Methods Applied to Matrix Equations Found in Calculating Spheroidal Functions*, Journal of Computational Physics, 159, 329-343 (2000).
- [19] V. Rokhlin, *A Procedure for the Design of Apparata for the Measurement and Generation of Band-Limited Signals*, Yale University Technical Report, YALEU/DCS/RR-1196, 2000.
- [20] H. Xiao, V. Rokhlin, N. Yarvin, *Prolate Spheroidal Wave Functions, Quadratures, and Interpolation*, Yale University Technical Report, YALEU/DCS/RR-1199, 2000.
- [21] W.L. Stutzman, G.A. Thiele, *Antenna Theory and Design*, Wiley, 1998.

- [22] T.T. Taylor, *Design of Line-Source Antennas for Narrow Beamwidth and Low Side Lobes*, IEEE Trans. on Antennas and Propagation, AP-3, pp. 16-28, 1955.
- [23] N. Yarvin and V. Rokhlin, *Generalized Gaussian Quadratures and Singular Value Decompositions of Integral Operators*, SIAM Journal of Scientific Computing, Vol. 20, No. 2, pp. 699-718 (1998).

**Personnel Supported:**

**F.M.A.& H. Corporation**

Vladimir Rokhlin, Ph.D., Vice President of FMA&H

Ronald Coifman, Ph. D., President of FMA&H

Frank Geshwind, Ph.D.

Hongwei Cheng, Ph.D.

Tomasz Hrycak, Ph.D.

Yu Chen, Ph.D.

**Yale University**

Norman Yarvin, Ph.D.

Petter Kolm, Ph.D.

Hong Xiao, Ph.D.



A Procedure for the Design of Apparata for the  
Measurement and Generation of Band-Limited Signals

V. Rokhlin  
Research Report YALEU/DCS/RR-1196  
March 29, 2000

YALE UNIVERSITY  
DEPARTMENT OF COMPUTER SCIENCE

Whenever physical signals are measured or generated, the locations of receivers or transducers have to be selected. Most of the time, this appears to be done on an ad hoc basis. For example, when a string of geophones is used in the measurements of seismic data in oil exploration, the receivers are located at equispaced points on an interval. When phased array antennae are constructed, their shapes are determined by certain aperture considerations; round and rectangular shapes are common. When antenna beams are steered electronically, it is done by changing the phases (and sometimes, the amplitudes) of the transducers. Again, these transducers are located in a region of predetermined geometry, and their actual locations within that geometry are chosen via some heuristic procedure. In all these (and many other) cases, the signals being received or generated are *band-limited*. Optimal representation of such signals has been studied in detail by Slepian et. al. more than 30 years ago, and some of the obtained results were applied by D. Rhodes to the design of antenna patterns; further development of this line of research appears to have been hindered by the absence at the time of necessary numerical tools. We combine these classical results with the recently developed apparatus of Generalized Gaussian Quadratures to construct optimal nodes for the measurement and generation of band-limited signals. In this report, we describe the procedure based on these techniques for the design of such receiver (and transducer) configurations in a variety of environments.

## A Procedure for the Design of Apparata for the Measurement and Generation of Band-Limited Signals

V. Rokhlin  
Research Report YALEU/DCS/RR-1196  
March 29, 2000

The author was supported in part by DARPA/AFOSR under Contract F49620/97/1/0011, in part by ONR under Grant N00014-96-1-0188, and in part by AFOSR under STTR number F49620/98/C/0051

Approved for public release: distribution is unlimited

**Keywords:** *Band-limited Signals, Antenna Arrays, Beam-forming*

# 1 Introduction

When measurements are performed, it often happens that the signal to be measured is well approximated by linear combinations of oscillatory exponentials, i.e. functions of the form

$$\sum_{j=1}^n \alpha_j \cdot e^{i \cdot \lambda_j \cdot x} \tag{1}$$

in one dimension, of the form

$$\sum_{j=1}^n \alpha_j \cdot e^{i \cdot (\lambda_j \cdot x + \mu_j \cdot y)} \tag{2}$$

in two dimensions, and of the form

$$\sum_{j=1}^n \alpha_j \cdot e^{i \cdot (\lambda_j \cdot x + \mu_j \cdot y + \nu_j \cdot z)} \tag{3}$$

in three dimensions. In most cases, the signal is band-limited, i.e. there exist such real positive  $a$  that all  $1 \leq j \leq n$ ,

$$|\lambda_j| \leq a \tag{4}$$

in one dimension,

$$\lambda_j^2 + \mu_j^2 \leq a^2 \tag{5}$$

in two dimensions, and

$$\lambda_j^2 + \mu_j^2 + \nu_j^2 \leq a^2, \tag{6}$$

in three dimensions.

As is well-known, most measurements of electromagnetic and acoustic data (especially at reasonably high frequencies) are of this form. Examples of such situations include geophone and hydrophone strings in geophysics, phased array antennae in radar

systems, multiple transceivers in ultrasound imaging, and a number of other applications in astrophysics, medical imaging, non-destructive testing, etc.

In this report, we describe a procedure for determining the optimal distribution of sources and receivers that maximizes accuracy and resolution in measuring band-limited data given a fixed number of receivers. Alternatively, the procedure can be used to determine the optimal distribution of receivers that will minimize their number given specified accuracy and resolution. While the techniques described in this note are fairly general, we describe them in detail in the case of linear antenna arrays; the changes needed to generalize the approach to other cases are summarized in Section 6.

**Remark 1.1** One of principal issues in the design of antenna arrays is the treatment (or avoidance) of the so-called supergain (or superdirectivity). Supergain is the condition that occurs when an antenna design is attempted that is prohibited (or nearly prohibited) by the Heisenberg principle; technically, it occurs in the form of very closely spaced elements operating out of phase, and leads to prohibitive Ohmic losses in transmitting antennae, loss of sensitivity in receiving ones, etc. Since the purpose of this note is to introduce techniques for selecting the locations of elements *for a prescribed antenna pattern*, we avoid the issue of choosing the antenna pattern altogether. Instead, we observe design optimal element distributions for several standard far-field patterns (see Section 5.1), and we observe that the scheme for choosing optimal distributions of elements is virtually independent of the patterns being approximated.

Technically, the approach taken here is to observe that designing an antenna array can be viewed as constructing a quadrature formula for the integration of certain special classes of functions. Using recently developed techniques for the construction of so-called Generalized Gaussian Quadratures, we obtain both nodes and weights that are optimal (in a very strong sense) for the required antenna pattern.

The structure of this note is as follows. In Section 2, we summarize some of the mathematical apparatus to be used: Chebychev Systems, Generalized Gaussian Quadratures,

etc. In Section 3, we recapitulate some of the standard antenna theory, primarily to introduce the necessary notation. In Section 4, element distributions given a specific antenna pattern. In Section 5, we illustrate our approach with several numerical examples, and Section 6 contains a discussion of the generality of the schemes presented.

## 2 Analytical Preliminaries

In this section, we summarize several known facts about classical Special functions. All of these facts can be found in the literature; detailed references are given in the text.

### 2.1 Chebyshev systems

**Definition 2.1** *A sequence of functions  $\phi_1, \dots, \phi_n$  will be referred to as a Chebyshev system on the interval  $[a, b]$  if each of them is continuous and the determinant*

$$\begin{vmatrix} \phi_1(x_1) & \cdots & \phi_1(x_n) \\ \vdots & & \vdots \\ \phi_n(x_1) & \cdots & \phi_n(x_n) \end{vmatrix} \quad (7)$$

*is nonzero for any sequence of points  $x_1, \dots, x_n$  such that  $a \leq x_1 < x_2 < \dots < x_n \leq b$ .*

An alternate definition of a Chebyshev system is that any linear combination of the functions with nonzero coefficients must have no more than  $n$  zeros.

Examples of Chebyshev and extended Chebyshev systems include the following (additional examples can be found in [8]).

**Example 2.1** *The powers  $1, x, x^2, \dots, x^n$  form an extended Chebyshev system on the interval  $(-\infty, \infty)$ .*

**Example 2.2** *The exponentials  $e^{-\lambda_1 x}, e^{-\lambda_2 x}, \dots, e^{-\lambda_n x}$  form an extended Chebyshev system for any  $\lambda_1, \dots, \lambda_n > 0$  on the interval  $[0, \infty)$ .*

**Example 2.3** *The functions  $1, \cos x, \sin x, \cos 2x, \sin 2x, \dots, \cos nx, \sin nx$  form a Chebyshev system on the interval  $[0, 2\pi]$ .*

**Example 2.4** Suppose that  $c > 0$  is a real number,  $w$  is a positive function  $[-1, 1] \rightarrow \mathbb{R}$  such that  $w \in C^1[-1, 1]$  and  $w(-x) = w(x)$  for all  $x \in [-1, 1]$ ,  $n$  is a natural number, and the operators  $P, Q : L^2[-1, 1] \rightarrow L^2[-1, 1]$  are defined by the formulae

$$P(\phi)(x) = \int_{-1}^1 w(t) \cdot e^{i \cdot c \cdot x \cdot t} \cdot \phi(t) dt \quad (8)$$

$$Q = P^* \circ P. \quad (9)$$

Suppose further that  $\phi_1, \phi_2, \dots$  are the eigenfunctions of  $Q$ ,  $\lambda_1, \lambda_2, \dots$  are the corresponding eigenvalues, and  $\lambda_1 > \lambda_2 > \lambda_3 \dots$ . Then all eigenfunctions of  $Q$  (also known as the right singular vectors of  $P$ ) can be chosen to be real. Furthermore, the functions  $\phi_1, \phi_2, \dots, \phi_n$  constitute a Chebychev system on the interval  $[-1, 1]$ .

## 2.2 Generalized Gaussian quadratures

A quadrature rule is an expression of the form

$$\sum_{j=1}^n w_j \cdot \phi(x_j), \quad (10)$$

where the points  $x_j \in \mathbb{R}$  and coefficients  $w_j \in \mathbb{R}$  are referred to as the nodes and weights of the quadrature, respectively. They serve as approximations to integrals of the form

$$\int_a^b \phi(x) \cdot \omega(x) dx \quad (11)$$

with  $\omega$  is an integrable non-negative function.

Quadratures are typically chosen so that the quadrature (10) is equal to the desired integral (11) for some set of functions, commonly polynomials of some fixed order. Of these, the classical Gaussian quadrature rules consist of  $n$  nodes and integrate polynomials of order  $2n - 1$  exactly. In [13], the notion of a Gaussian quadrature was generalized as follows:

**Definition 2.2** A quadrature formula will be referred to as Gaussian with respect to a set of  $2n$  functions  $\phi_1, \dots, \phi_{2n} : [a, b] \rightarrow \mathbb{R}$  and a weight function  $\omega : [a, b] \rightarrow \mathbb{R}^+$ , if it consists of  $n$  weights and nodes, and integrates the functions  $\phi_i$  exactly with the weight function  $\omega$  for all  $i = 1, \dots, 2n$ . The weights and nodes of a Gaussian quadrature will be referred to as Gaussian weights and nodes respectively.

The following theorem appears to be due to Markov [15, 16]; proofs of it can also be found in [10] and [8] (in a somewhat different form).

**Theorem 2.1** *Suppose that the functions  $\phi_1, \dots, \phi_{2n} : [a, b] \rightarrow \mathbb{R}$  form a Chebyshev system on  $[a, b]$ . Suppose in addition that  $\omega : [a, b] \rightarrow \mathbb{R}$  is a non-negative integrable function  $[a, b] \rightarrow \mathbb{R}$ . Then there exists a unique Gaussian quadrature for the functions  $\phi_1, \dots, \phi_{2n}$  on  $[a, b]$  with respect to the weight function  $\omega$ . The weights of this quadrature are positive.*

**Remark 2.1** While the existence of Generalized Gaussian Quadratures was observed more than 100 years ago, the constructions found in [15, 16], [3, 10], [7, 8] do not easily yield numerical algorithms for the design of such quadrature formulae; such algorithms have been constructed recently (see [13, 28, 2]). The version of the procedure found in [2] was used to produce the results presented in the Examples 5.1, 5.2, 5.3 in Section 5.1; the reader is referred to [2] for details.

Applying Theorem 2.1 to the Example 2.4, we obtain the following theorem.

**Theorem 2.2** *Suppose that under the conditions of Example 2.4,  $n$  is even. Then there exist  $n/2$  points  $t_1, t_2, \dots, t_{n/2}$  on the interval  $[-1, 1]$  and positive real numbers  $w_1, w_2, \dots, w_{n/2}$  such that*

$$\int_{-1}^1 w(t) \cdot \phi_i(t) dt = \sum_{j=1}^{n/2} w_j \cdot \phi_i(t_j), \quad (12)$$

for all  $i = 1, 2, \dots, n$ , with  $\phi_1, \phi_2, \dots, \phi_n$  the first  $n$  eigenfunctions of the operator  $Q$  defined in (9).

**Corollary 2.3** *The above theorem provides a tool for the efficient approximate evaluation of integrals of the form (12), as follows. Given a positive real  $\epsilon$ , we construct the*

*Singular Value Decomposition of the operator  $P$  defined in (8). Choosing  $n$  to be the smallest even integer such that*

$$\sum_{j=n+1}^{\infty} \lambda_j^2 < \epsilon^2, \quad (13)$$

*we construct an  $n/2$ -point quadrature that integrates  $n$  first right singular functions exactly (effective numerical schemes for the construction of such quadratures can be found in [13, 28, 2]). Now, we observe that due to the triangle inequality combined with the positivity of the obtained weights  $w_1, w_2, \dots, w_{n/2}$ ,*

$$\left| \sum_{j=1}^{n/2} w_j \cdot e^{i \cdot c \cdot x \cdot t_j} - \int_{-1}^1 w(x) \cdot e^{i \cdot c \cdot x \cdot t} dt \right| < \epsilon \quad (14)$$

*for any  $x \in [-1, 1]$ .*

**Remark 2.2** The principal subject of this note is the fact that the pattern of an antenna array is formed by a physical process amounting to a hardware implementation of a quadrature formula for functions of the form (9). Thus, designing a configuration of elements for such an antenna is equivalent to constructing a quadrature formula for functions of the form (9), and can be achieved via the techniques described in [13, 28, 2]).

### 3 Elements of Antenna Theory

In this section, we summarize certain facts about the theory of linear antenna arrays; all of these facts are well-known, and can be found, for example, in [9].

#### 3.1 Pattern of a linear array

A source distribution  $\sigma$  on the interval  $[-1, 1]$  creates the far-field pattern  $f : [0, \pi] \rightarrow \mathbb{C}$  given by the formula

$$f(\theta) = \int_{-1}^1 \sigma(u) \cdot e^{i \cdot k \cdot u \cdot \cos(\theta)} du, \quad (15)$$

where  $k$  is the free-space wavenumber,  $u$  is the point on the interval  $[-1, 1]$ , and  $\theta$  is the angle between the point on the horizon where the far field is being evaluated and the  $x$ -axis. It is customary to introduce the notation

$$x = \cos(\theta), \tag{16}$$

and define the function  $F : [-1, 1] \rightarrow \mathbb{C}$  by the formula

$$F(x) = f(\arccos(x)). \tag{17}$$

Now, defining the operator  $A : L^2[-1, 1] \rightarrow L^2[-1, 1]$  by the formula

$$A(\sigma)(x) = \int_{-1}^1 \sigma(u) \cdot e^{i \cdot k \cdot u \cdot x} du, \tag{18}$$

we observe that

$$F = A(\sigma) = \int_{-1}^1 \sigma(u) \cdot e^{i \cdot k \cdot u \cdot x} du. \tag{19}$$

The function  $F$  is usually more convenient to work with than  $f$ , and the following obvious lemma is the principal reason for this difference.

**Lemma 3.1** *Suppose that  $\sigma \in L^2[-1, 1]$ , the function  $F \in L^2[-1, 1]$  is defined by (19),  $\alpha$  is a real number, and the function  $\tilde{\sigma} \in L^2[-1, 1]$  is defined by the formula*

$$\tilde{\sigma}(u) = e^{i \cdot \alpha \cdot u} \cdot \sigma(u). \tag{20}$$

*Then*

$$A(\tilde{\sigma})(x) = A(\sigma)(x - \alpha) \tag{21}$$

*for all  $x \in (-\infty, \infty)$ . In other words, in order to translate the antenna pattern  $F$  (viewed as a function of  $x = \cos(\theta)$ ) by  $\alpha$ , one has to multiply by  $e^{i \cdot \alpha \cdot k}$  the source distribution  $\sigma$  generating the pattern  $F$ .*

**Observation 3.1** *While the obvious physical considerations lead to the antenna pattern  $F$  defined on the interval  $[-1, 1]$ , the formulae (15), (17) also define naturally the extension of  $F$  to the function  $\mathbb{R} \rightarrow \mathbb{C}$ ; in a mild abuse of notation, we will be denoting by  $F$  both the original mapping  $[-1, 1] \rightarrow \mathbb{C}$  and its extension to the mapping  $\mathbb{R} \rightarrow \mathbb{C}$ . Similarly, we will be denoting by  $A$  both the operator  $L^2[-1, 1] \rightarrow L^2[-1, 1]$  defined by (18) and its natural extension mapping  $L^2[-1, 1] \rightarrow c^\infty(\mathbb{R})$ . The restriction of  $F$  on  $\mathbb{R} \setminus [-1, 1]$  is referred to as the invisible spectrum of the source distribution  $\sigma$  and plays an important role in the antenna theory (this role is discussed briefly in the following subsection). By the same token, the restriction of  $F$  on the interval  $[-1, 1]$  is referred to as the visible spectrum.*

When an antenna array is implemented in hardware, it is (usually) constructed of a finite collection of elements, as opposed to being a continuous source distribution. Mathematically, it is equivalent to replacing the general function  $\sigma$  in (15), (19) with  $\sigma$  defined by the expression

$$\sigma(x) = \sum_{j=1}^n \beta_j \cdot \phi_j(u), \quad (22)$$

with  $\phi_1, \phi_2, \dots, \phi_n$  the source distributions generated by individual elements, and the coefficients  $\beta_1, \beta_2, \dots, \beta_n$  the intensities of the elements. As a rule, the elements are localized in space (i.e. the functions  $\phi_1, \phi_2, \dots, \phi_n$  are supported on small subintervals of  $[-1, 1]$ ), and very often, all of the elements are identical (i.e. the functions  $\phi_j$  are translates of each other), so that

$$\phi_j(u) = \phi(u - u_j), \quad (23)$$

with  $\phi$  the source distribution of a single element located at the point  $u = 0$ , and  $u_j$  the location of the element number  $j$ . Obviously, the far-field pattern of  $\phi$  is given by the formula

$$F_\phi(x) = \int_{-1}^1 \phi(u) \cdot e^{i \cdot k \cdot u \cdot x} du; \quad (24)$$

combining (24) with (22) and (23), we obtain the identity

$$\sigma(x) = \int_{-1}^1 \phi(u) \cdot e^{i \cdot k \cdot u \cdot x} du \cdot \sum_{j=1}^n \beta_j \cdot e^{i \cdot k \cdot u_j \cdot x}, \quad (25)$$

known in the antenna theory as the principle of pattern multiplication.

**Remark 3.2** The standard form of the principle of multiplication reads: “The field pattern of an array of nonisotropic but similar point sources is the product of the pattern of the individual source and the the pattern of an array of isotropic point sources, having the same locations, relative amplitudes and phases as the nonisotropic point sources” (see [9]). Needless to say, this is a special case of the well-known theorem from the theory of the Fourier Transform, stating that the Fourier transform of the product of two functions is the convolution of the Fourier Transforms of multiplicants.

## 4 Antenna Patterns and Corresponding Optimal Element Distributions

### 4.1 Characteristics of an antenna pattern

Depending on the situation, the design of an antenna array attempts to optimize certain characteristics of the resulting far-field pattern, subject to certain constraints on the number, power, etc. of the elements. Since the principal purpose of this note is to describe a technique for the selection of the *locations* of the elements that approximate a user-specified pattern, we could use any reasonable far-field pattern to be approximated. In subsection 4.2, 4.3, we construct optimal element distributions for the so-called sector patterns and cosecant pattern, respectively; a detailed discussion of these (and several other) pattern cans be found, for example in [14].

We will say that the antenna pattern has the  $\epsilon$ -bandwidth  $b$  if

$$\int_{b \leq \|x\| \leq 1} |F(x)|^2 dx = \epsilon^2 \cdot \int_{-1}^1 |F(x)|^2 dx \quad (26)$$

in other words, the proportion of the energy radiated outside the  $\epsilon$ -beamwidth from the axis of the beam is equal to  $\epsilon$ . The *supergain* of an antenna is defined (see, for example, [27]), as the ratio

$$\frac{\int_{-\infty}^{+\infty} |F(x)|^2 dx}{\int_{-1}^1 |F(x)|^2 dx} \quad (27)$$

The supergain (sometimes referred to as superdirectivity) measures the ratio of the energy associated with the total spectrum of the antenna to the energy in its visible spectrum; while detailed discussion of supergain and related issues is outside the scope of this note, we will observe that antenna arrays with large degrees of supergain would violate the uncertainty principle, and thus are physically impossible. Attempts to construct supergain antennae result in rapidly (exponentially) growing Ohmic losses, prohibitive accuracy requirements, extremely low bandwidth, etc. Thus, any potentially useful procedure for the design of antenna arrays has to limit the supergain of the resulting patterns.

## 4.2 Sector patterns

It is often desirable to construct antenna patterns that are as constant as possible within the main beam, and as small as possible outside it; in other words, ideally, the pattern would be defined by the formulae

$$F_b(x) = 1 \quad \text{for } |x| \leq b, \quad (28)$$

$$F_b(x) = 0 \quad \text{for } |x| > b, \quad (29)$$

with  $b$  a real number such that  $0 < b \leq k$ . Needless to say, the function  $F_b$  defined by the formulae (28), (29) is not band-limited, and some approximation has to be used. A standard procedure is to truncate the Fourier Transform of  $F_b$ , approximating it by the function  $\tilde{F}_b$  defined by the formula

$$\tilde{F}_b(x) = \int_{-1}^1 \frac{\sin(b \cdot t)}{t} \cdot e^{i \cdot k \cdot x \cdot t} \quad (30)$$

(see, for example, [26]). An important special case occurs when  $b = k$ , with (30) assuming the form

$$\tilde{F}_k(x) = \int_{-1}^1 \frac{\sin(k \cdot t)}{t} \cdot e^{i \cdot k \cdot x \cdot t}, \quad (31)$$

obviously, the latter expression is a band-limited approximation of the  $\delta$ -function. Another frequently encountered situation is that of  $b = k/2$ , so that (30) assumes the form

$$\tilde{F}_k(x) = \int_{-1}^1 \frac{\sin(\frac{k}{2} \cdot t)}{t} \cdot e^{i \cdot k \cdot x \cdot t}, \quad (32)$$

which is a band-limited approximation to the beam that is equal to 1 for  $-1/2 < x < 1/2$  and to zero elsewhere.

In Section 4.4 below, we demonstrate optimal element configurations that produce approximations to the patterns (31), (32) with  $k = 20\pi, 10\pi, 32.4676\pi$ .

**Remark 4.1** While (30) is by no means the only possible band-limited approximations to  $F_b$ , it is quite satisfactory in most cases, in addition to being simple. Furthermore, the principal purpose of this note is to describe a technique for the selection of *locations* of the nodes, given a pattern to be approximated. Thus, we ignore the issue of the optimal choice of  $F_b$ .

### 4.3 Cosecant patterns

Another standard far-field radiation pattern is the so-called cosecant pattern (see, for example, [19]). Given two real numbers  $0 < a < b < 1$ , the cosecant pattern  $F_{a,b}$  is defined by the formula

$$F_{a,b}(x) = \frac{1}{x} \quad (33)$$

for all  $x \in [a, b]$ , and

$$F_{a,b}(x) = 0 \quad (34)$$

for all  $x \in ([-1, 1] \setminus [a, b])$ . Again, the function  $F_{a,b}$  defined by the formulae (33), (34) is not band-limited, and can not be represented by the expression of the form (24). Before the scheme of this note can be applied to  $F_{a,b}$ , the latter has to be approximated with a band-limited function; as discussed in Section 4.1 above, if such an approximation is to be useful as an antenna pattern, its supergain factor has to be controlled. Fortunately, a procedure for such an approximation has been in existence for more than 35 years (see, [18]); the algorithm of [18] is a modification of the least-squares approach *permitting the user to limit the supergain factor of the obtained pattern explicitly*. At the time, the utility of the scheme of [18] was limited by the (perceived) difficulty in the numerical evaluation of Prolate Spheroidal Wave functions; given the present state of numerical analysis, this difficulty is non-existent, and it is this author's impression that the insights of [18], [19] deserve more attention than they have been receiving.

#### 4.4 Optimal distributions of elements

In this subsection, we briefly describe an algorithm for the construction of optimal (in the sense defined below) element configurations for the generation of antenna patterns given by (15), of which the patterns (29)-(31) are special cases. As will be seen, the procedure is in fact applicable to the design of element configurations for very general far-field patterns.

We start with observing that (15) expresses the far-field pattern  $F$  as an integral over the interval  $[-1, 1]$  of functions of the form

$$\sigma(u) \cdot e^{i \cdot k \cdot x \cdot u}, \quad (35)$$

with  $x = \cos(\theta)$  determined by the direction  $\theta$  in which the far-field is being evaluated. In other words, the problem of finding efficient antenna element distributions is equivalent to that of constructing quadrature formulae for integrals of the form (8), with

$$w(t) = \sigma(t). \quad (36)$$

In the cases when  $\sigma$  is non-negative everywhere on the interval  $[-1, 1]$ , Theorem 2.2 guarantees the existence of Generalized Gaussian Quadratures, and [13, 28]) provide a satisfactory numerical apparatus for the construction of such quadratures. Obviously, the patterns given by the formula (28) are not generated by non-negative source distributions, except when

$$b \leq \pi. \tag{37}$$

Thus, for these (and many other) patterns, the conditions of Theorem 2.2 are violated, and the existence of Generalized Gaussian Quadratures is not guaranteed. In our numerical experiments, the techniques of [2]) (after some tuning) have always been successful in finding the Gaussian quadratures for integrals of the form (28); some of our results are presented in Section 5 below.

## 5 Numerical Examples

In this section, we present examples of optimal element distributions generating the patterns of the preceding Section; all of the results presented here have been obtained numerically. Antenna patterns we present are compared to the antenna patterns given by uniform source distributions; configurations of elements approximating these antenna patterns are compared to equispaced distributions of elements generating the same antenna patterns.

### 5.1 Optimal distributions of elements

In this section, we demonstrate the results of the application of the techniques of Section 4.4 of this note to the types of antenna patterns described in the Sections 4.2, 4.3.

In all cases, we choose the size of an antenna array and a pattern to be reproduced, and use the scheme outlined in Section 4.4 to design a distribution of antenna elements (both the locations and the intensities) located within the chosen array that reproduces the required pattern. For comparison, we also generate optimal (in the least squares sense)

approximations to the desired pattern generated by equispaced elements located within the same array. Since the number of equispaced nodes required to obtain a reasonable approximation to the desired pattern is (in many cases) much greater than the number of optimally chosen nodes, for each example we demonstrate patterns generated by several such configurations. In this manner, the numbers of optimally chosen nodes necessary to obtain reasonable approximations to the desired patterns can be compared to the numbers of equispaced nodes required to obtain similar results.

### 5.1.1 Sector patterns

**Example 5.1** *The first example we consider is of the pattern defined by the formula (32), with  $k = 62.8312$ , so that the size of the array is 20 wavelengths.*

*In Figure 5, we display an approximation to the pattern obtained with 19 elements, overlaid with the exact pattern; the locations of the elements are displayed in Figure 5a; the relative error of the obtained approximation is 5.01%.*

*Similarly, in Figure 5g, we display the approximation to the pattern obtained with 21 elements, overlaid with the exact pattern; the relative error of the obtained approximation is 0.443%; in Figure 5h, we display the the approximation obtained with 17 elements. In the latter case, the relative error of the obtained approximation is 6.43%; Figure 5i depicts the 17-node distribution producing the approximation illustrated in Figure 5h. Finally, Figure 5j contains a graph of the values of the sources located at the 17 nodes depicted in Figure 5i and generating the pattern shown in Figure 5h.*

*For comparison, the optimal approximation obtained with 19, 24, 29, 31, and 34 equispaced elements are displayed in Figures 5b, 5c, 5d, 5e, 5f, respectively; these are also overlaid with the exact pattern.*

**Example 5.2** *Our second example is identical to the first one, with the exception that  $k = 31.416$ , so that the size of the array is 10 wavelengths.*

*In Figure 6, we display an approximation to the pattern obtained with 9 elements, overlaid with the exact pattern; the locations of the elements are displayed in Figure 6a; the relative error of the obtained approximation is 11.2%.*

Similarly, in Figure 6f, we display the approximation to the pattern obtained with 11 elements, overlaid with the exact pattern; the relative error of the obtained approximation is 0.600%.

For comparison, the optimal approximation obtained with 9, 14, 16, and 18 equispaced elements are displayed in Figures 6b, 6c, 6d, 5e, respectively; these are also overlaid with the exact pattern.

**Example 5.3** Our third example is identical to the preceding two, with the exception that  $k = 102$ , so that the size of the array is about 32.45 wavelengths.

In Figure 7a, we display an approximation to the pattern obtained with 23 optimally distributed elements, overlaid with the exact pattern and with the pattern obtained with 23 equispaced elements.

The relative error of the obtained approximation is 5.4%; needless to say, the error of the approximation obtained with the equispaced nodes is more than 70%. As can be seen from Figure 7c, the actual size of the obtained 23-element array is about 21 wavelengths; in other words, in order to obtain this precision, the array needs to be about 2/3 of the nominal (maximum permitted) length.

In Figure 7b, we display the approximation to the pattern obtained with 42 and 48 elements, overlaid with the exact pattern.

It is worth noting that with 33 optimally distributed elements, the pattern is approximated to the precision 0.12%; we do not display the obtained pattern since it is visually indistinguishable from the pattern being approximated.

**Example 5.4** Our final example is somewhat different from the preceding ones, in that instead of approximating a sector pattern, we approximate a cosecant pattern (see (33), (34) in Subsection 4.3 above).

In this example, we set

$$a = \sin(15^\circ), \tag{38}$$

$$b = \sin(75^\circ), \quad (39)$$

and use the procedure of [18] to approximate  $F_{a,b}$  with a band-limited function. The band-limit has been more or less arbitrarily set to 110, resulting in an antenna array about 35 wavelengths in size, and the supergain factor of the approximation was set to 1.1.

In Figure 8a, we display an approximation to the pattern obtained with 53 optimally distributed elements, overlaid with the exact bandlimited pattern and with the pattern obtained with 53 equispaced elements.

The relative error of the obtained approximation is 1.79%; the error of the approximation obtained with the equispaced nodes is about 42%.

In Figure 8b, we display the approximation to the pattern obtained with 47 optimally distributed elements, overlaid with the exact pattern; the purpose of this final figure is to demonstrate the behavior of the scheme when the number of elements is insufficient (i.e. when the array is underresolved).

It is worth noting that it takes about 70 equispaced nodes to obtain the resolution obtained with 47 optimally chosen ones.

The following observations can be made from Figures 5 - 8b, and from the more detailed numerical experiments performed by the author.

1. In order to obtain reasonable precision, the scheme requires about 1 point per wavelength in the antenna array; this is more or less independent from the structure of the beam as long as the pattern is symmetric about the point  $x = 0$ . This fact is observed numerically, even for modest numbers of nodes; for large-scale arrays, this statement (interpreted asymptotically) can be proved rigorously. For certain beam structures, the required number of nodes is even less (see Example 5.3). The reasons for these additional savings are subtle, and have to do with the fact that the continuous source distribution generating the pattern is relatively small on a large part of the antenna array; the algorithm of [2] takes advantage of this fact to reduce the number of nodes. When the beam is not symmetric about  $x = 0$ , the number of elements required does depend on

the structure of the pattern, and the dependence is fairly complicated. Generally, the improvement for non-symmetric beams is less than that for the symmetric ones.

2. The qualitative behavior of the scheme is similar to that of the Gaussian quadratures in that it displays no convergence at all until a certain minimum number of nodes is achieved; after that, the convergence is very fast. This behavior is not surprising, since the scheme is based on a Generalized Gaussian quadrature.

3. For the sector pattern with the sector  $[-1/2, 1/2]$ , the scheme reduces the required number of nodes by a factor of about 1.5 for small-scale problems, and roughly by a factor of 2 for large-scale ones; again, for large-scale problems, an asymptotic version of this statement can be proven rigorously.

4. For the cosecant pattern with the parameters specified by (38), (39), the number of nodes required is reduced by approximately a factor of 1.4. As the sidelobe level is reduced, the improvement obtained by going from the equispaced discretization to the optimal one increases rapidly.

5. An examination of Figures 5a, 6a shows that while the optimal nodes are by no means uniform, they display no clustering behavior.

6. An examination of Figure 5j shows that the intensities of individual elements do not become large; this is confirmed by the more extensive numerical experiments performed by the author.

7. The combination of the preceding two paragraphs (combined with additional numerical experiments and analysis) provide evidence that configurations of this type should pose no supergain problems.

## 6 Generalizations

The results described above admit radical generalizations in several directions; several such directions are discussed below,

**1. Conformal one-dimensional arrays.** The extension of the techniques of this note to one-dimensional arrays located on curves in  $R^3$  is completely straightforward, involving only a modest increase of the CPU time requirements of the procedure. Improvement in the number of nodes required to produce a prescribed pattern is similar to that in the case of a linear array.

**2. Planar two-dimensional arrays.** A straightforward generalization of the results of Sections 4, 5, is to rectangular planar arrays. Here, a tensor product quadrature can be constructed from the quadratures of Sections 4, 5, possessing all of the desirable properties of the latter. Obviously, the advantage in the number of transducers is squared, so that (for example) replacing 50 nodes in each of the two directions by 23 nodes (see Example 5.3 above) will lead to a factor of  $(50/23)^2 \sim 4.7$  savings in the number of elements.

The theory of Section 4 has been extended for disk-shaped arrays, via (*inter alia*) the techniques developed in [23]. The improvement in the number of nodes is comparable to that obtained in the rectangular geometry, and the CPU time requirements do not differ appreciably from those in the case of linear one-dimensional arrays.

The extension of the theory to more general geometries in the plane is in progress. At the present time, our only numerical experiments have been with arrays on triangles; the results are encouraging, but the CPU time requirements of the algorithms are excessive (we have only been able to design triangular arrays about 6 wavelengths in size). We are now in the process of constructing a more efficient numerical procedure for such computations.

**3. Conformal two-dimensional arrays.** The only environment in which we have a satisfactory theory is when the array is located on a surface of revolution; even in this environment, no experiments have been performed. We have not investigated more general conformal two-dimensional arrays in sufficient detail.

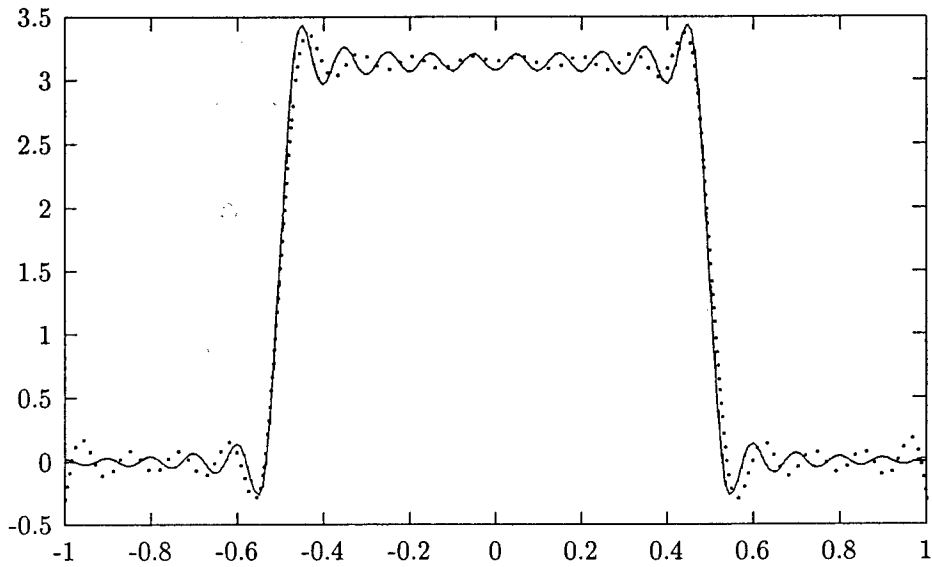


Figure 5: The pattern created by the 19 optimal elements, depicted in Figure 5a as described in Example 5.1

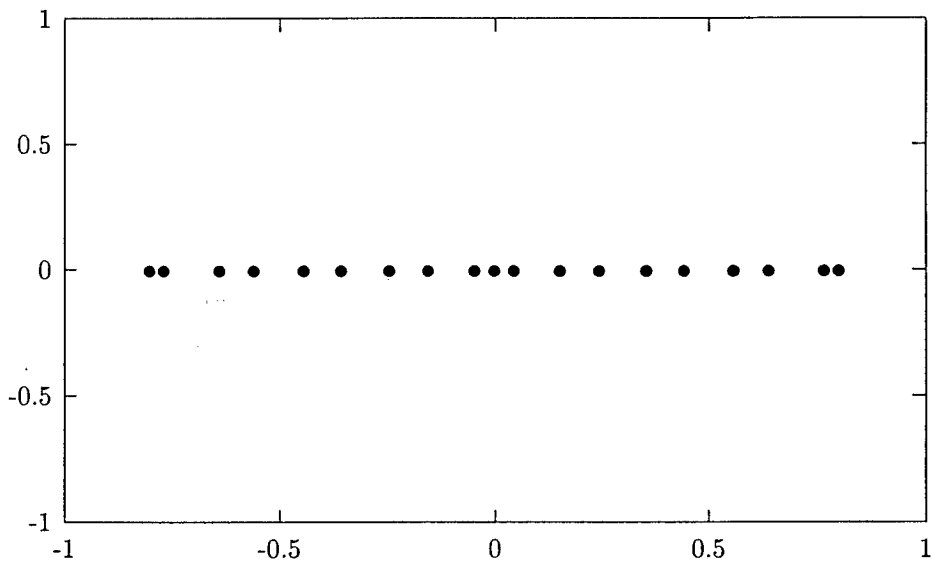


Figure 5a: The distribution of elements creating the pattern depicted in Figure 5, as described in Example 5.1

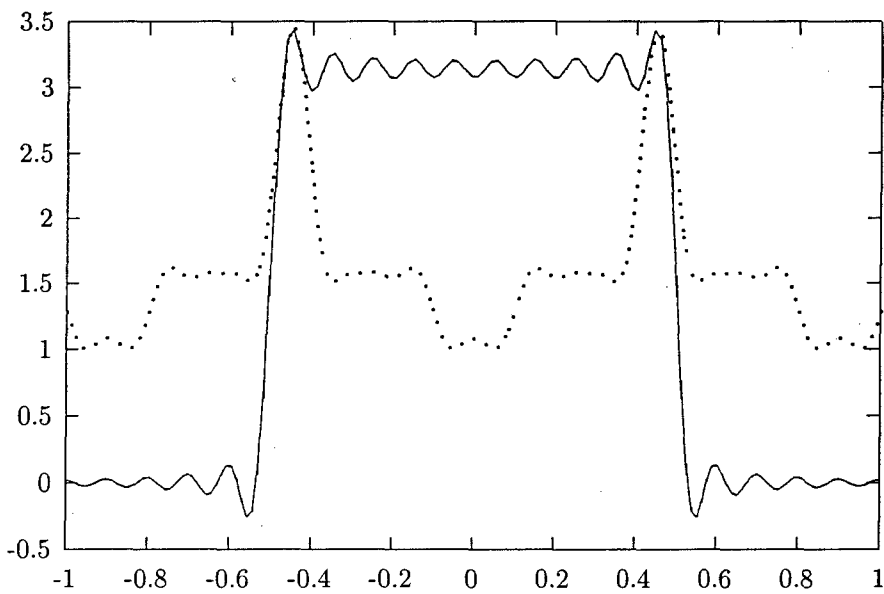


Figure 5b: The optimal approximation to the sector pattern generated by 19 equispaced nodes, as described in Example 5.1

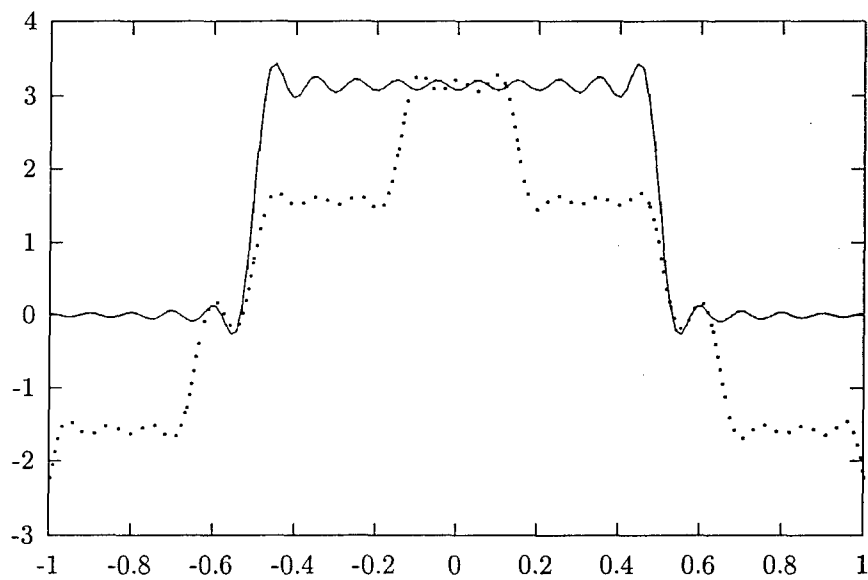


Figure 5c: The optimal approximation to the sector pattern generated by 24 equispaced nodes, as described in Example 5.1

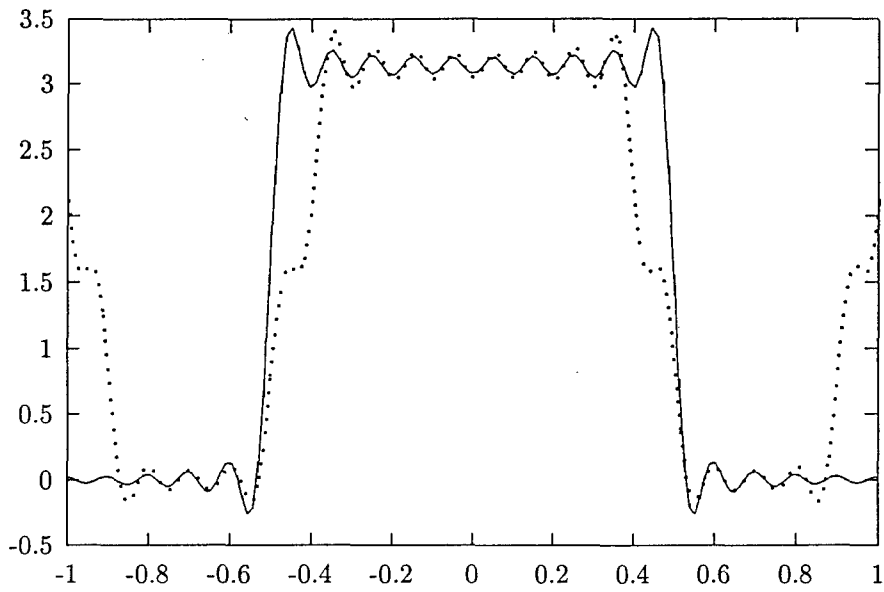


Figure 5d: The optimal approximation to the sector pattern generated by 29 equispaced nodes, as described in Example 5.1

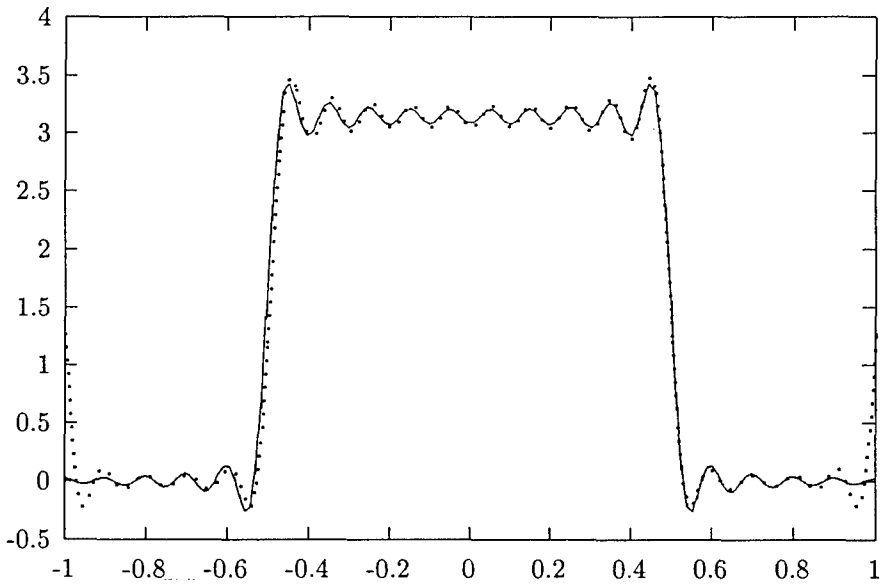


Figure 5e: The optimal approximation to the sector pattern generated by 31 equispaced nodes, as described in Example 5.1

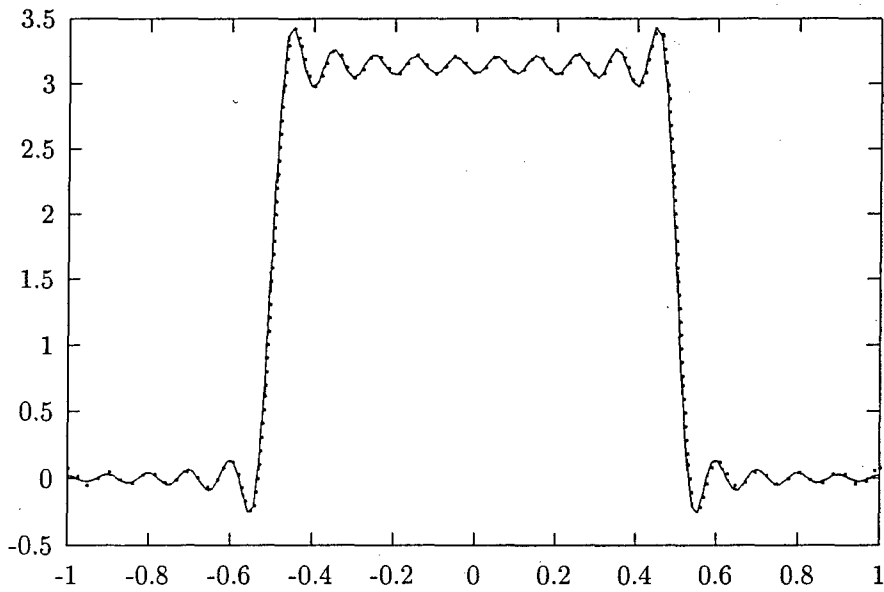


Figure 5f: The optimal approximation to the sector pattern generated by 34 equispaced nodes, as described in Example 5.1

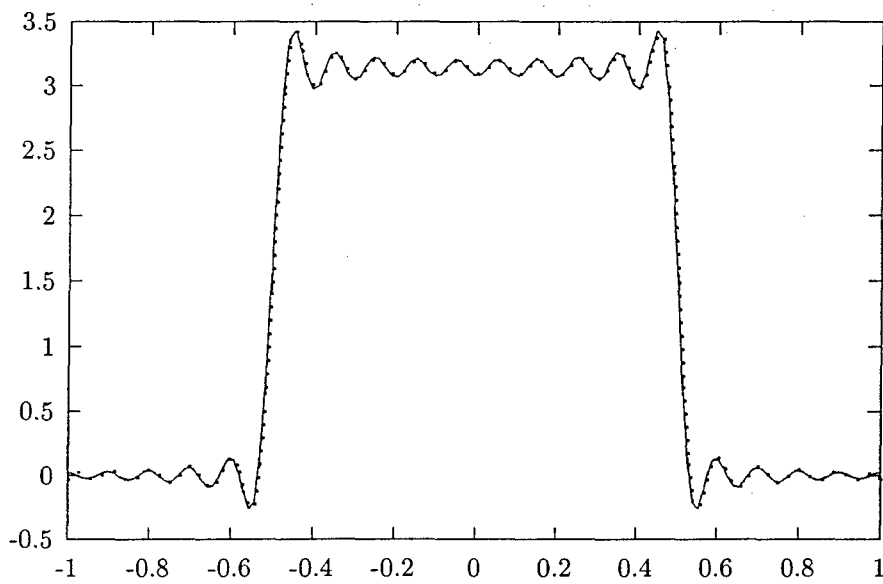


Figure 5g: The optimal approximation to the sector pattern generated by 21 optimal nodes, as described in Example 5.1

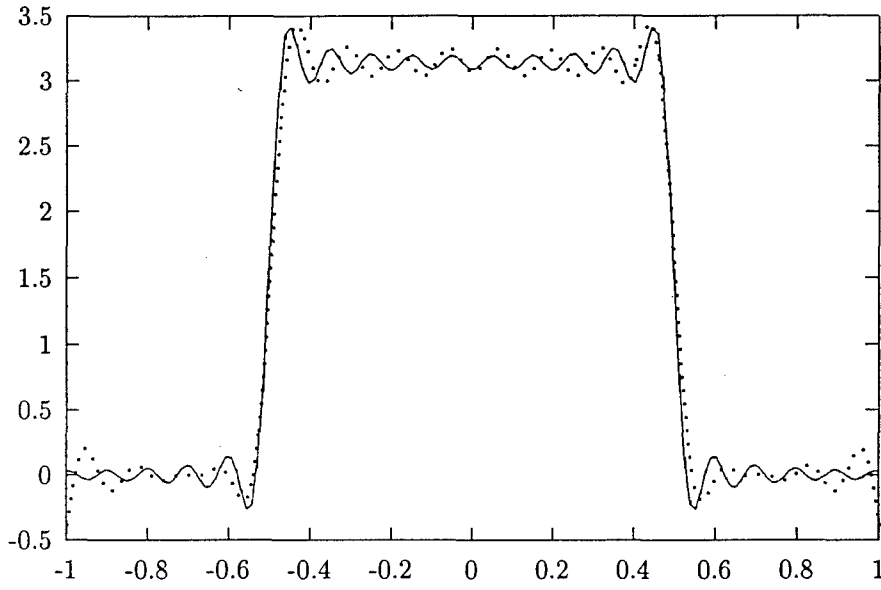


Figure 5h: The optimal approximation to the sector pattern generated by 17 optimal nodes, as described in Example 5.1

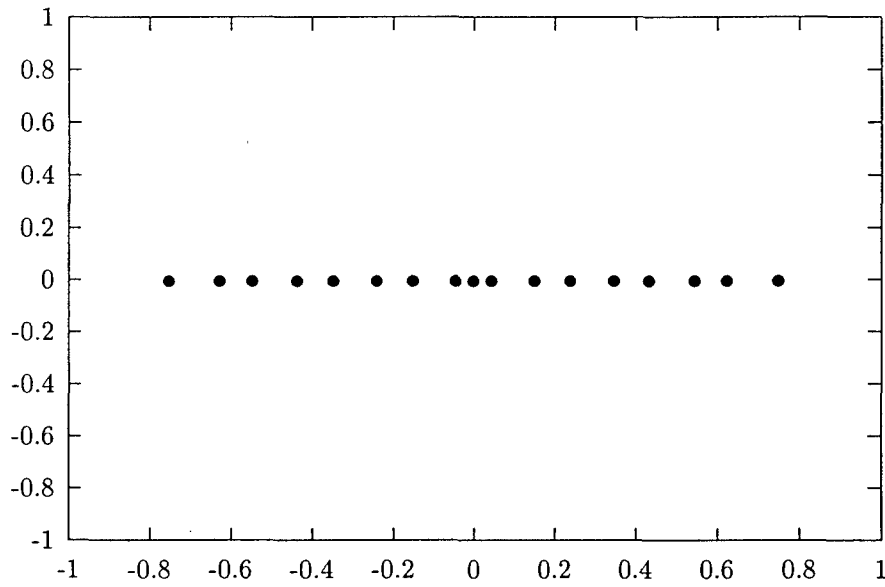


Figure 5i: The distribution of 17 elements creating the pattern depicted in Figure 5h, as described in Example 5.1

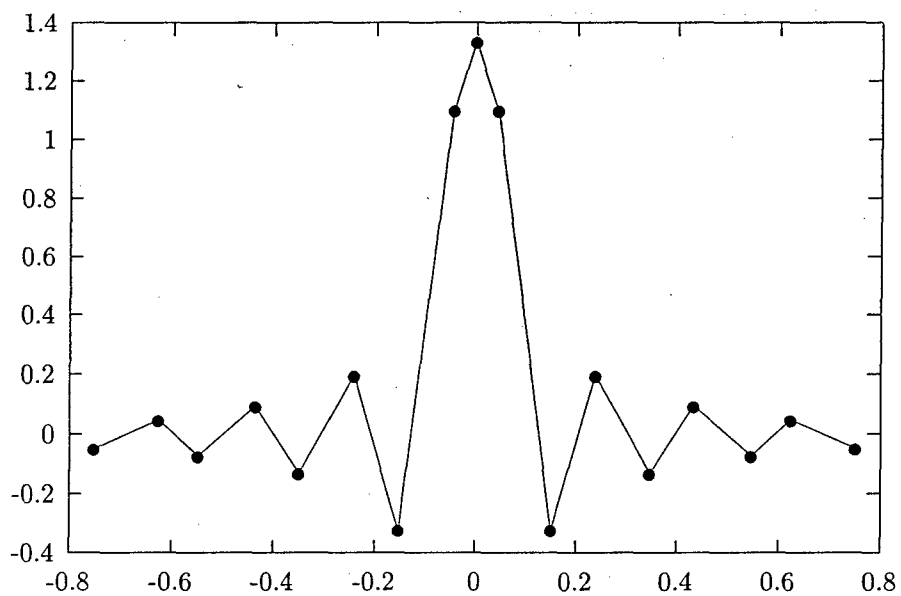


Figure 5j: The values of the sources located at the nodes depicted in Figure 5i and generating the pattern depicted in Figure 5h, as described in Example 5.1

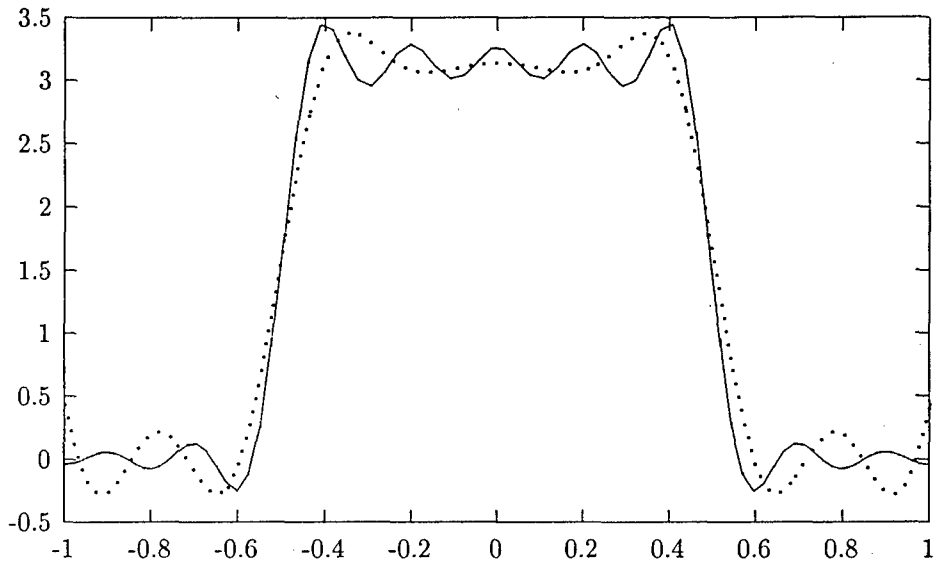


Figure 6: The pattern created by the 9 optimal elements, depicted in Figure 6a as described in Example 5.2

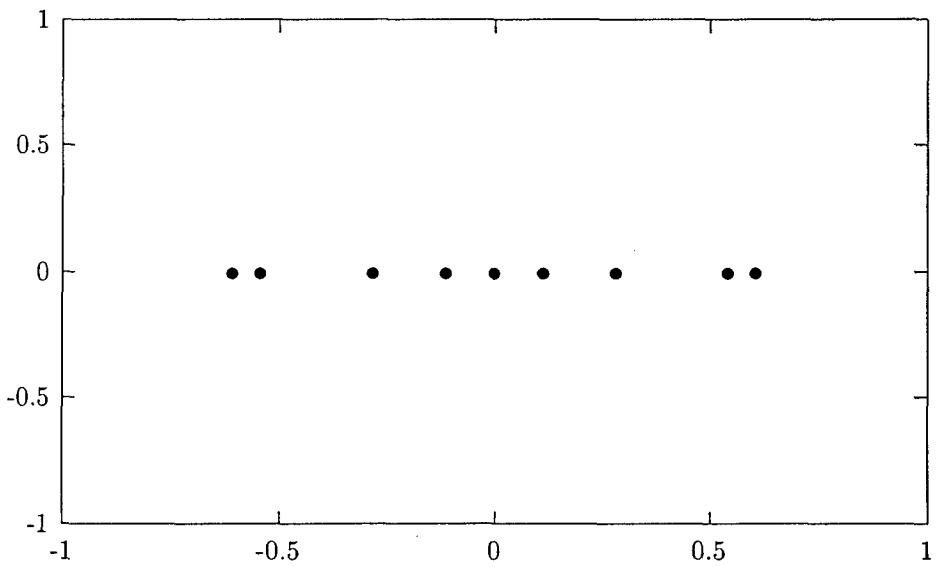


Figure 6a: The distribution of elements creating the pattern depicted in Figure 6, as described in Example 5.2

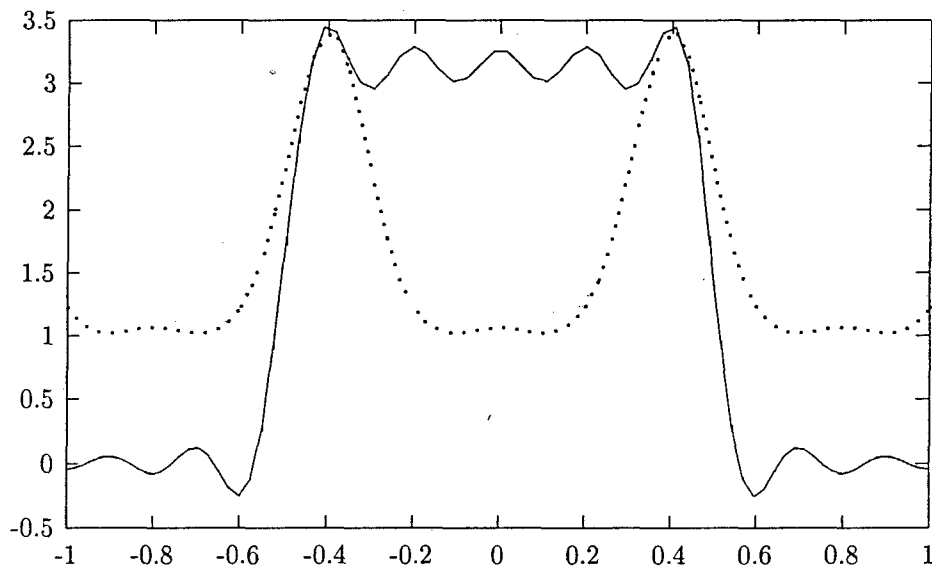


Figure 6b: The optimal approximation to the sector pattern generated by 9 equispaced nodes, as described in Example 5.2

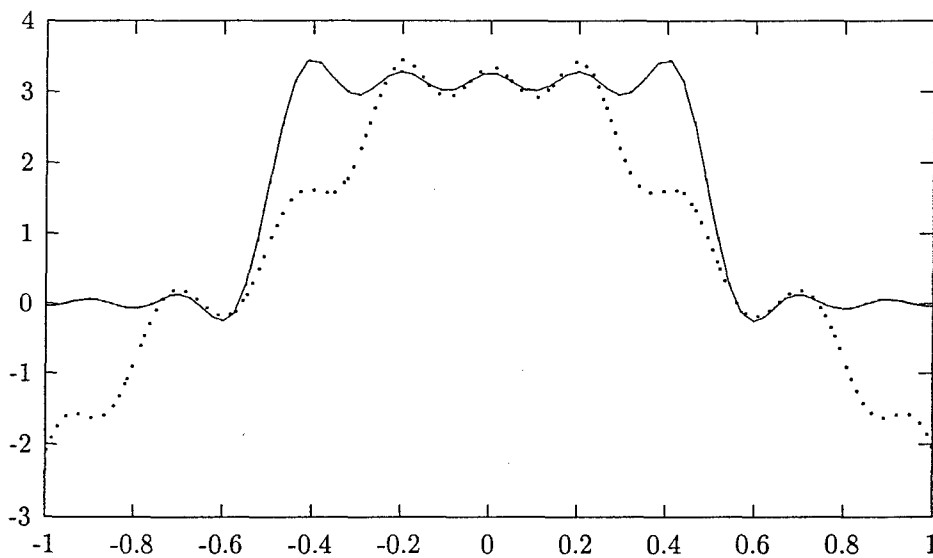


Figure 6c: The optimal approximation to the sector pattern generated by 14 equispaced nodes, as described in Example 5.2

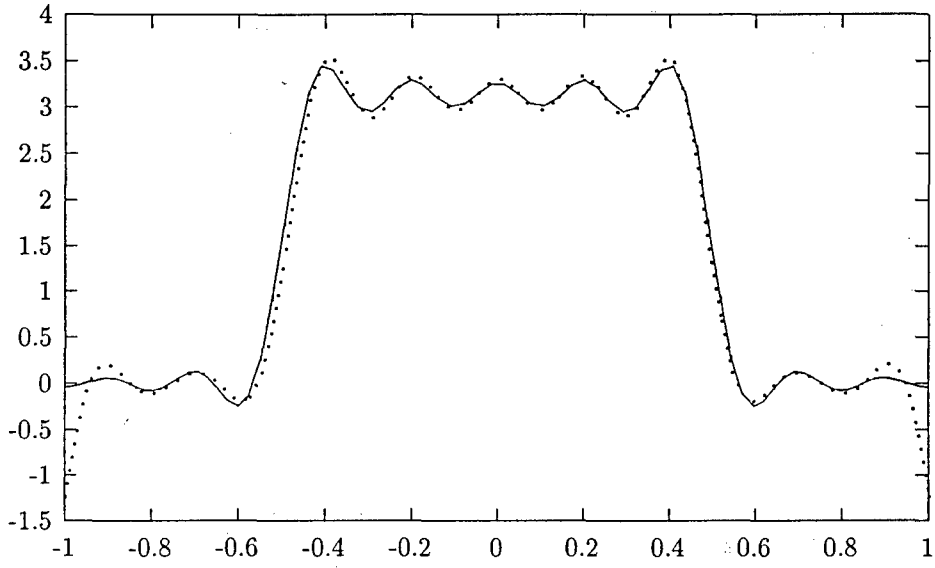


Figure 6d: The optimal approximation to the sector pattern generated by 16 equispaced nodes, as described in Example 5.2

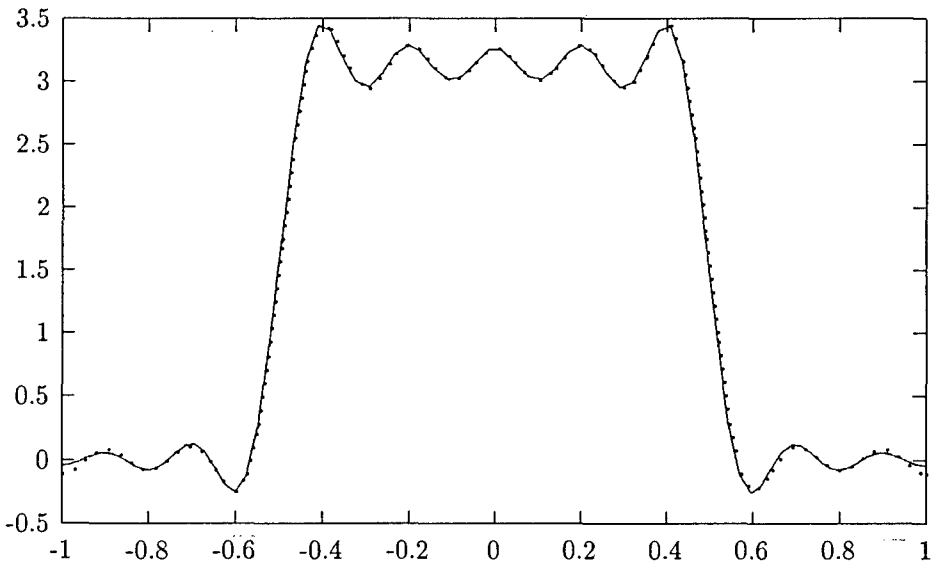


Figure 6e: The optimal approximation to the sector pattern generated by 18 equispaced nodes, as described in Example 5.2

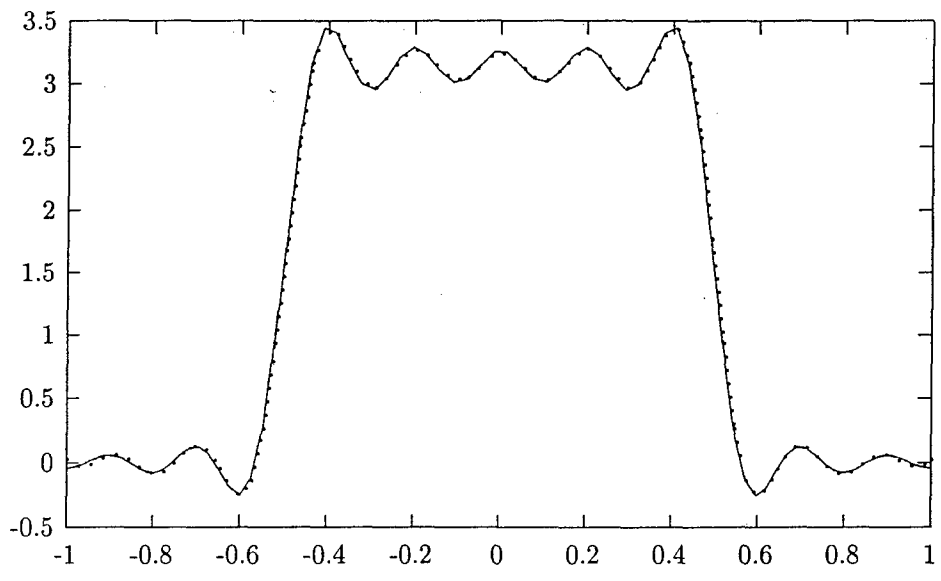


Figure 6f: The pattern created by the 11 optimal elements, in Example 5.2

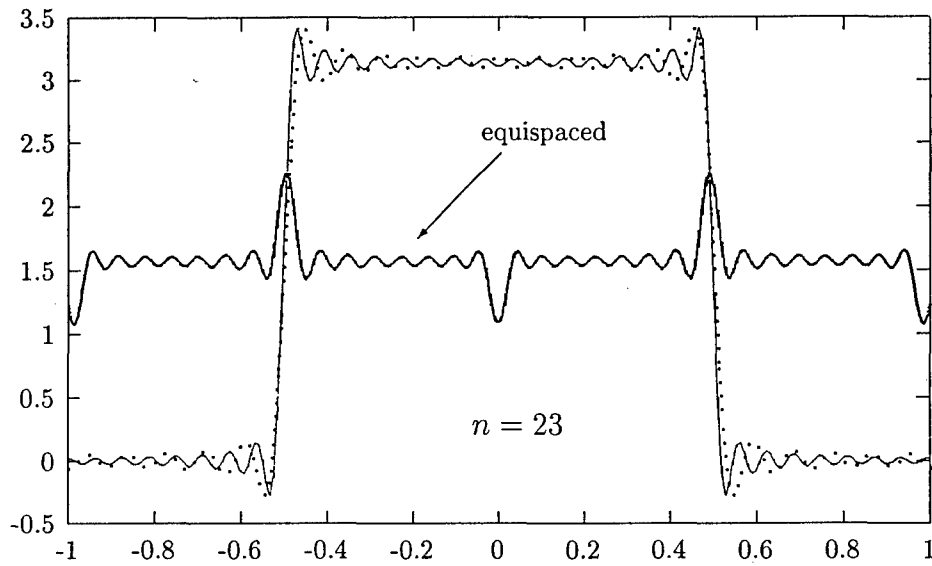


Figure 7a: The approximation to the sector pattern generated by 23 optimal elements, vs. optimal approximation by 23 equispaced nodes, as described in Example 5.3

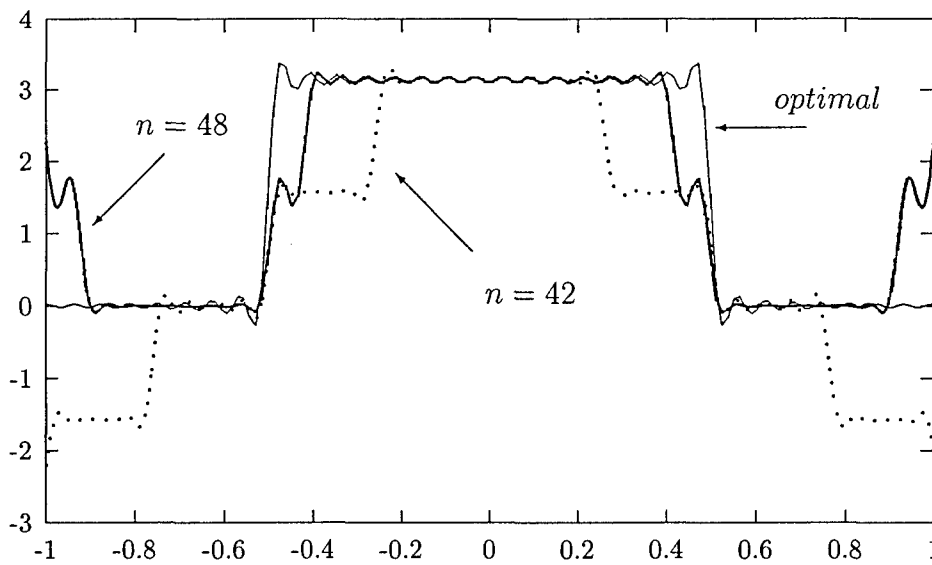


Figure 7b: The optimal approximations to the sector pattern generated by 42 and 48 equispaced nodes, as described in Example 5.3

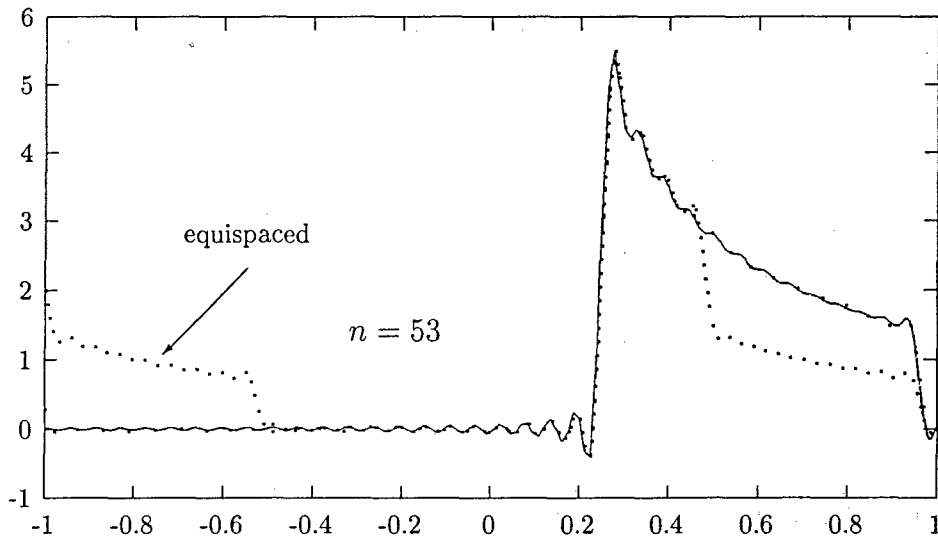


Figure 8a: The approximation to the cosecant pattern generated by 53 optimal elements, vs. optimal approximation by 53 equispaced nodes, as described in Example 5.4

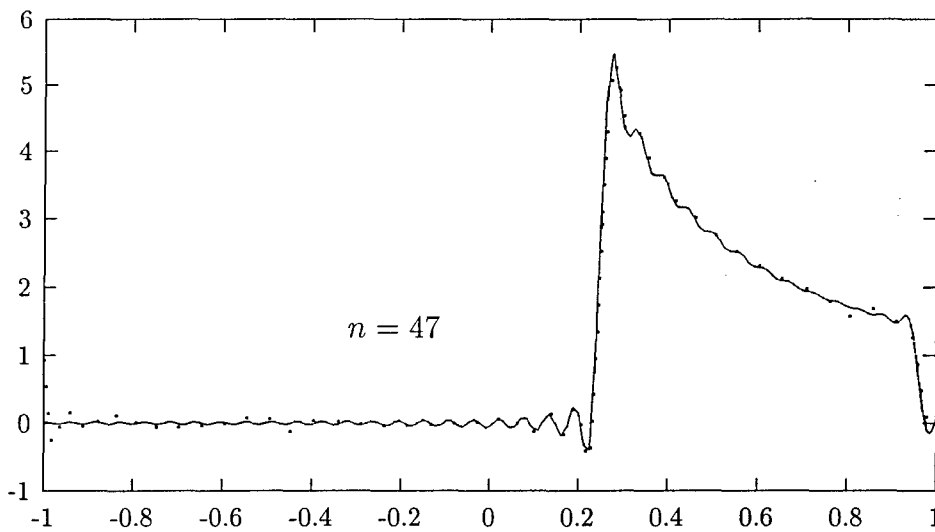


Figure 8a: The approximation to the cosecant pattern generated by 47 optimal elements, as described in Example 5.4

## References

- [1] M. Abramovitz, I. Stegun, *Handbook of Mathematical Functions*, Applied Math. Series (National Bureau of Standards), Washington, DC, 1964.
- [2] H. Cheng, N. Yarvin, V. Rokhlin, *Non-Linear Optimization, Quadrature, and Interpolation*, Yale University Technical Report, YALEU/DCS/RR-1169, 1998, to appear in the SIAM Journal of Non-linear Optimization.
- [3] F. GANTMACHER AND M. KREIN, *Oscillation matrices and kernels and small oscillations of mechanical systems*, 2nd ed., Gosudarstv. Izdat. Tehn-Teor. Lit., Moscow, 1950 (Russian).
- [4] F. A. Grünbaum, *Toeplitz Matrices Commuting With Tridiagonal Matrices*, J. Linear Alg. and Appl., 40, (1981).
- [5] F. A. Grünbaum, *Eigenvectors of a Toeplitz Matrix: Discrete Version of the Prolate Spheroidal Wave Functions*, SIAM J. Alg. Disc. Math., 2(1981).
- [6] F. A. Grünbaum, L. Longhi, M. Perlstadt, *Differential Operators Commuting with Finite Convolution Integral Operators: Some Non-Abelian Examples*, SIAM J. Appl. Math. 42(1982).
- [7] S. KARLIN, *The Existence of Eigenvalues for Integral Operators*, Trans. Am. Math. Soc. v. 113, pp. 1-17 (1964).
- [8] S. KARLIN, AND W. J. STUDDEN, *Tchebycheff Systems with Applications In Analysis And Statistics*, John Wiley (Interscience), New York, 1966.
- [9] John D. Kraus, *Antennas*, McGraw-Hill, 1988.
- [10] M. G. KREIN, *The Ideas of P. L. Chebyshev and A. A. Markov in the Theory Of Limiting Values Of Integrals*, American Mathematical Society Translations, Ser. 2, Vol. 12, 1959, pp. 1-122.

- [11] H.J. Landau, H. Widom, *Eigenvalue Distribution of Time and Frequency Limiting*, Journal of Mathematical Analysis and Applications, 77, 469-481 (1980).
- [12] Y.T. Lo, S.W. Lee, editors, *Antenna Handbook, Theory, Applications, and Design*, Van Nostrand Reinhold Company, 1988.
- [13] J. MA, V. ROKHLIN, AND S. WANDZURA, *Generalized Gaussian Quadratures For Systems of Arbitrary Functions*, SIAM Journal of Numerical Analysis, v. 33, No. 3, pp. 971-996, 1996.
- [14] R.J. Mailloux, *Phased Array Antenna Handbook*, Artech House, 1994.
- [15] A. A. MARKOV, *On the limiting values of integrals in connection with interpolation*, Zap. Imp. Akad. Nauk. Fiz.-Mat. Otd. (8) 6 (1898), no.5 (Russian), pp. 146-230 of [16].
- [16] A. A. MARKOV, *Selected papers on continued fractions and the theory of functions deviating least from zero*, OGIZ, Moscow-Leningrad, 1948 (Russian).
- [17] P.M. Morse, H. Feshbach, *Methods of Theoretical Physics*, McGraw-Hill, New York, 1953.
- [18] D. Rhodes, *The optimum line source for the best mean-square approximation to a given radiation pattern*, IEEE Trans. AP, July 1963.
- [19] D. Rhodes, *Synthesis of planar antenna sources*, Clarendon Press, Oxford, 1974.
- [20] D. Slepian, H.O. Pollak, *Prolate Spheroidal Wave Functions, Fourier Analysis, and Uncertainty - I*, The Bell System Technical Journal, January 1961.
- [21] H.J. Landau, H.O. Pollak, *Prolate Spheroidal Wave Functions, Fourier Analysis, and Uncertainty - II*, The Bell System Technical Journal, January 1961.

- [22] H.J. Landau, H.O. Pollak, *Prolate Spheroidal Wave Functions, Fourier Analysis, and Uncertainty - III: The Dimension of Space of Essentially Time- and Band-Limited Signals*, The Bell System Technical Journal, July 1962.
- [23] D. Slepian, *Prolate Spheroidal Wave Functions, Fourier Analysis, and Uncertainty - IV: Extensions to Many Dimensions, Generalized Prolate Spheroidal Wave Functions*, The Bell System Technical Journal, November 1964.
- [24] D. Slepian, *Prolate Spheroidal Wave Functions, Fourier Analysis, and Uncertainty - V: The Discrete Case*, The Bell System Technical Journal, May-June 1978.
- [25] D. Slepian, *Some Comments on Fourier Analysis, Uncertainty, and Modeling* SIAM Review, V. 25, No. 3, July 1983.
- [26] W.L. Stutzman, G.A. Thiele, *Antenna Theory and Design*, Wiley, 1998.
- [27] T.T. Taylor, *Design of Line-Source Antennas for Narrow Beamwidth and Low Side Lobes*, IEEE Trans. on Antennas and Propagation, AP-3, pp. 16-28, 1955.
- [28] N. Yarvin and V. Rokhlin, *Generalized Gaussian Quadratures and Singular Value Decompositions of Integral Operators*, SIAM Journal of Scientific Computing, Vol. 20, No. 2, pp. 699-718 (1998).



**Prolate Spheroidal Wave Functions, Quadrature, and  
Interpolation**

H. Xiao, V. Rokhlin, N. Yarvin  
Research Report YALEU/DCS/RR-1199  
June 27, 2000

**YALE UNIVERSITY  
DEPARTMENT OF COMPUTER SCIENCE**

Polynomials are one of principal tools of classical numerical analysis. When a function needs to be interpolated, integrated, differentiated, etc., it is assumed to be approximated by a polynomial of a certain fixed order (though the polynomial is almost never constructed explicitly), and a treatment appropriate to such a polynomial is applied. We introduce analogous techniques based on the assumption that the function to be dealt with is band-limited, and use the well-developed apparatus of Prolate Spheroidal Wave Functions to construct quadratures, interpolation and differentiation formulae, etc. for band-limited functions. Since band-limited functions are often encountered in physics, engineering, statistics, etc. the apparatus we introduce appears to be natural in many environments. Our results are illustrated with several numerical examples.

## Prolate Spheroidal Wave Functions, Quadrature, and Interpolation

H. Xiao, V. Rokhlin, N. Yarvin  
Research Report YALEU/DCS/RR-1199  
June 27, 2000

The authors were supported in part by DARPA/AFOSR under Contract F49620/91/C/0084  
Approved for public release: distribution is unlimited.

**Keywords:** *Prolate Spheroidal Wave Functions, Quadrature, Interpolation, Band-Limited Functions*



# Prolate Spheroidal Wave Functions, Quadrature, and Interpolation

## 1 Introduction

Numerical quadrature and interpolation are a well-developed part of numerical analysis; polynomials are the classical tool for the design of such schemes. Conceptually speaking, one assumes that the function is well-approximated by expressions of the form

$$\sum_{j=0}^n a_j x^j, \tag{1}$$

with reasonably small  $n$ , and designs algorithms that are effective for functions of the form (1) (needless to say, one almost never actually computes the coefficients  $\{a_i\}$ ; one only uses the fact of their existence). Obviously, the polynomial approach is only effective for functions that are well-approximated by polynomials.

When one has to handle functions that are well-behaved on the whole line (for example, in signal processing), polynomials are not an appropriate tool. In such cases, trigonometric polynomials are used; existing tools are very satisfactory for dealing with functions defined and well-behaved on the whole of  $\mathbb{R}^1$ . Such tools, in effect, make the assumption that the functions are band-limited or nearly so; a function  $f : \mathbb{R} \rightarrow \mathbb{R}$  is said to be band-limited if there exist a positive real  $c$  and a function  $\sigma \in L^2[-1, 1]$  such that

$$f(x) = \int_{-1}^1 e^{icxt} \sigma(t) dt. \tag{2}$$

However, in many cases, we are confronted with band-limited functions defined on intervals (or, more generally, on compact regions in  $\mathbb{R}^n$ ). Wave phenomena are a rich source of such functions, both in the engineering and computational contexts; they are also encountered in fluid dynamics, signal processing, and many other areas. Often, such functions can be effectively approximated by polynomials via standard tools of classical analysis. However, even when such approximations are feasible, they are usually not optimal. Smooth periodic functions are a good illustration of this observation: while they *can* be approximated by polynomials (for example, via Chebyshev or Legendre expansions), they are more efficiently approximated by Fourier expansions, both for analytical and numerical purposes. It would appear that an approach explicitly based on trigonometric polynomials could be more efficient in dealing with band-limited functions.

In the engineering context, such an apparatus was constructed more than 30 years ago (see [20]-[21], [7]-[9]). The natural tool for analyzing band-limited functions on  $\mathbb{R}^1$  is the Fourier Transform, unless the functions are periodic, in which case the natural tool is

the Fourier Series. The authors of [20]-[21] observe that for the analysis of band-limited functions on the interval, Prolate Spheroidal Wave Functions are likewise a natural approach. The authors also construct a multidimensional version of the theory, though their apparatus is only complete for the case of spherical regions.

The present paper constructs tools for the use of the approach of [20]-[21] in the modern computational environment. We construct a class of quadratures for band-limited functions that closely parallel the Gaussian quadratures for polynomials. The nodes are very close to being roots of appropriately chosen Prolate Spheroidal Wave Functions, the resulting quadratures are stable, and all weights are positive. As in the case of polynomials, there are interpolation, differentiation and indefinite integration schemes associated with the obtained quadratures, exact on certain classes of band-limited functions. These procedures are the main tools necessary for the numerical use of spectral discretizations based on Prolate Spheroidal Wave Functions, instead of on the usual polynomial bases. When dealing with band-limited functions, the number of nodes required by these procedures to obtain a prescribed accuracy is much less than that required by their polynomial-based counterparts. An additional bonus is the fact that the condition number of differentiation of prolate spheroidal wave functions is less than that of differentiation of the usual polynomial basis functions (see Section 8 below).

This paper is organized as follows. Section 2 summarizes various standard mathematical facts used in the remainder of the paper. Section 3 contains derivations of various results used in the algorithms described in later sections. Section 4 describes algorithms for evaluation of prolate spheroidal wave functions and associated eigenvalues. Section 5 describes a construction of quadratures for band-limited functions. Section 6 describes an alternative approach to arriving at such quadratures; it shows that roots of appropriately chosen prolate spheroidal wave functions can serve as quadrature nodes. Section 7 analyzes the use of prolate spheroidal wave functions for interpolation. Section 8 contains results of our numerical experiments with quadratures and interpolation. Section 9 contains a number of miscellaneous properties of prolate spheroidal wave functions, and Section 10 contains generalizations and conclusions.

## 2 Mathematical Preliminaries

As a matter of convention, in this paper the norm of a function is, unless stated otherwise, its  $L^2$  norm:

$$\|f\| = \sqrt{\int |f(x)|^2 dx}. \quad (3)$$

## 2.1 Chebyshev systems

**Definition 2.1** A sequence of functions  $\phi_1, \dots, \phi_n$  will be referred to as a Chebyshev system on the interval  $[a, b]$  if each of them is continuous and the determinant

$$\begin{vmatrix} \phi_1(x_1) & \cdots & \phi_1(x_n) \\ \vdots & & \vdots \\ \phi_n(x_1) & \cdots & \phi_n(x_n) \end{vmatrix} \quad (4)$$

is nonzero for any sequence of points  $x_1, \dots, x_n$  such that  $a \leq x_1 < x_2 < \dots < x_n \leq b$ .

An alternate definition of a Chebyshev system is that any linear combination of the functions with nonzero coefficients must have fewer than  $n$  zeros.

Examples of Chebyshev and extended Chebyshev systems include the following (additional examples can be found in [11]).

**Example 2.1** The powers  $1, x, x^2, \dots, x^n$  form an extended Chebyshev system on the interval  $(-\infty, \infty)$ .

**Example 2.2** The exponentials  $e^{-\lambda_1 x}, e^{-\lambda_2 x}, \dots, e^{-\lambda_n x}$  form an extended Chebyshev system for any  $\lambda_1, \dots, \lambda_n > 0$  on the interval  $[0, \infty)$ .

**Example 2.3** The functions  $1, \cos x, \sin x, \cos 2x, \sin 2x, \dots, \cos nx, \sin nx$  form a Chebyshev system on the interval  $[0, 2\pi]$ .

## 2.2 Generalized Gaussian quadratures

A quadrature rule is an expression of the form

$$\sum_{j=1}^n w_j \phi(x_j), \quad (5)$$

where the points  $x_j \in \mathbb{R}$  and coefficients  $w_j \in \mathbb{R}$  are referred to as the nodes and weights of the quadrature, respectively. They serve as approximations to integrals of the form

$$\int_a^b \phi(x) \omega(x) dx, \quad (6)$$

with  $\omega$  being an integrable non-negative function.

Quadratures are typically chosen so that the quadrature (5) is equal to the desired integral (6) for some set of functions, commonly polynomials of some fixed order. Of these, the classical Gaussian quadrature rules consist of  $n$  nodes and integrate polynomials of order  $2n - 1$  exactly. In [13], the notion of a Gaussian quadrature was generalized as follows:

**Definition 2.2** A quadrature formula will be referred to as Gaussian with respect to a set of  $2n$  functions  $\phi_1, \dots, \phi_{2n} : [a, b] \rightarrow \mathbb{R}$  and a weight function  $\omega : [a, b] \rightarrow \mathbb{R}^+$ , if it consists of  $n$  weights and nodes, and integrates the functions  $\phi_i$  exactly with the weight function  $\omega$  for all  $i = 1, \dots, 2n$ . The weights and nodes of a Gaussian quadrature will be referred to as Gaussian weights and nodes respectively.

The following theorem appears to be due to Markov [14, 15]; proofs of it can also be found in [12] and [11] (in a somewhat different form).

**Theorem 2.1** Suppose that the functions  $\phi_1, \dots, \phi_{2n} : [a, b] \rightarrow \mathbb{R}$  form a Chebyshev system on  $[a, b]$ . Suppose in addition that  $\omega : [a, b] \rightarrow \mathbb{R}$  is a non-negative integrable function  $[a, b] \rightarrow \mathbb{R}$ . Then there exists a unique Gaussian quadrature for the functions  $\phi_1, \dots, \phi_{2n}$  on  $[a, b]$  with respect to the weight function  $\omega$ . The weights of this quadrature are positive.

While the existence of Generalized Gaussian Quadratures was observed more than 100 years ago, the constructions found in [14, 15], [6, 12], [10, 11] do not easily yield numerical algorithms for the design of such quadrature formulae; such algorithms have been constructed recently (see [13, 25, 2]).

**Remark 2.1** It might be worthwhile to observe here that when a Generalized Gaussian quadrature is to be constructed, the determination of its nodes tends to be the critical step (though the procedure of [13, 25, 2] determines the nodes and weights simultaneously). Indeed, once the nodes  $x_1, x_2, \dots, x_n$  have been found, the weights  $w_1, w_2, \dots, w_n$  can be determined easily as the solution of the  $n \times n$  system of linear equations

$$\sum_{j=1}^n w_j \cdot \phi_i(x_j) = \int_a^b \phi_i(x) dx, \quad (7)$$

with  $i = 1, 2, \dots, n$ .

### 2.3 Legendre Polynomials

In agreement with standard practice, we will be denoting by  $P_n$  the classical Legendre polynomials, defined by the three-term recursion

$$P_{n+1}(x) = \frac{2n+1}{n+1} x P_n(x) - \frac{n}{n+1} P_{n-1}(x), \quad (8)$$

with the initial conditions

$$\begin{aligned} P_0(x) &= 1, \\ P_1(x) &= x; \end{aligned} \quad (9)$$

as is well-known,

$$P_k(1) = 1 \quad (10)$$

for all  $k = 0, 1, 2, \dots$ , and each of the polynomials  $P_k$  satisfies the differential equation

$$(1 - x^2) \frac{d^2 P_k(x)}{dx^2} - 2x \frac{dP_k(x)}{dx} + k \cdot (k+1) P_k(x) = 0. \quad (11)$$

The polynomials defined by the formulae (8),(9) are orthogonal on the interval  $[-1, 1]$ ; however, they are not orthonormal, since for each  $n \geq 0$ ,

$$\int_{-1}^1 (P_n(x))^2 dx = \frac{1}{n + 1/2}; \quad (12)$$

the normalized version of the Legendre polynomials will be denoted by  $\overline{P}_n$ , so that

$$\overline{P}_n(x) = P_n(x) \cdot \sqrt{n + 1/2}. \quad (13)$$

The following lemma follows immediately from the Cauchy-Schwartz inequality and from the orthogonality of the Legendre polynomials on the interval  $[-1, 1]$ :

**Lemma 2.2** *For all integer  $k \geq n$ ,*

$$\left| \int_{-1}^1 x^k \overline{P}_n(x) dx \right| < \sqrt{\frac{2}{k+1}}. \quad (14)$$

*For all integer  $0 \leq k < n$ ,*

$$\left| \int_{-1}^1 x^k \overline{P}_n(x) dx \right| = 0. \quad (15)$$

## 2.4 Convolutional Volterra Equations

A convolutional Volterra equation of the second kind is an expression of the form

$$\varphi(x) = \int_a^x K(x-t) \varphi(t) dt + \sigma(x) \quad (16)$$

where  $a, b$  are a pair of numbers such that  $a < b$ , the functions  $\sigma, K : [a, b] \rightarrow \mathbb{C}$  are square-integrable, and  $\varphi : [a, b] \rightarrow \mathbb{C}$  is the function to be determined. Proofs of the following theorem can be found in [4], as well as in many other sources.

**Theorem 2.3** *The equation (16) always has a unique solution on the interval  $[a, b]$ . If both functions  $K, \sigma$  are  $k$  times continuously differentiable, the solution  $\varphi$  is also  $k$  times continuously differentiable.*

## 2.5 Prolate Spheroidal Wave Functions

In this subsection, we summarize certain facts about the Prolate Spheroidal Wave Functions. Unless stated otherwise, all these facts can be found in [20, 17].

Given a real  $c > 0$ , we will denote by  $F_c$  the operator  $L^2[-1, 1] \rightarrow L^2[-1, 1]$  defined by the formula

$$F_c(\varphi)(x) = \int_{-1}^1 e^{icxt} \varphi(t) dt. \quad (17)$$

Obviously,  $F_c$  is compact; we will denote by  $\lambda_0, \lambda_1, \dots, \lambda_n, \dots$  the eigenvalues of  $F_c$  ordered so that  $|\lambda_{j-1}| \geq |\lambda_j|$  for all natural  $j$ . For each non-negative integer  $j$ , we will denote by  $\psi_j$  the eigenfunctions corresponding to  $\lambda_j$ , so that

$$\lambda_j \psi_j(x) = \int_{-1}^1 e^{icxt} \psi_j(t) dt, \quad (18)$$

for all  $x \in [-1, 1]$ ; we adopt the convention that the functions are normalized such that  $\|\psi_j\|_{L^2[-1,1]} = 1$ , for all  $j$ .<sup>1</sup> The following theorem is a combination of several lemmas from [20],[6],[11].

**Theorem 2.4** *For any positive real  $c$ , the eigenfunctions  $\psi_0, \psi_1, \dots$ , of the operator  $F_c$  are purely real, are orthonormal, and are complete in  $L^2[-1, 1]$ . The even-numbered eigenfunctions are even, and the odd-numbered ones are odd. All eigenvalues of  $F_c$  are non-zero and simple; the even-numbered eigenvalues are purely real, and the odd-numbered ones are purely imaginary; in particular,  $\lambda_j = i^j |\lambda_j|$ . The functions  $\psi_i$  constitute a Chebychev system on the interval  $[-1, 1]$ ; in particular, the function  $\psi_i$  has exactly  $i$  zeroes on that interval, for any  $i = 0, 1, \dots$ .*

We will define the self-adjoint operator  $Q_c : L^2[-1, 1] \rightarrow L^2[-1, 1]$  by the formula

$$Q_c(\varphi) = \frac{1}{\pi} \int_{-1}^1 \frac{\sin(c \cdot (x - t))}{x - t} \varphi(t) dt; \quad (19)$$

a simple calculation shows that

$$Q_c = \frac{c}{2\pi} \cdot F_c^* \cdot F_c, \quad (20)$$

that  $Q_c$  has the same eigenfunctions as  $F_c$ , and that the  $j$ -th (in descending order) eigenvalue  $\mu_j$  of  $Q_c$  is connected with  $\lambda_j$  by the formula

$$\mu_j = \frac{c}{2\pi} \cdot |\lambda_j|^2. \quad (21)$$

---

<sup>1</sup>This convention differs from that used in [20]; however, the present paper is concerned almost exclusively with approximation of functions on  $[-1, 1]$ , and in that context, the convention that the functions  $\{\psi_j\}$  have unit norm on that interval is by far the most convenient.

The operator  $Q_c$  is obviously closely related to the operator  $P_c : L^2[-\infty, \infty] \rightarrow [-\infty, \infty]$  defined by the formula

$$P_c(\varphi) = \frac{1}{\pi} \cdot \int_{-\infty}^{\infty} \frac{\sin(c \cdot (x - t))}{x - t} \cdot \varphi(t) dt, \quad (22)$$

which, as is well known, is the orthogonal projection operator onto the space of functions of band limit  $c$  on  $(-\infty, \infty)$ .

For large  $c$ , the spectrum of  $Q_c$  consists of three parts: about  $2c/\pi$  eigenvalues that are very close to 1, followed by order  $\log(c)$  eigenvalues which decay exponentially from 1 to nearly 0; the remaining eigenvalues are all very close to zero. The following theorem, proven (in a slightly different form) in [19], describes the spectrum of  $Q_c$  more precisely.

**Theorem 2.5** *For any positive real  $c$  and  $0 < \alpha < 1$  the number  $N$  of eigenvalues of the operator  $Q_c$  that are greater than  $\alpha$  satisfies the inequality*

$$\begin{aligned} \frac{2c}{\pi} + \left( \frac{1}{\pi^2} \log \frac{1 - \alpha}{\alpha} \right) \log(c) - 10 \cdot \log(c) < N < \\ \frac{2c}{\pi} + \left( \frac{1}{\pi^2} \log \frac{1 - \alpha}{\alpha} \right) \log(c) + 10 \cdot \log(c). \end{aligned} \quad (23)$$

By a remarkable coincidence, the eigenfunctions  $\psi_0, \psi_1, \dots, \psi_n$  of the operator  $Q_c$  turn out to be the Prolate Spheroidal Wave functions, well-known from classical Mathematical Physics (see, for example, [16]). The following theorem formalizes this statement; it is proven in a considerably more general form in [21].

**Theorem 2.6** *For any  $c > 0$ , there exists a strictly increasing sequence of positive real numbers  $\chi_0, \chi_1, \dots$  such that for each  $j \geq 0$ , the differential equation*

$$(1 - x^2) \psi''(x) - 2x \psi'(x) + (\chi_j - c^2 x^2) \psi(x) = 0 \quad (24)$$

*has a solution that is continuous on the interval  $[-1, 1]$ . For each  $j \geq 0$ , the function  $\psi_j$  (defined in Theorem 2.4) is the solution of (24).*

## 3 Analytical Apparatus

### 3.1 Prolate Series

Since the functions  $\psi_0, \psi_1, \dots, \psi_n, \dots$  are a complete orthonormal basis in  $L^2[-1, 1]$ , any formula for the inner product of prolate spheroidal wave functions with another function  $f$  is also a formula for the coefficients of an expansion of  $f$  into prolate spheroidal functions (which we will refer to as the prolate expansion of  $f$ ). Thus the following theorem

provides the coefficients of the prolate expansion of the derivative of a prolate spheroidal function, and also the coefficients of the prolate expansion of a prolate spheroidal wave function multiplied by  $x$ . Those coefficients are also the entries of the matrix for differentiation of a prolate expansion (producing another prolate expansion), and the entries of the matrix for multiplication of a prolate expansion by  $x$ , respectively. (These formulae are not, however, suitable for producing such matrices numerically, since in many cases they exhibit catastrophic cancellation.)

**Theorem 3.1** *Suppose that  $c$  is real and positive, and that the integers  $m$  and  $n$  are non-negative. If  $m = n \pmod{2}$ , then*

$$\int_{-1}^1 \psi'_n(x) \psi_m(x) dx = \int_{-1}^1 x \psi_n(x) \psi_m(x) dx = 0. \quad (25)$$

*If  $m \neq n \pmod{2}$ , then*

$$\int_{-1}^1 \psi'_n(x) \psi_m(x) dx = \frac{2 \lambda_m^2}{\lambda_m^2 + \lambda_n^2} \psi_m(1) \psi_n(1), \quad (26)$$

$$\int_{-1}^1 x \psi_n(x) \psi_m(x) dx = \frac{2}{ic} \frac{\lambda_m \lambda_n}{\lambda_m^2 + \lambda_n^2} \psi_m(1) \psi_n(1). \quad (27)$$

**Proof.** Since the functions  $\psi_j$  are alternately even and odd, (25) is obvious. In order to prove (26), we start with the identity

$$\lambda_n \psi_n = \int_{-1}^1 e^{icxt} \psi_n(t) dt \quad (28)$$

(see (18) in Subsection 2.5). Differentiating (28) with respect to  $x$ , we obtain

$$\lambda_n \psi'_n(x) = ic \int_{-1}^1 t e^{icxt} \psi_n(t) dt. \quad (29)$$

Projecting both sides of (29) on  $\psi_m$  and using the identity (28) (with  $n$  replaced with  $m$ ) again, we have

$$\begin{aligned} & \lambda_n \int_{-1}^1 \psi'_n(x) \psi_m(x) dx \\ &= ic \int_{-1}^1 \psi_m(x) \int_{-1}^1 t e^{icxt} \psi_n(t) dt dx \\ &= ic \int_{-1}^1 t \psi_n(t) \int_{-1}^1 e^{icxt} \psi_m(x) dx dt \\ &= ic \lambda_m \int_{-1}^1 t \psi_n(t) \psi_m(t) dt. \end{aligned} \quad (30)$$

Obviously, the above calculation can be repeated with  $m$  and  $n$  exchanged, yielding the identity

$$\lambda_m \int_{-1}^1 \psi'_m(x) \psi_n(x) dx = ic \lambda_n \int_{-1}^1 t \psi_n(t) \psi_m(t) dt; \quad (31)$$

combining (30) with (31), we have

$$\int_{-1}^1 \psi'_m(x) \psi_n(x) dx = \frac{\lambda_n^2}{\lambda_m^2} \int_{-1}^1 \psi_m(x) \psi'_n(x) dx. \quad (32)$$

On the other hand, integrating the left side of (32) by parts, we have

$$\begin{aligned} \int_{-1}^1 \psi'_m(x) \psi_n(x) dx \\ = \psi_m(1) \psi_n(1) - \psi_m(-1) \psi_n(-1) - \int_{-1}^1 \psi'_n(x) \psi_m(x) dx. \end{aligned} \quad (33)$$

Since  $m \neq n \pmod{2}$ , we rewrite (33) as

$$\begin{aligned} \int_{-1}^1 \psi'_m(x) \psi_n(x) dx \\ = 2 \psi_m(1) \psi_n(1) - \int_{-1}^1 \psi'_n(x) \psi_m(x) dx. \end{aligned} \quad (34)$$

Now, combining (32) and (34) and rearranging terms, we get

$$\int_{-1}^1 \psi'_n(x) \psi_m(x) dx = \frac{2 \lambda_m^2}{\lambda_m^2 + \lambda_n^2} \psi_m(1) \psi_n(1). \quad (35)$$

Substituting (30) into (35), we get

$$\begin{aligned} \int_{-1}^1 x \psi_n(x) \psi_m(x) dx \\ = \frac{1}{ic} \frac{\lambda_n}{\lambda_m} \int_{-1}^1 \psi'_n(x) \psi_m(x) dx \\ = \frac{1}{ic} \frac{\lambda_n}{\lambda_m} \frac{2 \lambda_m^2}{\lambda_m^2 + \lambda_n^2} \psi_m(1) \psi_n(1) \\ = \frac{2}{ic} \frac{\lambda_m \lambda_n}{\lambda_m^2 + \lambda_n^2} \psi_m(1) \psi_n(1). \end{aligned} \quad (36)$$

□

The following corollary, which is an immediate consequence of (32), finds use in the numerical evaluation of the eigenvalues  $\{\lambda_j\}$ :

**Corollary 3.2** Suppose that  $c$  is real and positive, and that the integers  $m$  and  $n$  are non-negative. If  $m \neq n \pmod{2}$ , then

$$\frac{\lambda_m^2}{\lambda_n^2} = \frac{\int_{-1}^1 \psi'_n(x) \psi_m(x) dx}{\int_{-1}^1 \psi'_m(x) \psi_n(x) dx}. \quad (37)$$

### 3.2 Decay of Legendre Coefficients of Prolate Spheroidal Wavefunctions

Since each of the functions  $\psi_j$  is analytic on  $\mathbb{C}$ , on the interval  $[-1, 1]$  it can be expanded in a Legendre series of the form

$$\psi_j(x) = \sum_{k=0}^{\infty} \beta_k \overline{P}_k(x), \quad (38)$$

with the coefficients  $\beta_k$  decaying superalgebraically; the following two theorems establish bounds for the decay rate.

**Lemma 3.3** Let  $\overline{P}_n(x)$  be the  $n$ -th normalized Legendre polynomial (defined in (13)). Then for any real  $a$ ,

$$\begin{aligned} & \int_{-1}^1 e^{iax} \overline{P}_n(x) dx \\ &= \sum_{k=k_0}^{\infty} \alpha_k \int_{-1}^1 x^{2k} \overline{P}_n(x) dx + i \sum_{k=k_0}^{\infty} \beta_k \int_{-1}^1 x^{2k+1} \overline{P}_n(x) dx. \end{aligned} \quad (39)$$

where

$$\alpha_k = (-1)^k \frac{a^{2k}}{(2k)!}, \quad (40)$$

$$\beta_k = (-1)^k \frac{a^{2k+1}}{(2k+1)!}, \quad (41)$$

$$k_0 = \lfloor n/2 \rfloor. \quad (42)$$

Furthermore, for all integer  $m \geq \lfloor e \cdot |a| \rfloor + 1$ ,

$$\begin{aligned} & \left| \int_{-1}^1 e^{iax} \overline{P}_n(x) dx - \sum_{k=k_0}^{m-1} \alpha_k \int_{-1}^1 x^{2k} \overline{P}_n(x) dx \right. \\ & \left. - i \sum_{k=k_0}^{m-1} \beta_k \int_{-1}^1 x^{2k+1} \overline{P}_n(x) dx \right| < \left( \frac{1}{2} \right)^{2m}. \end{aligned} \quad (43)$$

In particular, if

$$n \geq 2 (\lfloor e \cdot |a| \rfloor + 1), \quad (44)$$

then

$$\left| \int_{-1}^1 e^{iax} \overline{P}_n(x) dx \right| < \left( \frac{1}{2} \right)^{n-1}. \quad (45)$$

**Proof.** The formula (39) follows immediately from Lemma 2.2 and Taylor's expansion of  $e^{iax}$ . In order to prove (43), we assume that  $m$  is an integer such that

$$m \geq \lfloor e \cdot |a| \rfloor + 1. \quad (46)$$

Introducing the notation

$$R_m = \sum_{k=m}^{\infty} \alpha_k \int_{-1}^1 x^{2k} \overline{P}_n(x) dx + i \sum_{k=m}^{\infty} \beta_k \int_{-1}^1 x^{2k+1} \overline{P}_n(x) dx, \quad (47)$$

we immediately observe that, due to Lemma 2.2 and the triangle inequality,

$$\begin{aligned} |R_m| &\leq \sum_{k=2m}^{\infty} \left( \frac{|a|^k}{k!} \cdot \sqrt{\frac{2}{k+1}} \right) \\ &< \sum_{k=2m}^{\infty} \frac{|a|^k}{k!}. \end{aligned} \quad (48)$$

Since (46) implies that

$$\frac{|a|}{2m+k} < \frac{|a|}{2m} < \frac{1}{2e} < \frac{1}{2}, \quad (49)$$

for all integer  $m, k > 0$ , we rewrite (48) as

$$\begin{aligned} |R_m| &< \frac{|a|^{2m}}{(2m)!} \cdot \left( 1 + \frac{1}{2} + \frac{1}{4} + \dots \right) \\ &< 2 \frac{|a|^{2m}}{(2m)!}, \end{aligned} \quad (50)$$

and obtain (43) immediately using Stirling's formula. Finally, we obtain (45) by choosing

$$m = \lfloor e \cdot |a| \rfloor + 1. \quad (51)$$

□

**Theorem 3.4** Let  $\psi_m(x)$  be the  $m$ -th prolate spheroidal function with band limit  $c$ , let  $\overline{P}_k(x)$  be the  $k$ -th normalized Legendre polynomial (defined in (13)), and let  $\lambda_m$  be the eigenvalue which corresponds to  $\psi_m(x)$  (as in Theorem 2.4). Then for all integer  $m \geq 0$  and all real positive  $c$ , if

$$k \geq 2 (\lfloor e \cdot c \rfloor + 1), \quad (52)$$

then

$$\left| \int_{-1}^1 \psi_m(x) \overline{P}_k(x) dx \right| < \frac{1}{\lambda_m} \cdot \left(\frac{1}{2}\right)^{k-1}. \quad (53)$$

Moreover, given any  $\varepsilon > 0$ , if

$$k \geq 2 (\lfloor e \cdot c \rfloor + 1) + \log_2 \left(\frac{1}{\varepsilon}\right) + \log_2 \left(\frac{1}{\lambda_m}\right), \quad (54)$$

then

$$\left| \int_{-1}^1 \psi_m(x) \overline{P}_k(x) dx \right| < \varepsilon. \quad (55)$$

**Proof.** Obviously

$$\begin{aligned} & \left| \int_{-1}^1 \psi_m(x) \overline{P}_k(x) dx \right| \\ &= \frac{1}{|\lambda_m|} \cdot \left| \int_{-1}^1 \psi_m(x) \left( \int_{-1}^1 e^{icxt} \overline{P}_k(t) dt \right) dx \right| \\ &< \frac{1}{|\lambda_m|} \int_{-1}^1 |\psi_m(x)| \cdot \left| \int_{-1}^1 e^{icxt} \overline{P}_k(t) dt \right| dx. \end{aligned} \quad (56)$$

Introducing the notation

$$a = cx, \quad (57)$$

and remembering that

$$\int_{-1}^1 |\psi_m(x)| dx = 1, \quad (58)$$

we observe that the combination of (56), (57), (58), and Lemma 3.3 implies that

$$\begin{aligned} & \left| \int_{-1}^1 \psi_m(x) P_k(x) dx \right| \\ &< \frac{1}{|\lambda_m|} \cdot \left(\frac{1}{2}\right)^{k-1} \int_{-1}^1 |\psi_m(x)| dx \\ &= \frac{1}{|\lambda_m|} \left(\frac{1}{2}\right)^{k-1}. \end{aligned} \quad (59)$$

Substituting (54) into (53), we immediately see (55).  $\square$

## 4 Numerical Evaluation of Prolate Spheroidal Wavefunctions

Both the classical Bouwkamp algorithm (see, for example, [1]) for the evaluation of the functions  $\psi_j$ , and the algorithm presented in this paper for the same task, are based on the expression of those functions as a Legendre series of the form

$$\psi_j(x) = \sum_{k=0}^{\infty} \alpha_k P_k(x); \quad (60)$$

since the functions  $\psi_j$  are smooth, the coefficients  $\alpha_k$  decay superalgebraically (with bounds for that decay being given in Theorem 3.4). Substituting (60) into (24), and using (8) and (11), we obtain the well-known three-term recursion

$$\begin{aligned} & \frac{(k+2)(k+1)}{(2k+3)(2k+5)} \cdot c^2 \cdot \alpha_{k+2} + \\ & \left( k(k+1) + \frac{2k(k+1)-1}{(2k+3)(2k-1)} \cdot c^2 - \chi_j \right) \cdot \alpha_k + \\ & \frac{k(k-1)}{(2k-3)(2k-1)} \cdot c^2 \cdot \alpha_{k-2} = 0. \end{aligned} \quad (61)$$

Combining (61) with (13), we obtain the three-term recursion

$$\begin{aligned} & \frac{(k+2)(k+1)}{(2k+3)\sqrt{(2k+5)(2k+1)}} \cdot c^2 \cdot \beta_{k+2}^j + \\ & \left( k(k+1) + \frac{2k(k+1)-1}{(2k+3)(2k-1)} \cdot c^2 - \chi_j \right) \cdot \beta_k^j + \\ & \frac{k(k-1)}{(2k-1)\sqrt{(2k-3)(2k+1)}} \cdot c^2 \cdot \beta_{k-2}^j = 0 \end{aligned} \quad (62)$$

for the coefficients  $\beta_0^j, \beta_1^j, \dots$  of the expansion

$$\psi_j(x) = \sum_{k=0}^{\infty} \beta_k^j \cdot \overline{P}_k(x); \quad (63)$$

for each  $j = 0, 1, 2, \dots$ , we will denote by  $\beta^j$  the vector in  $l^2$  defined by the formula

$$\beta^j = (\beta_0^j, \beta_1^j, \beta_2^j, \dots). \quad (64)$$

The following theorem restates the recursion (62) in a slightly different form.

**Theorem 4.1** *The coefficients  $\chi_i$  are the eigenvalues and the vectors  $\beta^i$  are the corresponding eigenvectors of the operator  $l^2 \rightarrow l^2$  represented by the symmetric matrix  $A$  given by the formulae*

$$A_{k,k} = k(k+1) + \frac{2k(k+1) - 1}{(2k+3)(2k-1)} \cdot c^2, \quad (65)$$

$$A_{k,k+2} = \frac{(k+2)(k+1)}{(2k+3)\sqrt{(2k+1)(2k+5)}} \cdot c^2, \quad (66)$$

$$A_{k+2,k} = \frac{(k+2)(k+1)}{(2k+3)\sqrt{(2k+1)(2k+5)}} \cdot c^2, \quad (67)$$

for all  $k = 0, 1, 2, \dots$ , with the remainder of the entries of the matrix being zero.

In other words, the recursion (62) can be rewritten in the form

$$(A - \chi_j \cdot I)(\beta^j) = 0, \quad (68)$$

where  $A$  is separable into two symmetric tridiagonal matrices  $A_{\text{even}}$  and  $A_{\text{odd}}$ , the first consisting of the elements of  $A$  with even-numbered rows and columns and the second consisting of the elements of  $A$  with odd-numbered rows and columns. While these two matrices are infinite, and their entries do not decay much with increasing row or column number, the eigenvectors  $\{\beta^j\}$  of interest (those corresponding to the first  $m$  prolate spheroidal functions) lie almost entirely in the leading rows and columns of the matrices (as shown by Theorem 3.4). Thus the evaluation of prolate spheroidal functions can be performed by the following procedure:

- 1. Generate the leading  $k$  rows and columns of  $A$ , where  $k$  is given by (54).
- 2. Split the generated portion of  $A$  into  $A_{\text{even}}$  and  $A_{\text{odd}}$ , and use a solver for the symmetric tridiagonal eigenproblem (such as that in LAPACK) to compute their eigenvectors  $\{\beta^j\}$  and eigenvalues  $\{\chi_j\}$ .
- 3. Use the obtained values of the coefficients  $\beta_0^j, \beta_1^j, \beta_2^j, \dots$  in the expansion (63) to evaluate the function  $\psi_j$  at arbitrary points on the interval  $[-1, 1]$ .

Obviously steps 1 and 2 can be performed as a precomputation, for any given value of  $c$ . As a numerical diagonalization of a positive definite tridiagonal matrix with well-separated eigenvalues, this precomputation stage is numerically robust and efficient, requiring  $O(cm)$  operations to construct the Legendre expansions of the form (64) for the first  $m$  prolate spheroidal functions; each subsequent evaluation of a prolate spheroidal function takes  $O(c)$  operations.

## 4.1 Numerical Evaluation of Eigenvalues

Although the above algorithm for the evaluation of prolate spheroidal wave functions also produces the eigenvalues  $\{\chi_j\}$  of the differential operator (24), it does not produce the eigenvalues  $\{\lambda_j\}$  of the integral operator  $F_c$  (defined in (17)). Some of those eigenvalues can be computed using the formula

$$\lambda_j \psi_j(x) = \int_{-1}^1 e^{icxt} \psi_j(t) dt, \quad (69)$$

evaluating the integral on the right hand side numerically; however, that evaluation obviously has a condition number of about  $1/\lambda_j$ , and is thus inappropriate for computing small  $\lambda_j$ . A well-conditioned procedure is as follows:

- 1. Use (69) to calculate  $\lambda_0$ , evaluating the right hand side numerically, and with  $x = 0$  (so that  $\psi_0(x)$  is not small).
- 2. Use the calculated  $\lambda_0$ , together with Corollary 3.2, to compute the absolute values  $|\lambda_j|$ , for  $j = 1, 2, \dots, m$ , computing each  $|\lambda_j|$  from  $|\lambda_{j-1}|$  (and again, evaluating the required integrals numerically).
- 3. Use the fact that  $\lambda_j = i^j |\lambda_j|$  (see Theorem 2.4) to finish the computation.

## 5 Quadratures for Band-Limited Functions

Since the prolate spheroidal wave functions  $\psi_0, \psi_1, \dots, \psi_n, \dots$  constitute a complete orthonormal basis in  $L^2[-1, 1]$  (see Theorem 2.4),

$$e^{icxt} = \sum_{j=0}^{\infty} \left( \int_{-1}^1 e^{icx\tau} \psi_j(\tau) d\tau \right) \psi_j(t), \quad (70)$$

for all  $x, t \in [-1, 1]$ ; substituting (18) into (70) yields

$$e^{icxt} = \sum_{j=0}^{\infty} \lambda_j \psi_j(x) \psi_j(t), \quad (71)$$

Thus if a quadrature integrates exactly the first  $n$  eigenfunctions, that is, if

$$\sum_{k=1}^m w_k \psi_j(x_k) = \int_{-1}^1 \psi_j(x) dx, \quad (72)$$

for all  $j = 0, 1, \dots, n-1$ , then the error of the quadrature when applied to a function  $f(x) = e^{icax}$ , with  $a \in [-1, 1]$ , is given by

$$\begin{aligned} & \sum_{k=1}^m w_k e^{icax_k} - \int_{-1}^1 e^{icax} dx \\ &= \sum_{k=1}^m w_k \left( \sum_{j=0}^{\infty} \lambda_j \psi_j(a) \psi_j(x_k) \right) - \int_{-1}^1 \left( \sum_{j=0}^{\infty} \lambda_j \psi_j(a) \psi_j(x) \right) dx \\ &= \sum_{k=1}^m w_k \left( \sum_{j=n}^{\infty} \lambda_j \psi_j(a) \psi_j(x_k) \right) - \int_{-1}^1 \left( \sum_{j=n}^{\infty} \lambda_j \psi_j(a) \psi_j(x) \right) dx. \end{aligned} \quad (73)$$

Due to the orthonormality of the functions  $\{\psi_j\}$ ,

$$\left\| \sum_{j=n}^{\infty} \lambda_j \psi_j(a) \psi_j(x) \right\| = \sqrt{\sum_{j=n}^{\infty} |\lambda_j|^2}. \quad (74)$$

From (74), it is obvious that the error of integration (73) is of roughly the same magnitude as  $\lambda_n$ , provided that  $n$  is in the range where the eigenvalues  $\{\lambda_j\}$  are decreasing exponentially (as is the case for quadratures of any useful accuracy; see Theorem 2.5) and provided in addition that the weights  $\{w_k\}$  are not large.

Now, the existence of an  $n/2$ -point quadrature that is exact for the first  $n$  Prolate Spheroidal Wave functions follows from the combination of Theorems 2.1, 2.4; an algorithm for the numerical evaluation of nodes and weights of such quadratures can be found in [2]. An alternative procedure for the construction of quadrature formulae for band-limited functions (leading to slightly different nodes and weights) is described in the following section; a numerical comparison of the two can be found in Section 8 below.

**Remark 5.1** The above text considers only the error of integration of a single exponential. For a band-limited function  $g : [-1, 1] \rightarrow \mathbb{C}$  given by the formula

$$g(x) = \int_{-1}^1 G(t) e^{ixt} dt, \quad (75)$$

for some function  $G : [-1, 1] \rightarrow \mathbb{C}$ , the error is obviously bounded by the formula

$$\left| \sum_{k=1}^m w_k g(x_k) - \int_{-1}^1 g(x) dx \right| \leq \varepsilon \cdot \|G\|, \quad (76)$$

where  $\varepsilon$  is the maximum error of integration (73) of a single exponential, for any  $t \in [-1, 1]$ . While  $\|G\|$  might be much larger than  $\|g\|_{[-1,1]}$  (as it is if, for instance,  $g = \psi_{30-n}$ ), if the same equation (75) is used to extend  $g$  to the rest of the real line, then by Parseval's formula  $\|G\| = \|g\|_{(-\infty, \infty)}$ ; that is to say, although the error of such a quadrature when applied to a band-limited function is not bounded proportional to the norm of that function on the interval of integration, it is bounded proportional to the norm of that function on the entire real line.

## 6 Quadrature Nodes from Roots of Prolate Functions

An alternative to the approach of the previous section is to use roots of appropriate prolate spheroidal wave functions as quadrature nodes, with the weights determined via the procedure described in Remark 2.1. The following theorems provide a basis for this; numerically (see Section 8) the resulting quadrature nodes tend to be inferior to those produced by the optimization scheme of [13, 25, 2]; however, they are useful as starting points for that scheme, or as somewhat less efficient nodes which can be computed much more quickly.

### 6.1 Euclid Division Algorithm for Band-Limited Functions

The following two theorems constitute a straightforward extension to band-limited functions of Euclid's division algorithm for polynomials. Their proofs are quite simple, and are provided here for completeness, since the author failed to find them in the literature.

**Theorem 6.1** *Suppose that  $\sigma, \varphi : [0, 1] \rightarrow \mathbb{C}$  are a pair of  $c^2$ -functions such that*

$$\varphi(1) \neq 0, \tag{77}$$

*$c$  is a positive real number, and the functions  $f, p$  are defined by the formulae*

$$f(x) = \int_0^1 \sigma(t) e^{2icxt} dt, \tag{78}$$

$$p(x) = \int_0^1 \varphi(t) e^{icxt} dt. \tag{79}$$

*Then there exist two  $c^1$ -functions  $\eta, \xi : [0, 1] \rightarrow \mathbb{C}$  such that*

$$f(x) = p(x)q(x) + r(x) \tag{80}$$

*for all  $x \in \mathbb{R}$ , with the functions  $q, r : [0, 1] \rightarrow \mathbb{R}$  defined by the formulae*

$$q(x) = \int_0^1 \eta(t) e^{icxt} dt, \tag{81}$$

$$r(x) = \int_0^1 \xi(t) e^{icxt} dt. \tag{82}$$

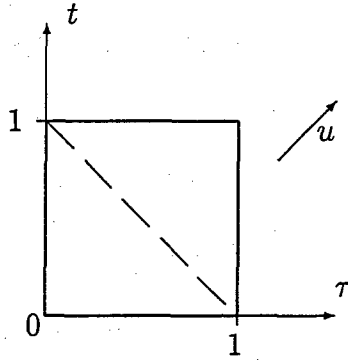


Figure 1: The split of integration range that yields (85)

**Proof.**

Obviously, for any functions  $p, q$  given by (79), (81),

$$\begin{aligned} p(x)q(x) &= \int_0^1 \varphi(t) e^{icxt} dt \cdot \int_0^1 \eta(\tau) e^{icx\tau} d\tau \\ &= \int_0^1 \int_0^1 \varphi(t) \eta(\tau) e^{icx(t+\tau)} d\tau dt. \end{aligned} \quad (83)$$

Defining the new independent variable  $u$  by the formula

$$u = t + \tau, \quad (84)$$

we rewrite (83) as

$$\begin{aligned} p(x)q(x) &= \int_0^1 e^{icux} \int_0^u \varphi(u-\tau) \eta(\tau) d\tau du \\ &\quad + \int_1^2 e^{icux} \int_{u-1}^1 \varphi(u-\tau) \eta(\tau) d\tau du \end{aligned} \quad (85)$$

(see Figure 1). Substituting (78), (82), and (85) into (80), we get

$$\begin{aligned} &\int_0^1 e^{icux} \int_0^u \varphi(u-\tau) \eta(\tau) d\tau du \\ &+ \int_1^2 e^{icux} \int_{u-1}^1 \varphi(u-\tau) \eta(\tau) d\tau du + \int_0^1 \xi(t) e^{icxt} dt \\ &= \int_0^{1/2} \sigma(t) e^{2icxt} dt + \int_{1/2}^1 \sigma(t) e^{2icxt} dt. \end{aligned} \quad (86)$$

Due to the well known uniqueness of the Fourier Transform, (86) is equivalent to two independent equations:

$$\begin{aligned} &\int_0^1 e^{icux} \int_0^u \varphi(u-\tau) \eta(\tau) d\tau du + \int_0^1 \xi(t) e^{icxt} dt \\ &= \int_0^{1/2} \sigma(t) e^{2icxt} dt, \end{aligned} \quad (87)$$

$$\int_1^2 e^{icux} \int_{u-1}^1 \varphi(u-\tau) \eta(\tau) d\tau du = \int_{1/2}^1 \sigma(t) e^{2icxt} dt. \quad (88)$$

Now, we observe that (88) does not contain  $\xi$ , and use it to obtain an expression for  $\eta$  as a function of  $\varphi$ ,  $\sigma$ . After that, we will view (87) as an expression for  $\xi$  via  $\varphi$ ,  $\sigma$ ,  $\eta$ .

From (88) and the uniqueness of the Fourier Transform, we obtain

$$\int_{u-1}^1 \varphi(u-\tau) \eta(\tau) d\tau = \sigma\left(\frac{u}{2}\right), \quad (89)$$

for all  $u \in [1, 2]$ . Introducing the new variable  $v$  via the formula

$$v = u - 1, \quad (90)$$

we convert (89) into

$$\int_v^1 \varphi(v+1-\tau) \eta(\tau) d\tau = \sigma\left(\frac{v+1}{2}\right), \quad (91)$$

which is a Volterra equation of the first kind with respect to  $\eta$ ; differentiating (91) with respect to  $v$ , we get

$$-\varphi(1) \eta(v) + \int_v^1 \varphi'(v+1-\tau) \eta(\tau) d\tau = \frac{1}{2} \sigma'\left(\frac{v+1}{2}\right), \quad (92)$$

which is a Volterra equation of the second kind. Now, the existence and uniqueness of the solution of (92) (and, therefore, of (89) and (88)) follows from Theorem 2.3 of Section 2.

With  $\eta$  defined as the solution of (89), we use (87) together with the uniqueness of the Fourier Transform, to finally obtain

$$\xi(u) = \sigma\left(\frac{u}{2}\right) - \int_0^u \varphi(u-\tau) \eta(\tau) d\tau, \quad (93)$$

for all  $u \in [0, 1]$ . □

The following theorem is a consequence of the preceding one.

**Theorem 6.2** *Suppose that  $\sigma, \varphi : [-1, 1] \rightarrow \mathbb{C}$  are a pair of  $c^2$ -functions such that  $\varphi(-1) \neq 0$ ,  $\varphi(1) \neq 0$ ,  $c$  is a positive real number, and the functions  $f, p$  are defined by the formulae*

$$f(x) = \int_{-1}^1 \sigma(t) e^{2icxt} dt, \quad (94)$$

$$p(x) = \int_{-1}^1 \varphi(t) e^{icxt} dt. \quad (95)$$

Then there exist two  $C^1$ -functions  $\eta, \xi : [-1, 1] \rightarrow \mathbb{C}$  such that

$$f(x) = p(x)q(x) + r(x) \quad (96)$$

for all  $x \in \mathbb{R}$ , with the functions  $q, r : [-1, 1] \rightarrow \mathbb{R}$  defined by the formulae

$$q(x) = \int_{-1}^1 \eta(t) e^{icxt} dt, \quad (97)$$

$$r(x) = \int_{-1}^1 \xi(t) e^{icxt} dt. \quad (98)$$

**Proof.**

Defining the functions  $f_+, f_-, p_+, p_-$ , by the formulae

$$f_+(x) = \int_0^1 \sigma(t) e^{2icxt} dt, \quad (99)$$

$$f_-(x) = \int_{-1}^0 \sigma(t) e^{2icxt} dt, \quad (100)$$

$$p_+(x) = \int_0^1 \varphi(t) e^{icxt} dt, \quad (101)$$

$$p_-(x) = \int_{-1}^0 \varphi(t) e^{icxt} dt, \quad (102)$$

we observe that for all  $x \in \mathbb{R}^1$ ,

$$f(x) = f_+(x) + f_-(x), \quad (103)$$

$$p(x) = p_+(x) + p_-(x). \quad (104)$$

Due to Theorem 6.1, there exist such  $\eta_+, \eta_-, \xi_+, \xi_-$ , that

$$f_+(x) = p_+(x)q_+(x) + r_+(x), \quad (105)$$

$$f_-(x) = p_-(x)q_-(x) + r_-(x), \quad (106)$$

with the functions  $q_+, q_-, r_+, r_-$  defined by the formulae

$$q_+(x) = \int_0^1 \eta_+(t) e^{icxt} dt, \quad (107)$$

$$q_-(x) = \int_{-1}^0 \eta_-(t) e^{icxt} dt, \quad (108)$$

$$r_+(x) = \int_0^1 \xi_+(t) e^{icxt} dt, \quad (109)$$

$$r_-(x) = \int_{-1}^0 \xi_-(t) e^{icxt} dt. \quad (110)$$

Now, defining  $q$ , by the formula

$$q(x) = q_-(x) + q_+(x) \quad (111)$$

for all  $x \in [-1, 1]$ , we have

$$\begin{aligned} p(x)q(x) &= (p_-(x) + p_+(x)) \cdot (q_-(x) + q_+(x)) \\ &= p_+(x)q_+(x) + p_-(x)q_-(x) + p_-(x)q_+(x) + p_+(x)q_-(x), \end{aligned} \quad (112)$$

and we define  $r(x)$  by the obvious formula

$$r(x) = r_-(x) + r_+(x) - (p_-(x)q_+(x) + p_+(x)q_-(x)). \quad (113)$$

□

## 6.2 Quadrature nodes from the division theorem

In much the same way that the division theorem for polynomials can be used to provide a constructive proof of Gaussian quadratures, Theorem 6.2 provides a method of constructing generalized Gaussian quadratures for band-limited functions. The method is as follows.

To construct a quadrature for functions of a bandwidth  $2c$ , prolate spheroidal wave functions corresponding to bandwidth  $c$  are used. (Thus the eigenvalues  $\{\lambda_j\}$  and eigenfunctions  $\{\psi_j\}$  are in this section, as elsewhere in the paper, those corresponding to bandwidth  $c$ ). The following theorem provides a bound of the error of a quadrature whose nodes are the roots of the  $n$ 'th prolate function  $\psi_n$ , when applied to a function  $f$  which satisfies the conditions of the division theorem, in terms of the norms of the quotient and remainder of  $f$  divided by  $\psi_n$ :

**Theorem 6.3** *Suppose that  $x_1, x_2, \dots, x_n \in \mathbb{R}$  are the roots of  $\psi_n$ . Let the numbers  $w_1, w_2, \dots, w_n \in \mathbb{R}$  be such that*

$$\sum_{k=1}^n w_k \psi_j(x_k) = \int_{-1}^1 \psi_j(x) dx, \quad (114)$$

for all  $j = 0, 1, \dots, n-1$ . Then for any function  $f : [-1, 1] \rightarrow \mathbb{C}$  which satisfies the conditions of Theorem 6.2,

$$\begin{aligned} & \left| \sum_{k=1}^n w_k f(x_k) - \int_{-1}^1 f(x) dx \right| \\ & \leq |\lambda_n| \cdot \|\eta\| + \|\xi\| \cdot \sum_{j=n}^{\infty} |\lambda_j| \cdot \|\psi_j\|_{\infty}^2 \cdot \left( 2 + \sum_{k=1}^m \|w_k\| \right), \end{aligned} \quad (115)$$

where the functions  $\eta, \xi : [-1, 1] \rightarrow \mathbb{C}$  are as defined in Theorem 6.2.

**Proof.** Since  $f$  satisfies the conditions of Theorem 6.2, there exist functions  $q, r : [-1, 1] \rightarrow \mathbb{R}$  defined by (97),(98) such that

$$f(x) = \psi_n(x) q(x) + r(x). \quad (116)$$

Then, defining the error of integration  $E_f$  for the function  $f$  by

$$E_f = \left| \sum_{k=1}^n w_k f(x_k) - \int_{-1}^1 f(x) dx \right| \quad (117)$$

we have

$$\begin{aligned} E_f &= \left| \sum_{k=1}^n w_k (\psi_n(x_k) q(x_k) + r(x_k)) - \int_{-1}^1 (\psi_n(x) q(x) + r(x)) dx \right| \\ &\leq \left| \sum_{k=1}^n w_k \psi_n(x_k) q(x_k) - \int_{-1}^1 \psi_n(x) q(x) dx \right| \\ &\quad + \left| \sum_{k=1}^n w_k r(x_k) - \int_{-1}^1 r(x) dx \right| \end{aligned} \quad (118)$$

Since the nodes  $\{x_k\}$  are the roots of  $\psi_n$ ,

$$\sum_{k=1}^n w_k \psi_n(x_k) q(x_k) = 0. \quad (119)$$

Thus

$$E_f \leq \left| \int_{-1}^1 \psi_n(x) q(x) dx \right| + \left| \sum_{k=1}^n w_k r(x_k) - \int_{-1}^1 r(x) dx \right|. \quad (120)$$

Now

$$\begin{aligned} \int_{-1}^1 \psi_n(x) q(x) dx &= \int_{-1}^1 \psi_n(x) \int_{-1}^1 \eta(t) e^{icxt} dt dx \\ &= \int_{-1}^1 \eta(t) \int_{-1}^1 \psi_n(x) e^{icxt} dx dt \\ &= \int_{-1}^1 \eta(t) \lambda_n \psi_n(t) dt. \end{aligned} \quad (121)$$

Using the Cauchy-Schwartz inequality and the fact that the function  $\psi_n$  has unit norm, we get from (121) that

$$\left| \int_{-1}^1 \psi_n(x) q(x) dx \right| \leq |\lambda_n| \cdot \|\eta\|. \quad (122)$$

Also,

$$\begin{aligned} & \sum_{k=1}^n w_k r(x_k) - \int_{-1}^1 r(x) dx \\ &= \sum_{k=1}^n w_k \left( \int_{-1}^1 \xi(t) e^{icx_k t} dt \right) - \int_{-1}^1 \left( \int_{-1}^1 \xi(t) e^{icx t} dt \right) dx \\ &= \int_{-1}^1 \xi(t) \left( \sum_{k=1}^n w_k e^{icx_k t} - \int_{-1}^1 e^{icx t} dx \right) dt. \end{aligned} \quad (123)$$

Substituting (73) into (123), and using the Cauchy-Schwartz inequality, we get

$$\begin{aligned} & \sum_{k=1}^n w_k r(x_k) - \int_{-1}^1 r(x) dx \\ &= \int_{-1}^1 \xi(t) \left( \sum_{k=1}^m w_k \left( \sum_{j=n}^{\infty} \lambda_j \psi_j(t) \psi_j(x_k) \right) \right. \\ & \quad \left. - \int_{-1}^1 \left( \sum_{j=n}^{\infty} \lambda_j \psi_j(t) \psi_j(x) \right) dx \right) dt \\ &\leq \|\xi\| \cdot \sum_{j=n}^{\infty} |\lambda_j| \cdot \|\psi_j\|_{\infty}^2 \cdot \left( 2 + \sum_{k=1}^m \|w_k\| \right). \end{aligned} \quad (124)$$

Combining (120), (122), and (124), we get

$$E_f \leq |\lambda_n| \cdot \|\eta\| + \|\xi\| \cdot \sum_{j=n}^{\infty} |\lambda_j| \cdot \|\psi_j\|_{\infty}^2 \cdot \left( 2 + \sum_{k=1}^m \|w_k\| \right). \quad (125)$$

□

**Remark 6.1** The use of Theorem 6.3 for the construction of quadrature rules for band-limited functions depends on the fact that the norms of the band-limited functions  $q$  and  $r$  in (116) are not large, compared to the norm of  $f$  (both sets of norms being on  $[-\infty, \infty]$ ). Such estimates have been obtained for all  $n > 2c/\pi + 10 \log(c)$ . The proofs are quite involved, and will be reported at a later date. In this paper, we demonstrate the performance of the obtained quadrature formulae numerically (see Section 8 below).

**Remark 6.2** It is natural to view (116) as an analogue for band-limited functions of the Euclid division theorem for polynomials. However, there are certain differences. In particular, Theorem 6.1 admits extensions to band-limited functions of several variables, while the classical Euclid algorithm does not. Such extensions (together with several applications) will be reported at a later date.

## 7 Interpolation via Prolate Spheroidal Wavefunctions

Interpolation is usually performed by the following general procedure: assuming that the function  $f : [a, b] \rightarrow \mathbb{C}$  to be interpolated is given by the formula

$$f(x) = c_1\phi_1(x) + c_2\phi_2(x) + \dots + c_n\phi_n(x), \quad (126)$$

where  $\phi_1, \phi_2, \dots, \phi_n : [a, b] \rightarrow \mathbb{C}$  are a fixed sequence of functions (often polynomials), solve an  $n \times n$  linear system to determine the coefficients  $c_1, c_2, \dots, c_n$  from the values of  $f$  at the  $n$  interpolation nodes, then use (126) to evaluate  $f$  wherever needed. As is well known, if  $f$  is well-approximated by a linear combination of the interpolation functions, and if the linear system to be solved is well-conditioned, then this procedure is accurate.

As shown in Section 5 in the context of quadratures, a linear combination of the first  $n$  prolate spheroidal functions  $\psi_0, \psi_1, \dots, \psi_{n-1}$  for a band limit  $c$  can provide a good approximation to functions of the form  $e^{icx}$ , with  $t \in [-1, 1]$  (see (71,74)); in the regime where the accuracy is numerically useful, the error is of the same order of magnitude as  $|\lambda_n|$ . This, in turn, shows that they provide a good approximation (in the same sense as in Remark 5.1) to any band-limited function of band limit  $c$ . Thus, if  $\psi_0, \psi_1, \dots, \psi_{n-1}$  are used as the interpolation functions in this procedure, they can be expected to yield an accurate interpolation scheme for band-limited functions, provided that the matrix to be inverted is well-conditioned. The following theorem shows that if the interpolation nodes are chosen to be quadrature nodes accurate up to twice the bandwidth of interpolation, with the quadrature formula being accurate to more than twice as many digits as the interpolation formula is to be accurate to, then the matrix inverted in the procedure is close to being a scaled version of an orthogonal matrix.

**Theorem 7.1** *Suppose the numbers  $w_1, w_2, \dots, w_n \in \mathbb{R}$  and  $x_1, x_2, \dots, x_n \in \mathbb{R}$  are such that*

$$\left| \int_{-1}^1 e^{2icax} dx - \sum_{j=1}^n w_j e^{2icax_j} \right| < \varepsilon, \quad (127)$$

for all  $a \in [-1, 1]$ , and for some  $c > 0$ . Let the matrix  $A$  be given by the formula

$$A = \begin{pmatrix} \psi_0(x_1) & \psi_1(x_1) & \dots & \psi_{n-1}(x_1) \\ \psi_0(x_2) & \psi_1(x_2) & \dots & \psi_{n-1}(x_2) \\ \vdots & \vdots & & \vdots \\ \psi_0(x_n) & \psi_1(x_n) & \dots & \psi_{n-1}(x_n) \end{pmatrix}, \quad (128)$$

let the matrix  $W$  be the diagonal matrix whose diagonal entries are  $w_1, w_2, \dots, w_n$ , and let the matrix  $E = [e_{jk}]$  be given by the formula

$$E = I - A^*WA. \quad (129)$$

Then

$$|e_{jk}| < \left| \frac{2\varepsilon}{\lambda_{j-1}\lambda_{k-1}} \right|. \quad (130)$$

**Proof.** Clearly

$$e_{jk} = \delta_{jk} - \sum_{l=1}^n w_l \psi_{j-1}(x_l) \psi_{k-1}(x_l), \quad (131)$$

where  $\delta_{ij}$  is the Kronecker delta function. Using (18), this becomes

$$\begin{aligned} e_{jk} &= \delta_{jk} - \sum_{l=1}^n w_l \cdot \left( \frac{1}{\lambda_{j-1}} \int_{-1}^1 e^{-icx_l t} \psi_{j-1}(t) dt \right) \\ &\quad \cdot \left( \frac{1}{\lambda_{k-1}} \int_{-1}^1 e^{icx_l \tau} \psi_{k-1}(\tau) d\tau \right) \\ &= \delta_{jk} - \frac{1}{\lambda_{j-1}\lambda_{k-1}} \int_{-1}^1 \int_{-1}^1 \psi_{j-1}(t) \psi_{k-1}(\tau) \sum_{l=1}^n w_l e^{-icx_l t} e^{icx_l \tau} dt d\tau. \end{aligned} \quad (132)$$

Using (127), this becomes

$$e_{jk} = \delta_{jk} - \frac{1}{\lambda_{j-1}\lambda_{k-1}} \int_{-1}^1 \int_{-1}^1 \psi_{j-1}(t) \psi_{k-1}(\tau) \cdot \left( \int_{-1}^1 e^{-icst} e^{ics\tau} ds - f_\varepsilon(t+\tau) \right) dt d\tau, \quad (133)$$

where  $f_\varepsilon : [-2, 2] \rightarrow \mathbb{C}$  is a function which satisfies the relation

$$|f_\varepsilon(x)| < \varepsilon, \quad (134)$$

for all  $x \in [-2, 2]$ . Thus

$$\begin{aligned} e_{jk} &= \delta_{jk} - \frac{1}{\lambda_{j-1}\lambda_{k-1}} \int_{-1}^1 \int_{-1}^1 \psi_{j-1}(t) \psi_{k-1}(\tau) \int_{-1}^1 e^{-icst} e^{ics\tau} ds dt d\tau \\ &\quad + \frac{1}{\lambda_{j-1}\lambda_{k-1}} \int_{-1}^1 \int_{-1}^1 \psi_{j-1}(t) \psi_{k-1}(\tau) f_\varepsilon(t+\tau) dt d\tau \end{aligned} \quad (135)$$

Using (18), this becomes

$$e_{jk} = \delta_{jk} - \int_{-1}^1 \psi_{j-1}(s) \psi_{k-1}(s) ds + \frac{1}{\lambda_{j-1} \lambda_{k-1}} \int_{-1}^1 \psi_{k-1}(\tau) \int_{-1}^1 \psi_{j-1}(t) f_\varepsilon(t + \tau) dt d\tau. \quad (136)$$

Due to the orthonormality of the functions  $\{\psi_j\}$ , this becomes

$$e_{jk} = \frac{1}{\lambda_{j-1} \lambda_{k-1}} \int_{-1}^1 \psi_{k-1}(\tau) \int_{-1}^1 \psi_{j-1}(t) f_\varepsilon(t + \tau) dt d\tau. \quad (137)$$

Using the Cauchy-Schwartz inequality, this becomes

$$\begin{aligned} |e_{jk}| &\leq \left| \frac{1}{\lambda_{j-1} \lambda_{k-1}} \right| \|\psi_{k-1}\| \sqrt{\int_{-1}^1 \left| \int_{-1}^1 \psi_{j-1}(t) f_\varepsilon(t + \tau) dt \right|^2 d\tau} \\ &\leq \left| \frac{1}{\lambda_{j-1} \lambda_{k-1}} \right| \sqrt{\int_{-1}^1 \|\psi_{j-1}\|^2 \int_{-1}^1 |f_\varepsilon(t + \tau)|^2 dt d\tau} \\ &= \left| \frac{1}{\lambda_{j-1} \lambda_{k-1}} \right| \sqrt{\int_{-1}^1 \int_{-1}^1 |f_\varepsilon(t + \tau)|^2 dt d\tau} \\ &< \frac{2\varepsilon}{\lambda_{j-1} \lambda_{k-1}}. \end{aligned} \quad (138)$$

□

From inspection of Theorem 2.5, it can easily be seen that the number  $N$  of eigenvalues needed for a bandwidth of  $2c$  and an accuracy of  $\varepsilon^2$  is roughly twice the number of eigenvalues needed for a bandwidth of  $c$  and an accuracy of  $\varepsilon$ . Thus a generalized Gaussian quadrature for a bandwidth  $2c$  and an accuracy  $\varepsilon^2$  has roughly the same number of nodes as are needed for interpolation of accuracy  $\varepsilon$ . In our numerical experiments, this correspondence was found to be much closer than the rough bounds in Theorem 2.5 indicate; in the results tabulated in Section 8, the number of nodes for an interpolation formula of a desired accuracy  $\varepsilon$  was always chosen to be the number of quadrature nodes for a desired accuracy  $\varepsilon^2$  for twice the band limit (that number, in turn, being chosen as indicated in Section 5); the correspondence between the desired accuracy and the experimentally measured maximum error can be seen in Tables 3 and 4.

The coefficients  $c_1, c_2, \dots, c_n$  produced by this interpolation procedure (see (126)) can, of course, just as easily be used for evaluating derivatives or indefinite integrals of the interpolated function, as they can for computing the function itself.

## 8 Numerical Results

The algorithms of Sections 5–7 have been implemented in double precision (64-bit floating point) arithmetic, with results shown in Tables 1–4. Tables 1 and 2 show the performance of quadrature nodes produced by the schemes of Sections 5 and 6, when used as quadrature nodes; Tables 3 and 4 show their performance when used as interpolation nodes. These are not actually the same sets of nodes; even with the bandwidth  $c$  for interpolation being half of the bandwidth for quadrature (as it is in the tables), more nodes are needed to achieve a given accuracy of interpolation than are needed to achieve a given accuracy of quadrature, as can be seen by comparing the number of nodes (printed in the column labeled  $n$  in each table). The error figures in the tables are approximations of the maximum error of interpolation or of the quadrature, when applied to functions of the form  $\cos(ax)$  and  $\sin(ax)$ , with  $0 \leq a \leq c$ ; they were computed by measuring the error at a large number of points in  $a$  (for interpolation, in both  $a$  and  $x$ ), including the extremes. The column labeled “Roots” contains the errors for the nodes produced by the scheme of Section 6; the column labeled “Refined” contains the errors after those nodes, used as a starting point, have been run through the scheme of Section 5. The variable  $\varepsilon$  which appears in the tables is the requested accuracy, used to determine the number of nodes in the ways described in Sections 5 and 7.

Also tabulated are the numbers of Legendre nodes required to achieve the same accuracy  $\varepsilon$  using polynomial interpolation or quadrature schemes. Since Chebyshev nodes are generally known to be superior for interpolation, for that case the numbers of Chebyshev nodes required to achieve the same accuracy are also tabulated.

Figure 2 contains the maximum norm of the derivative of each prolate function  $\psi_j(x)$ , for  $c = 200$  and  $x \in [-1, 1]$ , as a function of  $j$ ; also graphed, for comparison, is the maximum norm of the derivative of each normalized Legendre polynomial  $\bar{P}_j(x)$  over the same range; and graphed below, on the same horizontal scale, are the norms of the eigenvalues  $\lambda_j$ . The graph shows that, for this value of  $c$ , computing the derivatives of a function given by a prolate series is a better-conditioned operation than computing the derivatives of a function given by a Legendre series of the same number of terms. (Obviously, if the number of terms can also be reduced, as in the situations of Tables 1–4, there is a further improvement in the condition number.) The same general pattern of behavior is exhibited for other values of  $c$ ; as  $c$  approaches zero (and the prolate functions approach the Legendre polynomials), the value of  $j$  at which the maximum norm of the derivative rises sharply also approaches zero (as is to be expected, since for  $c = 0$  the prolate functions reduce to Legendre polynomials). Finally, Tables 5 and 6 contain samples of quadrature weights and nodes.

**Remark 8.1** In this paper, detailed discussion of issues encountered in the implementation of numerical algorithms has been deliberately avoided, as well as any discussion of

Mhz CPU time requirements, memory requirements, etc. Thus, we limit ourselves to observing that all algorithms have been implemented in FORTRAN, that with the exception of the procedure for the evaluation of Prolate Spheroidal Wave functions described in Section 4, we have not designed or implemented any new or original numerical algorithms, and that the procedure of Section 4 consists of applying standard tools of numerical analysis (diagonalization of a tridiagonal matrix) to the well-known recursion (61). The resulting algorithm for the evaluation of prolate spheroidal wave functions has the CPU time requirements proportional to  $c^2$ , with a fairly large proportionality constant. The procedure of [2], when applied to the system of functions  $\psi_0, \psi_1, \dots, \psi_{2n+1}$  requires order  $n^3$  operations, also with a fairly large proportionality constant. On the other hand, the cost of finding all roots  $n$  of the function  $\psi_n$  lying on the interval  $[-1, 1]$  is proportional to  $n$ , and the proportionality constant is not large. The largest  $c$  we have dealt with in our experiments was about 6000, with resulting quadratures having about 1900 nodes. In this regime, the construction of the quadrature (both nodes and weights) took several minutes on the 300-megaflop SUN workstation; while there are fairly obvious ways to reduce the cost of the calculation (both in terms of asymptotic CPU time requirements and in terms of associated proportionality constants) we have made no effort to do so.

The following observations can be made from the examples presented in this section, and from the more extensive tests performed by the authors.

1. When the nodes obtained via the algorithm of [2] are used for the integration of band-limited functions, the resulting quadrature rules are significantly more accurate than the quadratures obtained from the nodes of appropriately chosen prolate functions; however, the *difference* between the numbers of nodes required by the two approaches to obtain a *prescribed* precision is not large. When the nodes obtained via the two approaches are used for the interpolation (as opposed to the integration) of band-limited functions, the performances of the two are virtually identical.
2. For large  $c$ , the number of nodes required by a quadrature rule for the integration of band-limited functions with the band-limit  $c$  is close to  $\frac{c}{\pi}$ ; the dependence on the required precision of integration is weak (as one would expect from Theorem 2.5 and subsequent developments).
3. The numbers of nodes required by our quadratures rules to integrate band-limited functions is roughly  $\pi/2$  times less than the numbers of Gaussian nodes; the numbers of nodes required by our interpolation formulae in order to interpolate band-limited functions is roughly  $\pi/2$  times less than the number of Chebychev (or Gaussian) nodes. Again, the dependence of the required number of nodes on the accuracy requirements is weak.
4. The norm of the differentiation operator based on our nodes is of the order  $c^{3/2}$ , as

compared to the norm of the spectral differentiation operators obtained from classical polynomial expansions; this might be useful in the design of spectral (or pseudospectral) techniques.

## 9 Miscellaneous Properties

Prolate spheroidal wave functions possess a rich set of properties, vaguely resembling the properties of Bessel functions. This section establishes some of those properties. Some of the identities below can be found in [20],[17],[5]; others are easily derivable from the former.

The identity

$$e^{icxt} = \sum_{j=0}^{\infty} \lambda_j \psi_j(x) \psi_j(t), \quad (139)$$

(see Section 5) has a number of consequences which, while fairly obvious, seem worth recording, since similar properties of other special functions have often been found useful. Differentiating (139)  $m$  times with respect to  $x$  and  $n$  times with respect to  $t$  yields the formula

$$x^m t^n e^{icxt} = \left(\frac{1}{ic}\right)^{(m+n)} \sum_{j=0}^{\infty} \lambda_j \psi_j^{(m)}(x) \psi_j^{(n)}(t), \quad (140)$$

for all  $x, t \in [-1, 1]$ . Multiplying (139) by  $e^{-icut}$ , and integrating with respect to  $t$ , converts it into

$$\frac{\sin(c \cdot (x - u))}{x - u} = \frac{c}{2} \sum_{j=0}^{\infty} \lambda_j^2 \psi_j(x) \psi_j(u), \quad (141)$$

Taking the squared norm of (139), and integrating with respect to  $x$  and  $t$ , yields the formula

$$\sum_{j=0}^{\infty} |\lambda_j|^2 = 4; \quad (142)$$

combining this with (21) yields

$$\sum_{j=0}^{\infty} \mu_j = \frac{2c}{\pi}. \quad (143)$$

Setting  $x = t = 1$  converts (139) into

$$e^{ic} = \sum_{j=0}^{\infty} \lambda_j \psi_j^2(1). \quad (144)$$

The identity

$$\lambda_j \psi_j(x) = \int_{-1}^1 e^{icxt} \psi_j(t) dt \quad (145)$$

(see Section 2.5) also has a number of simple but potentially useful consequences. Differentiating it  $k$  times with respect to  $x$ , we get

$$\lambda_j \psi_j^{(k)}(x) = (ic)^k \int_{-1}^1 e^{icxt} t^k \psi_j(t) dt. \quad (146)$$

We next consider the integral

$$f(x) = f(a, x) = \int_{-1}^1 \frac{e^{icxt}}{t-a} \psi_j(t) dt. \quad (147)$$

Differentiating (147) with respect to  $x$ , we have

$$\frac{d}{dx} f(a, x) = ic \int_{-1}^1 \frac{te^{icxt}}{t-a} \psi_j(t) dt. \quad (148)$$

Multiplying (147) by  $ica$ , and subtracting it from (148), we obtain

$$\begin{aligned} \frac{d}{dx} f(a, x) - ica f(a, x) &= ic \int_{-1}^1 e^{icxt} \psi_j(t) dt \\ &= ic \lambda_j \psi_j(x). \end{aligned} \quad (149)$$

In other words,  $f$  satisfies the differential equation

$$f'(x) - ica f(x) = ic \lambda_j \psi_j(x). \quad (150)$$

The standard "variation of parameter" calculation provides the solution to (150):

$$f(x) = ic \lambda_j \int_0^x e^{-ica(x-t)} \psi_j(t) dt + f(0) e^{icax}. \quad (151)$$

Introducing the notation

$$\mathcal{D} = \frac{1}{ic} \circ \frac{d}{dx} \quad (152)$$

(i.e.  $\mathcal{D}$  is the product of multiplication by  $1/ic$  and differentiation), we rewrite (146) as

$$\mathcal{D}^k(\psi_j)(x) = \frac{1}{\lambda_j} \int_{-1}^1 t^k e^{icxt} \psi_j(t) dt; \quad (153)$$

for an arbitrary polynomial  $P$  (with real or complex coefficients),

$$P(\mathcal{D})(\psi_j)(x) = \frac{1}{\lambda_j} \int_{-1}^1 P(t) e^{icxt} \psi_j(t) dt. \quad (154)$$

By the same token, the function  $\phi$  defined by the formula

$$\phi(x) = \int_{-1}^1 \frac{e^{icxt}}{P(t)} \psi_j(t) dt \quad (155)$$

satisfies the differential equation

$$P(\mathcal{D})(\phi)(x) = \lambda_m \psi_m(x). \quad (156)$$

The following lemma provides a recursion connecting the values of the  $k$ -th derivative of the function  $\psi_m$  with its derivatives of orders  $k-1$ ,  $k-2$ ,  $k-3$ ,  $k-4$ .

**Lemma 9.1** *For any positive real  $c$ , integer  $m \geq 0$ , and  $x \in (-\infty, +\infty)$ ,*

$$\begin{aligned} & (1-x^2) \psi_m^{(k+2)}(x) - 2(k+1)x \psi_m^{(k+1)}(x) \\ & + (\chi_m - k(k+1) - c^2 x^2) \psi_m^{(k)}(x) \\ & - 2c^2 k x \psi_m^{(k-1)}(x) - c^2 k(k-1) \psi_m^{(k-2)}(x) = 0 \end{aligned} \quad (157)$$

for all  $k \geq 2$ . Furthermore,

$$\begin{aligned} & (1-x^2) \psi_m'''(x) - 4x \psi_m''(x) + (\chi_m - 2 - c^2 x^2) \psi_m'(x) \\ & - 2c^2 x \psi_m(x) = 0. \end{aligned} \quad (158)$$

In particular,

$$\begin{aligned} & -2(k+1) \psi_m^{(k+1)}(1) + (\chi_m - k(k+1) - c^2) \psi_m^{(k)}(1) \\ & - 2c^2 k \psi_m^{(k-1)}(1) - c^2 k(k-1) \psi_m^{(k-2)}(1) = 0 \end{aligned} \quad (159)$$

for all  $k \geq 2$ , and

$$-2 \psi_m'(1) + (\chi_m - c^2) \psi_m(1) = 0, \quad (160)$$

$$-4 \psi_m''(1) + (\chi_m - 2 - c^2) \psi_m'(1) - 2c^2 \psi_m(1) = 0. \quad (161)$$

Furthermore, for all integer  $m \geq 0$  and  $k \geq 2$ ,

$$\begin{aligned} \psi_m^{(k+2)}(0) + (\chi_m - k(k+1)) \psi_m^{(k)}(0) \\ - c^2 k(k-1) \psi_m^{(k-2)}(0) = 0. \end{aligned} \quad (162)$$

For all odd  $m$ ,

$$\psi_m'''(0) + (\chi_m - 2) \psi_m'(0) = 0, \quad (163)$$

and for all even  $m$ ,

$$\psi_m''(0) + \chi_m \psi_m(0) = 0. \quad (164)$$

Finally, for all integer  $m \geq 0$ ,  $k \geq 0$ ,

$$\psi_m(1) \neq 0, \quad (165)$$

$$\psi_{2m+1}^{(2k)}(0) = 0, \quad (166)$$

$$\psi_{2m}^{(2k+1)}(0) = 0. \quad (167)$$

**Proof.** All of the identities (157) – (164), (166), (167), are immediately obtained by repeated differentiation of (24).

In order to prove (165), we assume that

$$\psi_m(1) = 0 \quad (168)$$

for some integer  $m \geq 0$ , and observe that the combination of (168) with (159), (160), (161) implies that

$$\psi_m^{(k)}(1) = 0 \quad (169)$$

for all  $k = 0, 1, 2, \dots$ . Due to the analyticity of  $\psi_m(x)$  in the complex plane, this would imply that

$$\psi_m(x) = 0 \quad (170)$$

for all  $x \in \mathbb{R}^1$ .

□

The following is an immediate consequence of the identity (160) of Lemma 9.1.

**Corollary 9.2** For all integer  $m, n \geq 0$ ,

$$\psi_m'(1) \cdot \psi_n(1) - \psi_n'(1) \cdot \psi_m(1) = (\chi_n - \chi_m) \cdot \psi_n(1) \cdot \psi_m(1), \quad (171)$$

where  $\chi_m, \chi_n \in \mathbb{R}$  are as defined in Theorem 2.6.

Theorem 3.1, in Section 3.1, gives formulae for the entries of matrices for differentiation of prolate series and for multiplication of prolate series by  $x$ . Matrices for any combination of differentiation and of multiplication by a polynomial can obviously be constructed from these two matrices; for instance, calling the differentiation matrix  $D$ , and the multiplication-by- $x$  matrix  $X$ , the matrix for taking the second derivative of a prolate series, then multiplying it by  $5 - x^2$ , is equal to  $(5I - X^2)D^2$ .

In many cases, however, there are simpler formulae for the entries of such matrices, that is, for inner products of  $\psi_j(x)$  with its derivatives and with polynomials. The following theorems establish several such formulae, as well as a few formulae for inner products which do not involve  $\psi_j(x)$  itself but only its derivatives. We start with Theorem 3.1, restated here for consistency.

**Theorem 9.3** *Suppose that  $c$  is real and positive, and that the integers  $m$  and  $n$  are non-negative. If  $m = n \pmod{2}$ , then*

$$\int_{-1}^1 \psi_n'(x) \psi_m(x) dx = \int_{-1}^1 x \psi_n(x) \psi_m(x) dx = 0. \quad (172)$$

*If  $m \neq n \pmod{2}$ , then*

$$\int_{-1}^1 \psi_n'(x) \psi_m(x) dx = \frac{2\lambda_m^2}{\lambda_m^2 + \lambda_n^2} \psi_m(1) \psi_n(1), \quad (173)$$

$$\int_{-1}^1 x \psi_n(x) \psi_m(x) dx = \frac{2}{ic} \frac{\lambda_m \lambda_n}{\lambda_m^2 + \lambda_n^2} \psi_m(1) \psi_n(1). \quad (174)$$

**Theorem 9.4** *Suppose that  $c$  is real and positive, and that the integers  $m$  and  $n$  are non-negative. If  $m \neq n \pmod{2}$ , then*

$$\int_{-1}^1 x \psi_n'(x) \psi_m(x) dx = 0. \quad (175)$$

*If  $m = n \pmod{2}$ , then*

$$\int_{-1}^1 x \psi_n'(x) \psi_m(x) dx = \frac{\lambda_m}{\lambda_m + \lambda_n} (2\psi_m(1) \psi_n(1) - \delta_{mn}). \quad (176)$$

**Proof.** Identity (175) is obvious since the functions  $\psi_j$  are alternately even and odd (see Theorem 2.4). In order to prove (176), we consider the integral

$$\begin{aligned} & \int_{-1}^1 x \psi_n'(x) \psi_m(x) dx \\ &= \frac{1}{\lambda_n} \int_{-1}^1 x \left( \int_{-1}^1 e^{icxt} \psi_n(t) dt \right)'_x \psi_m(x) dx \end{aligned}$$

$$\begin{aligned}
&= \frac{ic}{\lambda_n} \int_{-1}^1 x \psi_m(x) \left( \int_{-1}^1 t \psi_n(t) e^{icxt} dt \right) dx \\
&= \frac{ic}{\lambda_n} \int_{-1}^1 t \left( \int_{-1}^1 x \psi_m(x) e^{icxt} dx \right) \psi_n(t) dt \\
&= \frac{\lambda_m}{\lambda_n} \int_{-1}^1 t \psi'_m(t) \psi_n(t) dt.
\end{aligned}$$

In other words,

$$\int_{-1}^1 x \psi'_n(x) \psi_m(x) dx = \frac{\lambda_m}{\lambda_n} \int_{-1}^1 x \psi'_m(x) \psi_n(x) dx. \quad (177)$$

On the other hand, integrating the left side of (177) by parts, we obtain

$$\begin{aligned}
&\int_{-1}^1 x \psi'_n(x) \psi_m(x) dx \\
&= 2\psi_m(1)\psi_n(1) - \int_{-1}^1 (\psi_n(x)\psi'_m(x)x + \psi_n(x)\psi_m(x)) dx \\
&= 2\psi_m(1)\psi_n(1) - \int_{-1}^1 x\psi_n(x)\psi'_m(x) dx - \delta_{mn}.
\end{aligned}$$

Combining (177) and (178), we have

$$\begin{aligned}
&\frac{\lambda_m}{\lambda_n} \int_{-1}^1 x \psi'_m(x) \psi_n(x) dx \\
&= 2\psi_m(1)\psi_n(1) - \int_{-1}^1 x \psi'_m(x) \psi_n(x) dx - \delta_{mn},
\end{aligned}$$

from which (176) follows directly.  $\square$

**Theorem 9.5** *Suppose that  $c$  is real and positive, and that the integers  $m$  and  $n$  are non-negative. If  $m \not\equiv n \pmod{2}$ , then*

$$\int_{-1}^1 x^2 \psi''_n(x) \psi_m(x) dx = 0. \quad (178)$$

*If  $m \equiv n \pmod{2}$  and  $m \neq n$ , then*

$$\begin{aligned}
&\int_{-1}^1 x^2 \psi''_m(x) \psi_n(x) dx \\
&= \frac{2\lambda_n}{\lambda_m - \lambda_n} (\psi'_n(1)\psi_m(1) - \psi'_m(1)\psi_n(1)) \\
&\quad - \frac{4\lambda_n}{\lambda_n + \lambda_m} \psi_n(1)\psi_m(1)
\end{aligned} \quad (179)$$

$$\begin{aligned}
&= \frac{\lambda_n}{\lambda_m - \lambda_n} (\chi_n - \chi_m) \psi_n(1) \psi_m(1) \\
&\quad - \frac{4\lambda_n}{\lambda_n + \lambda_m} \psi_n(1) \psi_m(1),
\end{aligned} \tag{180}$$

where  $\chi_m, \chi_n \in \mathbb{R}$  are as defined in Theorem 2.6.

**Proof.** Clearly (178) is true, since the functions  $\psi_j$  are alternately even and odd. In order to prove (179) and (180), supposing that  $m = n \pmod{2}$  and  $m \neq n$ , we consider the integral

$$\begin{aligned}
&\int_{-1}^1 x^2 \psi_n''(x) \psi_m(x) dx \\
&= \frac{1}{\lambda_n} \int_{-1}^1 x^2 \cdot \left( \int_{-1}^1 e^{icxt} \psi_n(t) dt \right)''_x \psi_m(x) dx \\
&= -\frac{c^2}{\lambda_n} \int_{-1}^1 \psi_m(x) x^2 \cdot \left( \int_{-1}^1 t^2 \psi_n(t) e^{icxt} dt \right) dx \\
&= -\frac{c^2}{\lambda_n} \int_{-1}^1 \left( \int_{-1}^1 \psi_m(x) x^2 e^{icxt} dx \right) \psi_n(t) t^2 dt \\
&= \frac{\lambda_m}{\lambda_n} \int_{-1}^1 t^2 \psi_n(t) \psi_m''(t) dt,
\end{aligned}$$

which is summarized as

$$\int_{-1}^1 x^2 \psi_n''(x) \psi_m(x) dx = \frac{\lambda_m}{\lambda_n} \int_{-1}^1 x^2 \psi_m''(x) \psi_n(x) dx. \tag{181}$$

On the other hand, integrating the left side of (181) by parts, we have

$$\begin{aligned}
&\int_{-1}^1 x^2 \psi_n''(x) \psi_m(x) dx \\
&= 2\psi_n'(1) \psi_m(1) - \int_{-1}^1 \psi_n'(x) (\psi_m'(x) x^2 + 2x \psi_m(x)) dx \\
&= 2\psi_n'(1) \psi_m(1) - 2 \int_{-1}^1 \psi_n'(x) \psi_m(x) x dx \\
&\quad - \int_{-1}^1 \psi_n'(x) \psi_m'(x) x^2 dx.
\end{aligned} \tag{182}$$

Due to Theorem 9.4 and the fact that  $m \neq n$ , we immediately rewrite (182) as

$$\begin{aligned}
&\int_{-1}^1 x^2 \psi_n''(x) \psi_m(x) dx \\
&= 2\psi_n'(1) \psi_m(1) - \frac{2\lambda_m}{\lambda_m + \lambda_n} 2\psi_n(1) \psi_m(1) \\
&\quad - \int_{-1}^1 x^2 \psi_n'(x) \psi_m'(x) dx,
\end{aligned} \tag{183}$$

which we rewrite as

$$\begin{aligned}
& \int_{-1}^1 x^2 \psi'_n(x) \psi'_m(x) dx \\
&= 2 \psi'_n(1) \psi_m(1) - \frac{4 \lambda_m}{\lambda_m + \lambda_n} \psi_n(1) \psi_m(1) \\
&\quad - \int_{-1}^1 x^2 \psi''_n(x) \psi_m(x) dx.
\end{aligned} \tag{184}$$

Swapping  $m$  with  $n$ , we convert (184) into

$$\begin{aligned}
& \int_{-1}^1 x^2 \psi'_n(x) \psi'_m(x) dx \\
&= 2 \psi'_m(1) \psi_n(1) - \frac{4 \lambda_n}{\lambda_m + \lambda_n} \psi_n(1) \psi_m(1) \\
&\quad - \int_{-1}^1 x^2 \psi''_m(x) \psi_n(x) dx.
\end{aligned} \tag{185}$$

Combining (184) and (185), we obtain

$$\begin{aligned}
& \int_{-1}^1 x^2 \psi''_n(x) \psi_m(x) dx - 2 \psi'_n(1) \psi_m(1) + \frac{4 \lambda_m}{\lambda_m + \lambda_n} \psi_n(1) \psi_m(1) \\
&= \int_{-1}^1 x^2 \psi''_m(x) \psi_n(x) dx - 2 \psi'_m(1) \psi_n(1) + \frac{4 \lambda_n}{\lambda_m + \lambda_n} \psi_n(1) \psi_m(1),
\end{aligned} \tag{186}$$

which is obviously equivalent to

$$\begin{aligned}
& \int_{-1}^1 x^2 \psi''_n(x) \psi_m(x) dx \\
&= \int_{-1}^1 x^2 \psi''_m(x) \psi_n(x) dx + 2 (\psi'_n(1) \psi_m(1) - \psi'_m(1) \psi_n(1)) \\
&\quad + 4 \frac{\lambda_n - \lambda_m}{\lambda_n + \lambda_m} \psi_n(1) \psi_m(1).
\end{aligned}$$

Finally, combining (181) with (187), we have

$$\begin{aligned}
& \frac{\lambda_m}{\lambda_n} \int_{-1}^1 x^2 \psi''_m(x) \psi_n(x) dx \\
&= \int_{-1}^1 x^2 \psi''_m(x) \psi_n(x) dx + 2 (\psi'_n(1) \psi_m(1) - \psi'_m(1) \psi_n(1)) \\
&\quad + 4 \frac{\lambda_n - \lambda_m}{\lambda_n + \lambda_m} \psi_n(1) \psi_m(1),
\end{aligned} \tag{187}$$

which is easily rewritten as

$$\begin{aligned} & \left( \frac{\lambda_m}{\lambda_n} - 1 \right) \int_{-1}^1 x^2 \psi_m''(x) \psi_n(x) dx \\ &= 2 (\psi_n'(1) \psi_m(1) - \psi_m'(1) \psi_n(1)) \\ & \quad + 4 \frac{\lambda_n - \lambda_m}{\lambda_n + \lambda_m} \psi_n(1) \psi_m(1), \end{aligned}$$

or

$$\begin{aligned} & \int_{-1}^1 x^2 \psi_m''(x) \psi_n(x) dx \\ &= \frac{2 \lambda_n}{\lambda_m - \lambda_n} (\psi_n'(1) \psi_m(1) - \psi_m'(1) \psi_n(1)) \\ & \quad - \frac{4 \lambda_n}{\lambda_n + \lambda_m} \psi_n(1) \psi_m(1). \end{aligned} \tag{188}$$

We finally rewrite (188) as (180) using Corollary 9.2.  $\square$

The following theorem is an immediate consequence of combining the preceding theorem with equation (184) from its proof.

**Theorem 9.6** *Suppose that  $c$  is real and positive, and that the integers  $m$  and  $n$  are non-negative. If  $m \not\equiv n \pmod{2}$ , then*

$$\int_{-1}^1 x^2 \psi_n'(x) \psi_m'(x) dx = 0. \tag{189}$$

If  $m \equiv n \pmod{2}$  and  $m \neq n$ ,

$$\begin{aligned} & \int_{-1}^1 x^2 \psi_m'(x) \psi_n'(x) dx \\ &= 2 \psi_m'(1) \psi_n(1) + \frac{2 \lambda_n}{\lambda_m - \lambda_n} (\psi_m'(1) \psi_n(1) - \psi_n'(1) \psi_m(1)) \end{aligned} \tag{190}$$

$$= 2 \psi_n'(1) \psi_m(1) + \frac{2 \lambda_m}{\lambda_n - \lambda_m} (\psi_n'(1) \psi_m(1) - \psi_m'(1) \psi_n(1)) \tag{191}$$

$$= \psi_m(1) \psi_n(1) \left( \frac{\lambda_m \lambda_m - \lambda_n \lambda_n}{\lambda_m - \lambda_n} - c^2 \right). \tag{192}$$

**Theorem 9.7** *Suppose that  $c$  is real and positive, and that the integers  $m$  and  $n$  are non-negative. If  $m \not\equiv n \pmod{2}$ , then*

$$\int_{-1}^1 \psi_n(x) \psi_m''(x) dx = \int_{-1}^1 x^2 \psi_n(x) \psi_m(x) dx = 0 \tag{193}$$

If  $m = n \pmod{2}$  and  $m \neq n$ , then

$$\begin{aligned} & \int_{-1}^1 \psi_n(x) \psi_m''(x) dx \\ &= \frac{2\lambda_n^2}{\lambda_m^2 - \lambda_n^2} (\psi_n'(1) \psi_m(1) - \psi_n(1) \psi_m'(1)) \end{aligned} \quad (194)$$

$$= \frac{\lambda_n^2}{\lambda_m^2 - \lambda_n^2} (\chi_n - \chi_m) \psi_m(1) \psi_n(1), \quad (195)$$

$$\begin{aligned} & \int_{-1}^1 x^2 \psi_n(x) \psi_m(x) dx \\ &= -\frac{2}{c^2} \frac{\lambda_m \lambda_n}{\lambda_m^2 - \lambda_n^2} (\psi_n'(1) \psi_m(1) - \psi_n(1) \psi_m'(1)) \end{aligned} \quad (196)$$

$$= -\frac{1}{c^2} \frac{\lambda_m \lambda_n}{\lambda_m^2 - \lambda_n^2} (\chi_n - \chi_m) \psi_m(1) \psi_n(1), \quad (197)$$

where  $\chi_m, \chi_n \in \mathbb{R}$  are as defined in Theorem 2.6.

**Proof.** Identity (193) is obvious, since the functions  $\psi_j$  are alternately even and odd. In order to prove (194)–(197), we start with the expression

$$\lambda_n \psi_n''(x) = -c^2 \int_{-1}^1 t^2 e^{icxt} \psi_n(t) dt. \quad (198)$$

Taking the inner product of (198) with  $\psi_m(x)$ , we have

$$\begin{aligned} & \lambda_n \int_{-1}^1 \psi_n''(x) \psi_m(x) dx \\ &= -c^2 \int_{-1}^1 \left( \int_{-1}^1 t^2 \psi_n(t) e^{icxt} dt \right) \psi_m(x) dx \\ &= -c^2 \int_{-1}^1 t^2 \psi_n(t) \left( \int_{-1}^1 \psi_m(x) e^{icxt} dx \right) dt \\ &= -c^2 \lambda_m \int_{-1}^1 t^2 \psi_n(t) \psi_m(t) dt, \end{aligned}$$

which we summarize as

$$\int_{-1}^1 x^2 \psi_n(x) \psi_m(x) dx = -\frac{1}{c^2} \frac{\lambda_n}{\lambda_m} \int_{-1}^1 \psi_n''(x) \psi_m(x) dx. \quad (199)$$

Swapping  $n, m$ , we rewrite (199) in the form of

$$\begin{aligned} & \int_{-1}^1 x^2 \psi_n(x) \psi_m(x) dx \\ &= -\frac{1}{c^2} \frac{\lambda_m}{\lambda_n} \int_{-1}^1 \psi_m''(x) \psi_n(x) dx. \end{aligned} \quad (200)$$

Combining (199) and (200), we get

$$\int_{-1}^1 \psi_n''(x) \psi_m(x) dx = \frac{\lambda_m^2}{\lambda_n^2} \int_{-1}^1 \psi_m''(x) \psi_n(x) dx. \quad (201)$$

On the other hand, integrating the left side of (201) by parts, we have

$$\begin{aligned} & \int_{-1}^1 \psi_n''(x) \psi_m(x) dx \\ &= \psi_n'(1) \psi_m(1) - \psi_n'(-1) \psi_m(-1) - \int_{-1}^1 \psi_n'(x) \psi_m'(x) dx \\ &= 2 \psi_n'(1) \psi_m(1) - (\psi_n(1) \psi_m'(1) - \psi_n(-1) \psi_m'(-1)) \\ & \quad + \int_{-1}^1 \psi_n(x) \psi_m''(x) dx. \end{aligned} \quad (202)$$

We rewrite (202) in the form of

$$\begin{aligned} & \int_{-1}^1 \psi_n''(x) \psi_m(x) dx \\ &= 2 (\psi_n'(1) \psi_m(1) - \psi_n(1) \psi_m'(1)) + \int_{-1}^1 \psi_n(x) \psi_m''(x) dx. \end{aligned}$$

We combine (201) and (203) and get

$$\begin{aligned} & \left( \frac{\lambda_m^2}{\lambda_n^2} - 1 \right) \int_{-1}^1 \psi_n(x) \psi_m''(x) dx \\ &= 2 (\psi_n'(1) \psi_m(1) - \psi_n(1) \psi_m'(1)). \end{aligned} \quad (203)$$

Since  $m \neq n$ , we easily rewrite (203) as (194). We obtain expression (196) by combining (200) and (194). The identities (195), (197) follow from (194), (196) immediately due to Corollary 9.2.  $\square$

**Theorem 9.8** *Suppose that  $c$  is real and positive, and that the integers  $m$  and  $n$  are non-negative. Let*

$$\Psi_n(y) = \int_0^y \psi_n(x) dx. \quad (204)$$

*If  $n$  is odd and  $m$  is even, then*

$$\int_{-1}^1 \frac{1}{t} \psi_n(t) \psi_m(t) dt \quad (205)$$

$$= ic \frac{2 \lambda_m \lambda_n}{\lambda_n^2 + \lambda_m^2} \Psi_n(1) \Psi_m(1) \quad (206)$$

$$+ 2 \frac{\lambda_m}{\lambda_n^2 + \lambda_m^2} \Psi_m(1) \int_{-1}^1 \frac{1}{t} \psi_n(t) dt. \quad (207)$$

If  $m = n \pmod{2}$ , then

$$\int_{-1}^1 \frac{1}{t} \psi_n(t) \psi_m(t) dt = 0. \quad (208)$$

**Proof.** We start with the identity

$$\lambda_n \psi_n(x) = \int_{-1}^1 e^{icxt} \psi_n(t) dt. \quad (209)$$

Integrating (209) with respect to  $x$ , we have

$$\begin{aligned} \lambda_n \int_0^y \psi_n(x) dx \\ &= \int_0^y \left( \int_{-1}^1 e^{icxt} \psi_n(t) dt \right) dx \end{aligned} \quad (210)$$

$$= \int_{-1}^1 \psi_n(t) \int_0^y e^{icxt} dx dt \quad (211)$$

$$= \frac{1}{ic} \int_{-1}^1 \frac{1}{t} \psi_n(t) e^{icyt} dt - \frac{1}{ic} \int_{-1}^1 \frac{1}{t} \psi_n(t) dt, \quad (212)$$

which we summarize as

$$\lambda_n \Psi_n(y) = \frac{1}{ic} \int_{-1}^1 \frac{1}{t} \psi_n(t) e^{icyt} dt - \frac{1}{ic} \int_{-1}^1 \frac{1}{t} \psi_n(t) dt. \quad (213)$$

Taking the inner product of (213) and  $\psi_m(y)$ , we obtain

$$\begin{aligned} \lambda_n \int_{-1}^1 \Psi_n(y) \psi_m(y) dy \\ &= \frac{1}{ic} \int_{-1}^1 \psi_m(y) \cdot \left( \int_{-1}^1 \frac{1}{t} \psi_n(t) e^{icyt} dt \right) dy \\ &\quad - \frac{1}{ic} \int_{-1}^1 \psi_m(y) \cdot \left( \int_{-1}^1 \frac{1}{t} \psi_n(t) dt \right) dy \end{aligned} \quad (214)$$

$$\begin{aligned} &= \frac{1}{ic} \int_{-1}^1 \frac{1}{t} \psi_n(t) \cdot \left( \int_{-1}^1 e^{icyt} \psi_m(y) dy \right) dt \\ &\quad - \frac{1}{ic} \int_{-1}^1 \frac{1}{t} \psi_n(t) dt \cdot \int_{-1}^1 \psi_m(y) dy \end{aligned} \quad (215)$$

$$\begin{aligned} &= \frac{\lambda_m}{ic} \int_{-1}^1 \frac{1}{t} \psi_n(t) \psi_m(t) dt \\ &\quad - \frac{1}{ic} \int_{-1}^1 \frac{1}{t} \psi_n(t) dt \cdot \int_{-1}^1 \psi_m(y) dy, \end{aligned} \quad (216)$$

which we summarize as

$$\begin{aligned}
& \int_{-1}^1 \frac{1}{t} \psi_n(t) \psi_m(t) dt \\
&= ic \frac{\lambda_n}{\lambda_m} \int_{-1}^1 \Psi_n(t) \psi_m(t) dt \\
&\quad + \frac{1}{\lambda_m} \int_{-1}^1 \frac{1}{t} \psi_n(t) dt \cdot \int_{-1}^1 \psi_m(y) dy
\end{aligned} \tag{217}$$

Exchanging  $m$  with  $n$ , we convert (217) into

$$\begin{aligned}
& \int_{-1}^1 \frac{1}{t} \psi_m(t) \psi_n(t) dt \\
&= ic \frac{\lambda_m}{\lambda_n} \int_{-1}^1 \Psi_m(t) \psi_n(t) dt \\
&\quad + \frac{1}{\lambda_n} \int_{-1}^1 \frac{1}{t} \psi_m(t) dt \cdot \int_{-1}^1 \psi_n(y) dy,
\end{aligned} \tag{218}$$

and combining (217), (218), we get

$$\begin{aligned}
& \frac{\lambda_n}{\lambda_m} ic \int_{-1}^1 \Psi_n(t) \psi_m(t) dt - \frac{\lambda_m}{\lambda_n} ic \int_{-1}^1 \Psi_m(t) \psi_n(t) dt \\
&= \frac{1}{\lambda_n} \int_{-1}^1 \frac{1}{t} \psi_m(t) dt \cdot \int_{-1}^1 \psi_n(t) dt \\
&\quad - \frac{1}{\lambda_m} \int_{-1}^1 \frac{1}{t} \psi_n(t) dt \cdot \int_{-1}^1 \psi_m(t) dt.
\end{aligned} \tag{219}$$

Suppose that  $m$  is even and  $n$  is odd; then the first product in the right hand side of (219) is zero, so

$$\begin{aligned}
& \frac{\lambda_n}{\lambda_m} ic \int_{-1}^1 \Psi_n(t) \psi_m(t) dt - \frac{\lambda_m}{\lambda_n} ic \int_{-1}^1 \Psi_m(t) \psi_n(t) dt \\
&= -\frac{1}{\lambda_m} \int_{-1}^1 \frac{1}{t} \psi_n(t) dt \cdot \int_{-1}^1 \psi_m(t) dt,
\end{aligned} \tag{220}$$

which is equivalent to

$$\begin{aligned}
& \int_{-1}^1 \Psi_n(t) \psi_m(t) dt \\
&= \frac{\lambda_m^2}{\lambda_n^2} \int_{-1}^1 \Psi_m(t) \psi_n(t) dt \\
&\quad - \frac{1}{\lambda_n} \frac{1}{ic} \int_{-1}^1 \frac{1}{t} \psi_n(t) dt \cdot \int_{-1}^1 \psi_m(t) dt,
\end{aligned} \tag{221}$$

or

$$\begin{aligned}
& \int_{-1}^1 \Psi_m(t) \psi_n(t) dt \\
&= \frac{\lambda_n^2}{\lambda_m^2} \int_{-1}^1 \Psi_n(t) \psi_m(t) dt \\
&\quad + \frac{\lambda_n}{\lambda_m^2} \frac{1}{ic} \int_{-1}^1 \frac{1}{t} \psi_n(t) dt \cdot \int_{-1}^1 \psi_m(t) dt.
\end{aligned} \tag{222}$$

On the other hand, integrating the left side of (222) by parts, we obtain

$$\begin{aligned}
& \int_{-1}^1 \Psi_m(t) \psi_n(t) dt \\
&= \Psi_n(1) \Psi_m(1) - \Psi_n(-1) \Psi_m(-1) - \int_{-1}^1 \Psi_n(t) \psi_m(t) dt.
\end{aligned} \tag{223}$$

Since the product  $\Psi_m(x) \Psi_n(x)$  is an odd function when  $m \neq n \pmod{2}$ , we rewrite (223) as

$$\begin{aligned}
& \int_{-1}^1 \Psi_m(t) \psi_n(t) dt \\
&= 2 \Psi_n(1) \Psi_m(1) - \int_{-1}^1 \Psi_n(t) \psi_m(t) dt.
\end{aligned} \tag{224}$$

The combination of (222) and (224) implies that

$$\begin{aligned}
& \int_{-1}^1 \Psi_n(t) \psi_m(t) dt + \frac{\lambda_n^2}{\lambda_m^2} \int_{-1}^1 \Psi_n(t) \psi_m(t) dt \\
&= 2 \Psi_n(1) \Psi_m(1) - \frac{\lambda_n}{\lambda_m^2} \frac{1}{ic} \int_{-1}^1 \frac{1}{t} \psi_n(t) dt \cdot \int_{-1}^1 \psi_m(t) dt,
\end{aligned} \tag{225}$$

or

$$\begin{aligned}
& \frac{\lambda_m^2 + \lambda_n^2}{\lambda_m^2} \int_{-1}^1 \Psi_n(t) \psi_m(t) dt \\
&= 2 \Psi_n(1) \Psi_m(1) - \frac{\lambda_n}{\lambda_m^2} \frac{1}{ic} \int_{-1}^1 \frac{1}{t} \psi_n(t) dt \cdot \int_{-1}^1 \psi_m(t) dt,
\end{aligned} \tag{226}$$

which is equivalent to

$$\begin{aligned}
& \int_{-1}^1 \Psi_n(t) \psi_m(t) dt \\
&= \frac{2 \lambda_m^2}{\lambda_n^2 + \lambda_m^2} \Psi_n(1) \Psi_m(1) \\
&\quad - \frac{\lambda_n}{\lambda_n^2 + \lambda_m^2} \frac{1}{ic} \int_{-1}^1 \frac{1}{t} \psi_n(t) dt \cdot \int_{-1}^1 \psi_m(t) dt.
\end{aligned} \tag{227}$$

Finally, combining (217) and (227), we have

$$\begin{aligned} & \int_{-1}^1 \frac{1}{t} \psi_n(t) \psi_m(t) dt \\ &= ic \frac{2 \lambda_m \lambda_n}{\lambda_n^2 + \lambda_m^2} \Psi_n(1) \Psi_m(1) \\ & \quad + \frac{\lambda_m}{\lambda_n^2 + \lambda_m^2} \int_{-1}^1 \frac{1}{t} \psi_n(t) dt \cdot \int_{-1}^1 \psi_m(t) dt. \end{aligned} \quad (228)$$

Equation (208) is easily proven since the product  $\frac{1}{t} \psi_m(x) \psi_n(x)$  is an odd function whenever  $m = n \pmod{2}$ .  $\square$

The above theorems do not use much of the detailed structure of the integral operators of which the functions  $\{\psi_j\}$  are eigenfunctions. Thus many of them generalize easily to the case of an operator  $L : L^2[0, 1] \rightarrow L^2[0, 1]$  defined via the formula

$$L(\psi)(x) = \int_0^1 K(xt) \psi(t) dt, \quad (229)$$

for some function  $K : [0, 1] \rightarrow \mathbb{C}$ ; the following theorem is an example of this.

**Theorem 9.9** *Let  $\lambda_1, \lambda_2$  be two eigenvalues of the operator  $L$  defined by (229), that is,*

$$\int_0^1 K(xt) \psi_1(t) dt = \lambda_1 \psi_1(x), \quad (230)$$

$$\int_0^1 K(xt) \psi_2(t) dt = \lambda_2 \psi_2(x). \quad (231)$$

Then

$$\frac{\lambda_2}{\lambda_1} = \frac{\int_0^1 x \psi_1'(x) \psi_2(x) dx}{\int_0^1 x \psi_2'(x) \psi_1(x) dx}, \quad (232)$$

provided that neither  $\lambda_1$  nor the denominator of the right hand side of (232) is zero.

**Proof.** Differentiating (230), (231) with respect to  $x$ , we get

$$\int_0^1 t K'(xt) \psi_1(t) dt = \lambda_1 \psi_1'(x), \quad (233)$$

$$\int_0^1 t K'(xt) \psi_2(t) dt = \lambda_2 \psi_2'(x). \quad (234)$$

Multiplying (233) by  $x \psi_2(x)$ , we have

$$\lambda_1 x \psi_1'(x) \psi_2(x) = x \psi_2(x) \int_0^1 t K'(xt) \psi_1(t) dt. \quad (235)$$

Integrating on the interval  $[0, 1]$ , we obtain

$$\lambda_1 \int_0^1 x \psi_1'(x) \psi_2(x) dx = \int_0^1 x \psi_2(x) \int_0^1 t K'(xt) \psi_1(t) dt dx \quad (236)$$

$$= \int_0^1 t \psi_1(t) \int_0^1 x K'(xt) \psi_2(x) dx dt. \quad (237)$$

Renaming the variables of integration on the right hand side from  $x$  to  $t$  and vice versa, we get

$$\lambda_1 \int_0^1 x \psi_1'(x) \psi_2(x) dx = \int_0^1 x \psi_1(x) \int_0^1 t K'(xt) \psi_2(t) dt dx. \quad (238)$$

Substituting (234) into (238), we obtain

$$\lambda_1 \int_0^1 x \psi_1'(x) \psi_2(x) dx = \lambda_2 \int_0^1 x \psi_1(x) \psi_2'(x) dx, \quad (239)$$

from which (232) follows immediately, as does its caveat.  $\square$

The following theorem establishes the relation between the norm of each function  $\psi_j$  on  $[-1, 1]$  (which in this paper is taken to be one), and its norm on  $(-\infty, \infty)$ .

**Theorem 9.10** *Suppose that  $c$  is real and positive, and that the integer  $n$  is non-negative. Then*

$$\int_{-\infty}^{\infty} \psi_n^2(x) dx = \frac{1}{\mu_n}. \quad (240)$$

where  $\mu_n$  is given by (21).

**Proof.**

$$\begin{aligned} \int_{-\infty}^{\infty} \psi_n^2(x) dx &= \int_{-\infty}^{\infty} \left( \frac{1}{\pi \mu_n} \int_{-1}^1 \psi_n(t) \frac{\sin(c \cdot (x-t))}{x-t} dt \right) \psi_n(x) dx \\ &= \frac{1}{\mu_n} \int_{-1}^1 \psi_n(t) \cdot \left( \frac{1}{\pi} \int_{-\infty}^{\infty} \frac{\sin(c \cdot (x-t))}{x-t} \psi_n(x) dx \right) dt \\ &= \frac{1}{\mu_n} \int_{-1}^1 \psi_n^2(t) dt \\ &= \frac{1}{\mu_n}. \end{aligned}$$

$\square$

The following theorem extends Theorem (9.10) to any band-limited function with band limit  $c$ .

**Theorem 9.11** Suppose that  $c$  is real and positive, that the integer  $n$  is non-negative, and that  $f : \mathbb{R} \rightarrow \mathbb{C}$  is a band-limited function with band limit  $c$ . Then

$$\int_{-\infty}^{\infty} \psi_n(x) f(x) dx = \frac{1}{\mu_n} \int_{-1}^1 \psi_n(x) f(x) dx. \quad (241)$$

**Proof.**

$$\begin{aligned} & \int_{-\infty}^{\infty} \psi_n(x) f(x) dx \\ &= \int_{-\infty}^{\infty} \left( \frac{1}{\pi \mu_n} \int_{-1}^1 \frac{\sin(c \cdot (x-t))}{x-t} \psi_n(t) dt \right) f(x) dx \\ &= \frac{1}{\mu_n} \int_{-1}^1 \psi_n(t) \cdot \left( \frac{1}{\pi} \int_{-\infty}^{\infty} \frac{\sin(c \cdot (x-t))}{x-t} f(x) dx \right) dt \\ &= \frac{1}{\mu_n} \int_{-1}^1 \psi_n(t) f(t) dt. \end{aligned}$$

□

**Theorem 9.12** Suppose that  $c$  is real and positive, and that the integer  $n$  is non-negative. Then

$$\int_{-\infty}^{\infty} e^{icxt} \psi_m(t) dt = \begin{cases} \frac{\lambda_m}{\mu_m} \psi_m(x), & \text{if } -1 < x < 1, \\ 0, & \text{if } x > 1 \text{ or } x < -1. \end{cases} \quad (242)$$

**Proof.** Since  $\psi_m$  is an eigenfunction of the operator  $Q_c$  defined in (19), and  $\mu_m$  is the corresponding eigenvalue,

$$\mu_m \psi_m(t) = \frac{1}{\pi} \int_{-1}^1 \frac{\sin(c \cdot (x-u))}{x-u} \psi_m(u) du. \quad (243)$$

Thus

$$\begin{aligned} & \int_{-\infty}^{\infty} e^{icxt} \psi_m(t) dt \\ &= \frac{1}{\mu_m} \int_{-\infty}^{\infty} e^{icxt} \left( \frac{1}{\pi} \int_{-1}^1 \frac{\sin(c \cdot (x-u))}{x-u} \psi_m(u) du \right) dt \end{aligned} \quad (244)$$

$$= \frac{1}{\mu_m} \int_{-1}^1 \psi_m(u) \left( \frac{1}{\pi} \int_{-\infty}^{\infty} \frac{\sin(c \cdot (x-u))}{x-u} e^{icxt} dt \right) du \quad (245)$$

Since the innermost integral is the orthogonal projection operator onto the space of functions of band limit  $c$  on  $(-\infty, \infty)$ , applied to the function  $e^{icxt}$ , it follows that:

$$\begin{aligned} & \int_{-\infty}^{\infty} e^{icxt} \psi_m(t) dt \\ &= \frac{1}{\mu_m} \int_{-1}^1 \psi_m(u) \left( \begin{cases} e^{icxu}, & \text{if } -1 < x < 1, \\ 0, & \text{if } x > 1 \text{ or } x < -1 \end{cases} \right) du \end{aligned} \quad (246)$$

$$= \begin{cases} \frac{1}{\mu_m} \int_{-1}^1 \psi_m(u) e^{icxu} du, & \text{if } -1 < x < 1, \\ 0, & \text{if } x > 1 \text{ or } x < -1, \end{cases} \quad (247)$$

from which (242) follows immediately.  $\square$

The following five theorems establish formulae for the derivatives of prolate functions and their associated eigenvalues with respect to  $c$ .

**Theorem 9.13** *For all positive real  $c$  and non-negative integer  $m$ ,*

$$\frac{\partial \lambda_m}{\partial c} = \lambda_m \frac{2 \psi_m^2(1) - 1}{2c}. \quad (248)$$

**Proof.** We start with

$$\lambda_m \psi_m(x) = \int_{-1}^1 e^{icxt} \psi_m(t) dt. \quad (249)$$

Differentiating (249) with respect to  $c$ , we obtain

$$\begin{aligned} & \frac{\partial \lambda_m}{\partial c} \psi_m(x) + \lambda_m \frac{\partial \psi_m(x)}{\partial c} \\ &= \int_{-1}^1 i x t e^{icxt} \psi_m(t) dt + \int_{-1}^1 e^{icxt} \frac{\partial \psi_m(t)}{\partial c} dt. \end{aligned} \quad (250)$$

Multiplying by  $\psi_m(x)$  on both sides of (250), and integrating on the interval  $[-1, 1]$ , we get

$$\begin{aligned} & \int_{-1}^1 \psi_m(x) \left( \frac{\partial \lambda_m}{\partial c} \psi_m(x) + \lambda_m \frac{\partial \psi_m(x)}{\partial c} \right) dx \\ &= \int_{-1}^1 \psi_m(x) \int_{-1}^1 i x t e^{icxt} \psi_m(t) dt dx \\ & \quad + \int_{-1}^1 \psi_m(x) \int_{-1}^1 e^{icxt} \frac{\partial \psi_m(t)}{\partial c} dt dx, \end{aligned} \quad (251)$$

which we rewrite as

$$\begin{aligned}
& \frac{\partial \lambda_m}{\partial c} + \lambda_m \int_{-1}^1 \frac{\partial \psi_m(x)}{\partial c} \psi_m(x) dx \\
&= \int_{-1}^1 i t \psi_m(t) \int_{-1}^1 e^{icxt} x \psi_m(x) dx dt \\
&\quad + \int_{-1}^1 \frac{\partial \psi_m(t)}{\partial c} \int_{-1}^1 e^{icxt} \psi_m(x) dx dt
\end{aligned} \tag{252}$$

$$\begin{aligned}
&= \lambda_m \int_{-1}^1 i t \psi_m(t) \frac{1}{ic} \frac{\partial \psi_m(t)}{\partial t} dt \\
&\quad + \lambda_m \int_{-1}^1 \frac{\partial \psi_m(t)}{\partial c} \psi_m(t) dt,
\end{aligned} \tag{253}$$

which we summarize as

$$\frac{\partial \lambda_m}{\partial c} = \frac{\lambda_m}{c} \int_{-1}^1 t \psi_m(t) \frac{\partial \psi_m(t)}{\partial t} dt. \tag{254}$$

On the other hand, integrating the right-hand side of (254) by parts, we have

$$\begin{aligned}
& \int_{-1}^1 t \psi_m(t) \frac{\partial \psi_m(t)}{\partial t} dt \\
&= \psi_m^2(1) + \psi_m^2(-1) - 1 - \int_{-1}^1 \psi_m(t) t \frac{\partial \psi_m(t)}{\partial t} dt,
\end{aligned} \tag{255}$$

which we rewrite as

$$\int_{-1}^1 t \psi_m(t) \frac{\partial \psi_m(t)}{\partial t} dt = \psi_m^2(1) - \frac{1}{2}. \tag{256}$$

Finally, substituting (256) into (254), we get

$$\frac{\partial \lambda_m}{\partial c} = \lambda_m \frac{2 \psi_m^2(1) - 1}{2c}. \tag{257}$$

□

**Theorem 9.14** For any positive real  $c$  and non-negative integer  $m$ ,

$$\frac{\partial \mu_m}{\partial c} = \frac{2}{c} \mu_m \psi_m^2(1). \tag{258}$$

**Proof.** We start with the identity

$$\mu_m = \frac{2c}{\pi} \bar{\lambda}_m \lambda_m. \quad (259)$$

Differentiating (259) with respect to  $c$ , we get

$$\frac{\partial \mu_m}{\partial c} = \frac{2c}{\pi} \left( \bar{\lambda}_m \frac{\partial \lambda_m}{\partial c} + \lambda_m \frac{\partial \bar{\lambda}_m}{\partial c} \right) + \frac{2}{\pi} \bar{\lambda}_m \lambda_m. \quad (260)$$

Substituting Lemma 9.13 into (260), we get

$$\frac{\partial \mu_m}{\partial c} = \frac{2c}{\pi} \cdot 2 \bar{\lambda}_m \lambda_m \frac{2\psi_m^2(1) - 1}{2c} + \frac{2}{\pi} \bar{\lambda}_m \lambda_m \quad (261)$$

$$\begin{aligned} &= 2 \mu_m \frac{2\psi_m^2(1) - 1}{2c} + \frac{1}{c} \mu_m \\ &= \frac{2}{c} \mu_m \psi_m^2(1) - \frac{1}{c} \mu_m + \frac{1}{c} \mu_m \\ &= \frac{2}{c} \mu_m \psi_m^2(1). \end{aligned} \quad (262)$$

□

The following theorem immediately follows from Theorems 9.13 and 9.14.

**Theorem 9.15** For all positive real  $c$  and non-negative integer  $m, n$ ,

$$\left( \frac{\lambda_m}{\lambda_n} \right)' = \frac{\lambda_m}{\lambda_n} \frac{1}{c} (\psi_m^2(1) - \psi_n^2(1)), \quad (263)$$

$$\left( \frac{\mu_m}{\mu_n} \right)' = \frac{\mu_m}{\mu_n} \frac{2}{c} (\psi_m^2(1) - \psi_n^2(1)). \quad (264)$$

**Theorem 9.16** Suppose that  $c$  is real and positive, and the integers  $m, n$  are non-negative. If  $m \neq n$ , then

$$\int_{-1}^1 \psi_m(t) \frac{\partial \psi_n}{\partial c}(t) dt = -\frac{2}{c} \frac{\lambda_n \lambda_m}{\lambda_m^2 - \lambda_n^2} \psi_m(1) \psi_n(1). \quad (265)$$

If  $m = n$ , then

$$\int_{-1}^1 \psi_m(t) \frac{\partial \psi_n}{\partial c}(t) dt = 0. \quad (266)$$

**Proof.** Since the norm of  $\psi_n$  on  $[-1, 1]$  remains constant as  $c$  varies,  $\psi_n$  must be orthogonal on  $[-1, 1]$  to its own derivative with respect to  $c$ , which immediately yields (266). To establish (265), we start with the identity

$$\lambda_n \psi_n(x) = \int_{-1}^1 e^{icxt} \psi_n(t) dt. \quad (267)$$

Differentiating (267) with respect to  $c$ , we get

$$\begin{aligned} \frac{\partial \lambda_n}{\partial c} \psi_n(x) + \lambda_n \frac{\partial \psi_n}{\partial c} \\ = \int_{-1}^1 \left( i x t e^{icxt} \psi_n(t) + e^{icxt} \frac{\partial \psi_n(t)}{\partial c} \right) dt. \end{aligned} \quad (268)$$

Multiplying both sides of (268) by  $\psi_m(x)$  and integrating with respect to  $x$ , we have

$$\begin{aligned} \lambda_n \int_{-1}^1 \psi_m(x) \frac{\partial \psi_n(x)}{\partial c} dx \\ = \frac{\lambda_n}{c} \int_{-1}^1 x \psi_n'(x) \psi_m(x) dx + \lambda_m \int_{-1}^1 \psi_m(t) \frac{\partial \psi_n(t)}{\partial c} dt, \end{aligned} \quad (269)$$

which, using (176), we rewrite as

$$\begin{aligned} (\lambda_n - \lambda_m) \int_{-1}^1 \psi_m(t) \frac{\partial \psi_n(t)}{\partial c} dt \\ = \frac{\lambda_n}{c} \frac{\lambda_m}{\lambda_m + \lambda_n} (2 \psi_m(1) \psi_n(1) - \delta_{mn}). \end{aligned} \quad (270)$$

Assuming that  $m \neq n$ , and dividing by  $\lambda_n - \lambda_m$ , we then get (265).  $\square$

**Theorem 9.17** *Suppose that  $c$  is real and positive, and the integer  $m$  is non-negative. Then*

$$\frac{\partial \chi_m}{\partial c} = 2c \int_{-1}^1 x^2 \psi_m^2(x). \quad (271)$$

**Proof.** Due to Theorem 2.6,

$$(1 - x^2) \psi_m''(x) - 2x \psi_m'(x) + (\chi_m - c^2 x^2) \psi_m(x) = 0. \quad (272)$$

Making the infinitesimal changes  $c = c + h$ ,  $\chi_m = \chi_m + \varepsilon$ , and  $\psi_m(x) = \psi_m(x) + \delta(x)$ , this becomes

$$\begin{aligned} (1 - x^2) \cdot (\psi_m''(x) + \delta''(x)) - 2x \cdot (\psi_m'(x) + \delta'(x)) \\ + (\chi_m + \varepsilon - (c + h)^2 x^2) \cdot (\psi_m(x) + \delta(x)) = 0. \end{aligned} \quad (273)$$

Expanding each term, discarding infinitesimals of the second order or greater (that is, products of two or more of the quantities  $h$ ,  $\varepsilon$ , and  $\delta(x)$ ), and subtracting (272), we get

$$(1 - x^2) \delta''(x) - 2x\delta'(x) + (\chi_m - c^2x^2) \delta(x) + (\varepsilon - 2chx^2)\psi_m(x) = 0. \quad (274)$$

Let the self-adjoint differential operator  $L$  be defined by the formula

$$L(f)(x) = (1 - x^2)f''(x) - 2xf'(x) + (\chi_m - c^2x^2)f(x). \quad (275)$$

Then, multiplying (274) by  $\psi_m(x)/h$  and integrating on  $[-1, 1]$ , we get

$$\int_{-1}^1 L\left(\frac{\partial\psi_m}{\partial c}\right)(x) \psi_m(x) dx + \frac{\varepsilon}{h} - \int_{-1}^1 2cx^2\psi_m^2(x) dx = 0. \quad (276)$$

Now  $\frac{\varepsilon}{h} = \frac{\partial\chi_m}{\partial c}$ . In addition, since  $L$  is self-adjoint,

$$\int_{-1}^1 L\left(\frac{\partial\psi_m}{\partial c}\right)(x) \psi_m(x) dx = \int_{-1}^1 \frac{\partial\psi_m}{\partial c}(x) L(\psi_m)(x) dx. \quad (277)$$

But due to (272),  $L(\psi_m)(x) = 0$  for all  $x \in [-1, 1]$ , so the integral (277) is zero. Thus (276) becomes

$$\frac{\partial\chi_m}{\partial c} = 2c \int_{-1}^1 x^2\psi_m^2(x) dx. \quad (278)$$

□

## 10 Generalizations and Conclusions

In this paper, we design quadrature rules for band-limited functions, based on the properties of Prolate Spheroidal Wave Functions (PSWFs), and the connections of the latter with certain fundamental integral operators (see (17), (19) in Section 2.5). The quadratures are a surprisingly close analogue for band-limited functions of Gaussian quadratures for polynomials, in that they have positive weights, are optimal in the appropriately defined sense, and their nodes, when used for approximation (as opposed to integration), result in extremely efficient interpolation formulae. Thus, Sections 5-7 of this paper can be viewed as reproducing for band-limited functions much of the standard polynomial-based approximation theory (for which see, for example, [24]). Generally, there is a striking analogy between the band-limited functions and polynomials.

Obviously, there are certain differences between the resulting apparatus and the standard numerical analysis. To start with, where the classical techniques are optimal for polynomials, the approach of this paper is optimal for band-limited functions; whenever

the functions to be dealt with are naturally represented by trigonometric expansions on finite intervals, our quadrature and interpolation formulae tend to be more efficient than those based on the polynomials. When the functions to be dealt with are naturally represented by polynomials, the classical approach is more efficient; however, many physical phenomena involve band-limited functions, and very few involve polynomials.

Qualitatively, the quadrature (and interpolation) nodes obtained in this paper behave like a compromise between the Gaussian nodes and the equispaced ones: near the middle of the interval, they are very nearly equispaced, and near the ends, they concentrate somewhat, but much less than the Gaussian (or Chebychev) nodes do. For large  $c$ , the distance between nodes near the ends of the interval is of the order  $\frac{1}{c^{3/2}}$ , with the total number of nodes close to  $\frac{c}{\pi}$ . In contrast, the distance between the Gaussian nodes near the ends of the interval is of the order  $\frac{1}{n^2}$ , with  $n$  the total number of nodes. A closely related phenomenon is the reduced norm of the differentiation operator based on the prolate expansions: for an  $n$ -point differentiation formula, the norm is of the order  $n^{3/2}$ , as opposed to  $n^2$  for polynomial-based spectral differentiation. Thus, PSWFs are likely to be a better tool for the design of spectral and pseudo-spectral techniques than the orthogonal polynomials and related functions.

Much of the analytical apparatus we use was developed more than 30 years ago (see [20]-[21], [17], [18]); the fundamental importance of these results in certain areas of electrical engineering and physics has also been understood for a long time. However, there appears to have been no prior attempt made to view band-limited functions as a source of *numerical* algorithms. Generally, there is a fairly limited amount of information in the literature about the PSWFs, especially when compared to the wealth of facts on many other special functions. Section 9 of this paper is an attempt to remedy this situation to a small degree.

The apparatus built in this paper is a strictly one-dimensional one. Obviously, one can construct discretizations of rectangles, cubes, etc. by using direct products of one-dimensional grids; the resulting numerical algorithms are satisfactory but not optimal. Furthermore, representation of band-limited functions on regions in higher dimensions is of both theoretical and engineering interest. Obvious applications include seismic data collection and processing, antenna theory, NMR imaging, and many others. When the region of interest is a sphere, most of the necessary analytical apparatus can be found in [21]. At the present time, we have constructed and implemented somewhat rudimentary versions of the relevant numerical algorithms; we are conducting numerical experiments with these, and will report the results at a later date. A much more difficult set of questions is presented by the structure of band-limited functions on more general regions.

## References

- [1] C.J. Bouwkamp, *On Spheroidal Wave Functions of Order Zero*, J. Math. Phys., 26, 1947, pp. 79-92.
- [2] H. Cheng, N. Yarvin, V. Rokhlin, *Non-Linear Optimization, Quadrature, and Interpolation*, Yale University Technical Report, YALEU/DCS/RR-1169, 1998, to appear in the SIAM Journal of Non-linear Optimization.
- [3] L. Debnath, *Integral Transforms and Their Applications*, CRC Press, New York, 1995.
- [4] G. Gripenberg, S.O. Londen, O. Staffans, *Volterra Integral and Functional Equations*, *Encyclopedia of Mathematics and its Applications*, Cambridge University Press, 1990.
- [5] C. Flammer, *Spheroidal Wave Functions*, Stanford University Press, Stanford, Ca, 1956.
- [6] F. GANTMACHER AND M. KREIN, *Oscillation matrices and kernels and small oscillations of mechanical systems*, 2nd ed., Gosudarstv. Izdat. Tehn-Teor. Lit., Moscow, 1950 (Russian).
- [7] F. A. Grünbaum, *Toeplitz Matrices Commuting With Tridiagonal Matrices*, J. Linear Alg. and Appl., 40, (1981).
- [8] F. A. Grünbaum, *Eigenvectors of a Toeplitz Matrix: Discrete Version of the Prolate Spheroidal Wave Functions*, SIAM J. Alg. Disc. Meth., 2(1981).
- [9] F. A. Grünbaum, L. Longhi, M. Perlstadt, *Differential Operators Commuting with Finite Convolution Integral Operators: Some Non-Abelian Examples*, SIAM J. Appl. Math. 42(1982).
- [10] S. KARLIN, *The Existence of Eigenvalues for Integral Operators*, Trans. Am. Math. Soc. v. 113, pp. 1-17 (1964).
- [11] S. KARLIN, AND W. J. STUDDEN, *Tchebycheff Systems with Applications In Analysis And Statistics*, John Wiley (Interscience), New York, 1966.
- [12] M. G. KREIN, *The Ideas of P. L. Chebyshev and A. A. Markov in the Theory Of Limiting Values Of Integrals*, American Mathematical Society Translations, Ser. 2, Vol. 12, 1959, pp. 1-122.

- [13] J. MA, V. ROKHLIN, AND S. WANDZURA, *Generalized Gaussian Quadratures For Systems of Arbitrary Functions*, SIAM Journal of Numerical Analysis, v. 33, No. 3, pp. 971-996, 1996.
- [14] A. A. MARKOV, *On the limiting values of integrals in connection with interpolation*, Zap. Imp. Akad. Nauk. Fiz.-Mat. Otd. (8) 6 (1898), no.5 (Russian), pp. 146-230 of [15].
- [15] A. A. MARKOV, *Selected papers on continued fractions and the theory of functions deviating least from zero*, OGIZ, Moscow-Leningrad, 1948 (Russian).
- [16] P.M. Morse, H. Feshbach, *Methods of Theoretical Physics*, McGraw-Hill, New York, 1953.
- [17] H.J. Landau, H.O. Pollak, *Prolate Spheroidal Wave Functions, Fourier Analysis, and Uncertainty - II*, The Bell System Technical Journal, January 1961.
- [18] H.J. Landau, H.O. Pollak, *Prolate Spheroidal Wave Functions, Fourier Analysis, and Uncertainty - III: The Dimension of Space of Essentially Time- and Band-Limited Signals*, The Bell System Technical Journal, July 1962.
- [19] H.J. Landau, H. Widom, *Eigenvalue Distribution of Time and Frequency Limiting*, Journal of Mathematical Analysis and Applications, 77, 469-481 (1980).
- [20] D. Slepian, H.O. Pollak, *Prolate Spheroidal Wave Functions, Fourier Analysis, and Uncertainty - I*, The Bell System Technical Journal, January 1961.
- [21] D. Slepian, *Prolate Spheroidal Wave Functions, Fourier Analysis, and Uncertainty - IV: Extensions to Many Dimensions, Generalized Prolate Spheroidal Wave Functions*, The Bell System Technical Journal, November 1964.
- [22] D. Slepian, *Prolate Spheroidal Wave Functions, Fourier Analysis, and Uncertainty - V: The Discrete Case*, The Bell System Technical Journal, May-June 1978.
- [23] D. Slepian, *Some Comments on Fourier Analysis, Uncertainty, and Modeling* SIAM Review, V. 25, No. 3, July 1983.
- [24] J. Stoer and R. Bulirsch, *Introduction To Numerical Analysis*, 2'nd ed., Springer-Verlag, 1992
- [25] N. Yarvin and V. Rokhlin, *Generalized Gaussian Quadratures and Singular Value Decompositions of Integral Operators*, SIAM Journal of Scientific Computing, Vol. 20, No. 2, pp. 699-718 (1998).

Table 1: Quadrature performance for varying band limits, for  $\varepsilon = 10^{-7}$

$c$	$n$	Maximum Errors		$N_{\text{pol}}$
		Roots	Refined	
10.0	9	0.96E-05	0.51E-07	13
20.0	13	0.17E-04	0.94E-07	19
30.0	17	0.12E-04	0.50E-07	25
40.0	20	0.70E-05	0.30E-06	31
50.0	24	0.35E-05	0.83E-07	37
60.0	27	0.25E-04	0.27E-06	43
70.0	31	0.11E-04	0.66E-07	48
80.0	34	0.48E-05	0.17E-06	54
90.0	38	0.21E-05	0.40E-07	59
100.0	41	0.12E-04	0.91E-07	65
200.0	74	0.24E-05	0.86E-07	118
300.0	106	0.32E-05	0.21E-06	171
400.0	139	0.52E-05	0.62E-07	223
500.0	171	0.56E-05	0.88E-07	275
600.0	203	0.58E-05	0.11E-06	326
700.0	235	0.57E-05	0.12E-06	377
800.0	267	0.55E-05	0.13E-06	428
900.0	299	0.53E-05	0.14E-06	479
1000.0	331	0.50E-05	0.14E-06	530
1200.0	395	0.44E-05	0.13E-06	632
1400.0	459	0.38E-05	0.11E-06	734
1600.0	523	0.31E-05	0.97E-07	835
1800.0	587	0.28E-05	0.80E-07	937
2000.0	651	0.23E-05	0.64E-07	1038
2400.0	778	0.29E-05	0.15E-06	1240
2800.0	906	0.19E-05	0.84E-07	1442
4000.0	1288	0.37E-05	0.17E-06	2047

Table 2: Quadrature performance for varying precisions, for  $c = 50$

$\varepsilon$	$n$	Maximum Errors		$N_{\text{pol}}$
		Roots	Refined	
0.10E-01	19	0.45E-01	0.10E-01	30
0.10E-02	20	0.70E-02	0.13E-02	32
0.10E-03	21	0.91E-03	0.14E-03	33
0.10E-04	22	0.82E-04	0.13E-04	34
0.10E-05	23	0.54E-04	0.11E-05	36
0.10E-06	24	0.35E-05	0.83E-07	37
0.10E-07	25	0.33E-05	0.57E-08	38
0.10E-08	26	0.18E-06	0.36E-09	39
0.10E-09	26	0.18E-06	0.36E-09	40
0.10E-10	27	0.17E-06	0.21E-10	42
0.10E-11	28	0.79E-08	0.11E-11	43
0.10E-12	29	0.78E-08	0.56E-13	45
0.10E-13	30	0.31E-09	0.27E-14	55

Table 3: Interpolation performance for varying band limits, for  $\varepsilon = 10^{-7}$

$c$	$n$	Maximum Errors		$N_{\text{pol}}$	
		Roots	Refined	Cheb.	Leg.
5.0	13	0.12E-06	0.12E-06	17	17
10.0	18	0.12E-06	0.13E-06	24	25
15.0	22	0.24E-06	0.25E-06	31	32
20.0	26	0.26E-06	0.28E-06	37	39
25.0	30	0.22E-06	0.23E-06	43	45
30.0	33	0.67E-06	0.73E-06	49	51
35.0	37	0.42E-06	0.46E-06	55	57
40.0	41	0.25E-06	0.27E-06	61	63
45.0	44	0.54E-06	0.60E-06	67	69
50.0	48	0.29E-06	0.33E-06	73	75
100.0	82	0.39E-06	0.46E-06	128	131
150.0	115	0.52E-06	0.64E-06	182	186
200.0	147	0.12E-05	0.15E-05	235	239
250.0	180	0.83E-06	0.11E-05	287	292
300.0	212	0.13E-05	0.17E-05	340	345
350.0	245	0.75E-06	0.10E-05	392	398
400.0	277	0.10E-05	0.14E-05	443	450
450.0	309	0.13E-05	0.18E-05	495	502
500.0	341	0.16E-05	0.22E-05	547	554
1000.0	662	0.16E-05	0.24E-05	1058	1068
1500.0	982	0.15E-05	0.25E-05	1566	1578
2000.0	1301	0.20E-05	0.35E-05	2072	2086

Table 4: Interpolation performance for varying precisions, for  $c = 25$

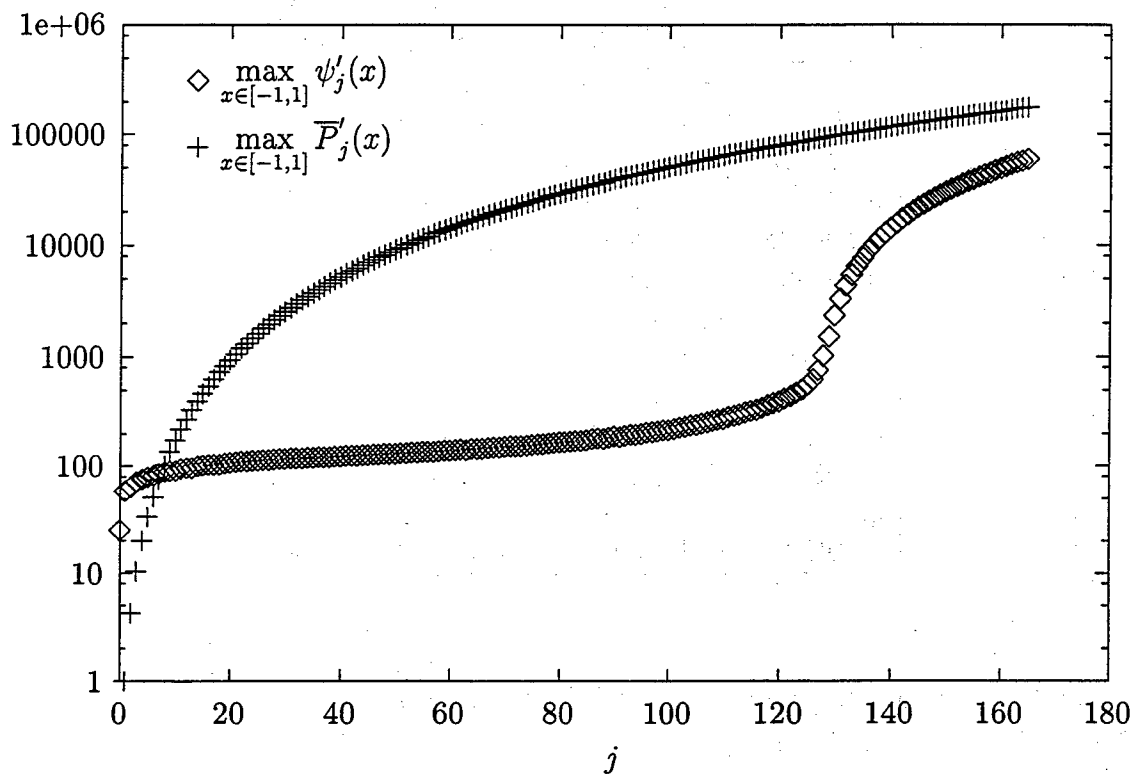
$\varepsilon$	$n$	Maximum Errors		$N_{\text{pol}}$	
		Roots	Refined	Cheb.	Leg.
0.10E-01	21	0.38E-01	0.43E-01	31	34
0.10E-02	23	0.37E-02	0.41E-02	34	36
0.10E-03	25	0.29E-03	0.31E-03	37	39
0.10E-04	26	0.74E-04	0.81E-04	39	41
0.10E-05	28	0.44E-05	0.47E-05	41	43
0.10E-06	30	0.22E-06	0.23E-06	43	45
0.10E-07	31	0.46E-07	0.49E-07	45	47
0.10E-08	32	0.95E-08	0.10E-07	47	49
0.10E-09	34	0.36E-09	0.38E-09	49	51
0.10E-10	35	0.67E-10	0.70E-10	51	52
0.10E-11	37	0.21E-11	0.22E-11	53	54
0.10E-12	38	0.36E-12	0.37E-12	54	56
0.10E-13	39	0.59E-13	0.63E-13	98	61

Table 5: Quadrature nodes for band-limited functions, with  $c = 50$  and  $\varepsilon = 10^{-7}$

This table contains only half of the nodes and weights, in particular those for which the node is less than or equal to zero; reflecting these nodes around zero yields the remaining nodes, the weight for the node at  $-x$  being the same as the weight for the node at  $x$ .

Node	Weight
-.9904522459960804E+00	0.2413064234922188E-01
-.9525601106643832E+00	0.5024347217095568E-01
-.8927960861459153E+00	0.6801787677830858E-01
-.8186117530609125E+00	0.7952155999100788E-01
-.7350624131965875E+00	0.8706680708376023E-01
-.6452878027260844E+00	0.9216240765763570E-01
-.5512554698695428E+00	0.9569254015486106E-01
-.4542505281525226E+00	0.9817257766311556E-01
-.3551568458127944E+00	0.9990914516102242E-01
-.2546173463813596E+00	0.1010880172648715E+00
-.1531287781860989E+00	0.1018214308931439E+00
-.5110121484050418E-01	0.1021735189986602E+00

Figure 2: Maximum norms of derivatives of prolate spheroidal wave functions for  $c = 200$ , and of normalized Legendre polynomials



Norms of eigenvalues  $\lambda_j$  for  $c = 200$ :

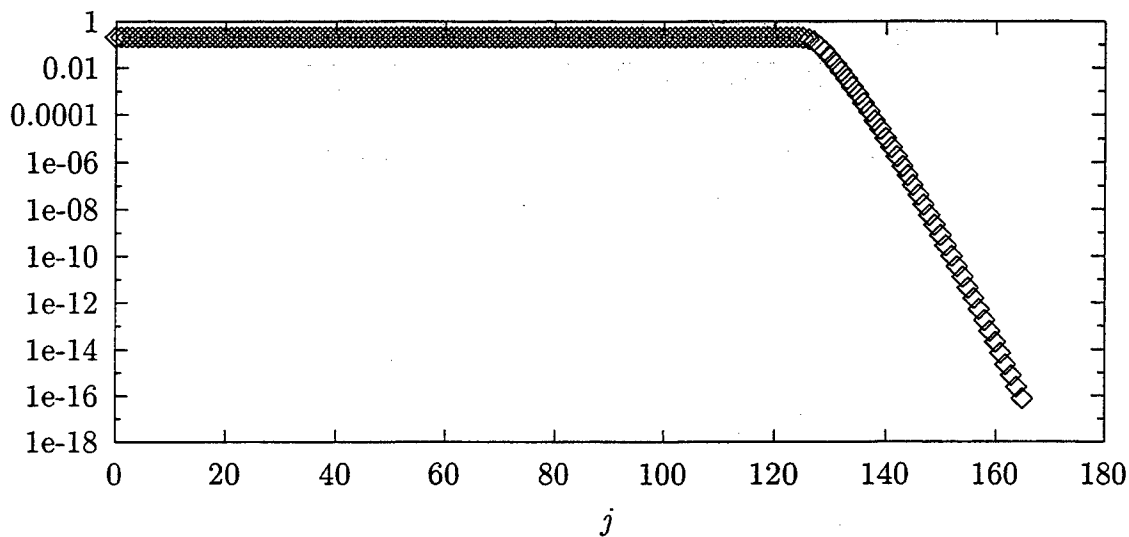


Table 6: Quadrature nodes for band-limited functions, with  $c = 150$  and  $\varepsilon = 10^{-14}$

This table contains only half of the nodes and weights, in particular those for which the node is less than or equal to zero; reflecting these nodes around zero yields the remaining nodes, the weight for the node at  $-x$  being the same as the weight for the node at  $x$ .

Node	Weight
-.9982883010959975E+00	0.4374483371752129E-02
-.9911354691596528E+00	0.9842619236149078E-02
-.9788315280982487E+00	0.1463518300250369E-01
-.9621348937901911E+00	0.1862396111287527E-01
-.9418386698454396E+00	0.2184988739217138E-01
-.9186509576802944E+00	0.2442858670932862E-01
-.8931541850293142E+00	0.2648864579258096E-01
-.8658083894041821E+00	0.2814375940413615E-01
-.8369709588254746E+00	0.2948528624795690E-01
-.8069187108185302E+00	0.3058356160435090E-01
-.7758670331396409E+00	0.3149181066633766E-01
-.7439849501152674E+00	0.3225015506203403E-01
-.7114064976175457E+00	0.3288893713079314E-01
-.6782391686910609E+00	0.3343126421620424E-01
-.6445701594098660E+00	0.3389488931551181E-01
-.6104710013384929E+00	0.3429358206877410E-01
-.5760010202980960E+00	0.3463812513892117E-01
-.5412099413257457E+00	0.3493704033879884E-01
-.5061398697742787E+00	0.3519712095895683E-01
-.4708268134473433E+00	0.3542382499917732E-01
-.4353018643598344E+00	0.3562156808557525E-01
-.3995921259242572E+00	0.3579394352776868E-01
-.3637214481257228E+00	0.3594388900778062E-01
-.3277110167114320E+00	0.3607381381247460E-01
-.2915798305819667E+00	0.3618569660385742E-01
-.2553450930388687E+00	0.3628116095737887E-01
-.2190225363501577E+00	0.3636153393399723E-01
-.1826266945721476E+00	0.3642789154364812E-01
-.1461711362450572E+00	0.3648109393796617E-01
-.1096686661347072E+00	0.3652181242257066E-01
-.7313150339365902E-01	0.3655054982303338E-01
-.3657144220122915E-01	0.3656765531685031E-01
0	0.3657333451556860E-01

## Fast Mathematical Algorithms & Hardware Corporation

Ronald R. Coifman  
Vladimir Rokhlin

1020 Sherman Avenue  
Hamden, CT 06514  
USA (203) 248-8212  
USA (203) 287-8765FAX

June 21, 2002

Defense Technical Information Center/OCP  
8725 John J. Kingman Road, Suite 0944  
Fort Belvoir, VA 22060-6218

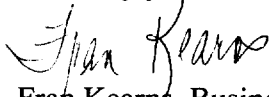
**Re: Contract #: F49620-98-C-0051**

To Whom It May Concern:

In regard to the above referenced contract, due to typographical errors, would you please correct the SF298 forms and the reports to read Contract #: F49620-98-C-0051, **not** F49620-97-C-0051. I apologize for any inconvenience this may have caused.

If you have any questions please feel free to call at the above number or email [fran@fmah.com](mailto:fran@fmah.com)

Sincerely yours,



Fran Kearns, Business Manager  
F.M.A. & H. Corporation